Sapienza Università di Roma

"Vito Volterra" Doctoral School in Astronomical, Chemical,

Earth, Mathematical and Physical Sciences.

Department of Earth Sciences

Archaeometric study on orichalcum coins

by

Melania Di Fazio

XXXII cycle

Thesis for the Degree of

Doctor of Philosophy

Advisors:

Dr. Anna Candida Felici

Dr. Caterina De Vito

Dr. Fiorenzo Catalli

“An investigator starts research in a new field with faith,
a foggy idea, and a few wild experiments.
Eventually the interplay of negative and positive results guides the work.
By the time the research is completed,
he or she knows how it should have been started and conducted.”

Donald Cram, Nobel laureates in Chemistry

Table of contents

Riassunto

I metalli, puri o in lega, hanno sempre giocato un ruolo fondamentale nella storia dell'uomo: la produzione regolare di oggetti in rame, ferro, bronzo e oricalco in antichità è infatti attestata dai numerosi ritrovamenti archeologici. In particolare, l'oricalco è una lega a base di rame e zinco, simile al moderno ottone, considerata dagli antichi un'invenzione degli dei. L'antica tecnica utilizzata per la produzione dell'oricalco era la cementazione, diffusa sia in Oriente che tra i popoli del bacino mediterraneo. Usato sin dal primo millennio a.C. in Asia Minore, l'oricalco fu introdotto come lega per la monetazione nel secondo secolo a.C. in Anatolia e solo successivamente nella penisola italica. Qui, Giulio Cesare per primo produsse monete in oricalco, come emissione sperimentale. Ottaviano Augusto, nel 23 a.C., promulgò una riforma monetaria in cui introdusse l'emissione di due nominali in oricalco. Successivamente, con la riforma monetaria di Nerone nel 63-64 d.C. furono introdotti altri tre nominali in oricalco.

La tesi di dottorato di seguito presentata ha lo scopo di caratterizzare la lega di oricalco e valutarne il degrado, attraverso uno studio archeometrico di monete antiche emesse tra il primo secolo a.C. e la fine del primo secolo d.C. Allo scopo, sono state impiegate tecniche non distruttive, nano-invasive e distruttive. In particolare, metodologie superficiali (XRF, FTIR-ATR, VIMP) hanno permesso una prima caratterizzazione delle monete in oricalco e degli strati superficiali della patina. Con tecniche di microscopia (SEM-EDS, FIB-FESEM-EDS, HR-FESEM-EDS) è stato possibile studiare le microstrutture tipiche della lega oricalco, il pattern corrosivo delle patine e il loro sviluppo all'interno dei campioni. L'analisi quantitativa (attraverso l'EMPA) dei nuclei non corrosi e delle patine dei campioni ha consentito la caratterizzazione dell'oricalco e la descrizione del processo di dezincificazione. Attraverso l'approccio multianalitico è stato possibile identificare caratteri di autenticità dei campioni, differenziare le monete per emissione e riesaminare le precedenti teorie utilizzate per la datazione di campioni in oricalco.

Per tanto, con questa tesi di dottorato si è voluto contribuire alle attuali conoscenze sulla coniazione romana in oricalco e si è tentato di approfondire i meccanismi dei processi corrosivi a carico delle leghe antiche.

Abstract

Metals, pure or in alloy, have always played a fundamental role in human history. Indeed, the regular production in antiquity of objects in copper, iron, bronze and orichalcum is attested by the numerous archaeological findings. In particular, the orichalcum is a copper-zinc based alloy, similar to the modern brass, considered by the ancient populations an invention of the gods. The cementation was the ancient technique used for the production of the orichalcum, common both in the East and in the Mediterranean basin. Used since the first millennium BC in Asia Minor, the orichalcum was introduced as alloy for coinage in Anatolia in the second century BC and only later was adopted in the Italian peninsula. Here, *Julius Caesar* first produced coins in orichalcum, as an experimental emission. *Octavianus Augustus*, in the 23 BC, promulgated a monetary reform, introducing two denominations in orichalcum. Subsequently, with the monetary reform of *Nero* in 63-64 AD three other denominations in orichalcum were introduced.

The PhD thesis presented below aims to characterise the orichalcum alloy and to evaluate its degradation, through an archaeometric study of ancient coins issued between the first century BC and the end of the first century AD. For this purpose, non-destructive, nano-invasive and destructive techniques were used. In particular, surface methodologies (XRF, FTIR-ATR, VIMP) allowed a first characterization of the orichalcum coins and the superficial investigation of the patinas. With microscopy techniques (SEM-EDS, FIB-FESEM-EDS, HR-FESEM-EDS) it was possible to study the typical microstructures of the orichalcum alloy, the corrosive pattern of the patinas and their development within the samples. The quantitative analysis (through the EMPA) of non-corroded cores and patinas of the samples allowed the characterization of the ancient orichalcum and the description of the dezincification process. Therefore, using a multi-analytical approach it was possible to define the authenticity of the samples, to grouping the coins by emission and to review the previous theories used for dating samples in orichalcum.

This PhD thesis wanted to contribute to the current knowledge on Roman coinage in orichalcum and to attempt investigating the mechanisms of corrosive processes affecting ancient alloys.

Introduction

Among all the ancient metallic objects, coins are the most common findings in archaeological excavations, due to their production in series, strictly related to their daily use by Romans since the Republican Age. Nevertheless, there are some denominations that seem rarer than others, as they belong to peculiar issues or because they were coined in uncommon alloys.

The Roman coins minted in orichalcum fit in this description of rarity. Indeed, they were issued for a not so long period in a short number of specimens, if compared to the large amount of different denominations simultaneously circulating in Roman territories. In addition, the orichalcum alloy was considered a high value material by the ancient populations, for the aesthetic features as well as to the difficulty in its production.

Therefore, the focus of this PhD thesis is the Roman orichalcum coinage and the aim of the related three-year project, yet concluded, was to characterize the ancient Cu-Zn based alloy, similar to the modern brass, and to define the technological level reached by ancient population to produce it. For this purpose, a representative number of samples from private collections were studied, using a multidisciplinary approach and, thus, multi-analytical methods. This resulted to be the best line to acquire new information about the cementation process, because of the lack of scientific sources on the Cu-Zn alloy production.

Previous analyses on archaeological specimen were frequently conducted melting the objects under study (or part of them); even, the sampling method was not mentioned in the research papers. In addition, it often happened that the analytical methods employed to obtain qualitative and/or quantitative information on ancient alloys were not described in scientific articles. In all these cases, it is not known how the degraded patina was treated, if it was removed or molten and, thus, if it was analysed together with the uncorroded nucleus. In the last case, all the data could be affected by errors. Indeed, archaeological orichalcum samples suffer of dealloying of the patinas, i.e. dezincification (the loss of zinc) or, in the worst cases, decuprification (the subsequent loss of copper), causing the formation of a porous layer, resulting different in composition from the undegraded inner core of the object. For these reasons, all the chemical data obtained

from the external layer of the specimens or from a non-defined area of analysis could not be considered as representative of the real composition of the ancient alloy.

For all the reasons mentioned above, new considerations about ancient orichalcum alloy could be useful in different fields. Indeed, new analyses can help to better understand the technological development of metallurgical processes in ancient times and they can also fill the gap of the absence of real quantitative data not only from the undegraded core of the metal object, but also from patinas. In fact, information about orichalcum patinas can give evidences about the development of the dezincification process that can extend in deep in samples. This process can be related to both the aging of the alloy as to its composition, since the presence of minor elements in the alloy can, for instance, prevent object to the degradation and, thus, to the dealloying.

Destructive and non-destructive analyses were performed, aiming to characterize the whole set of samples, investigating both the corroded external layers and the uncorroded core of the coins. Combining techniques as X-ray fluorescence (XRF), voltammetry of immobilized particles (VIMP), attenuated total reflectance – Fourier transform infrared spectroscopy (ATR-FTIR) and focused ion beams – field emission scanning electron microscopy (FIB-FESEM-EDS), the organic and inorganic compounds of the patinas were identified. Moreover, the use of scanning electron microscopy (SEM-EDS), X-ray distribution maps of elements, high resolution field emission scanning electron microscopy (HR-FESEM) and electron microprobe analysis (EMPA) on cross section allowed to characterize the real composition of the orichalcum. The information obtained in this way helped to distinguish different technological levels of cementation process achieved by the Roman in different historical periods. Information about the chemical composition of the patinas and of the uncorroded nucleus, in addition to the investigation of the micro and nanostructures of the orichalcum, were a powerful tool to understand the trigger of corrosion and degradation processes on this ancient alloy.

This thesis aims to contribute to the current knowledge about the orichalcum coinage during the Roman Empire and to deepen knowledge of corrosive processes of ancient alloys.

This PhD thesis is presented as a collection of peer-reviewed original papers, yet published or under review.

All the scientific data were acquired and processed by me as PhD student, under the supervision of my advisor (Dr. Anna Candida Felici), my co-advisor (Dr. Caterina De Vito) and the supervisors of the hosting institutions, during the international mobility period in Spain (Prof. María Teresa Doménech-Carbó and Prof. Antonio Doménech-Carbó). The numismatic characterization of the studied samples was conducted with the help of Dr. Fiorenzo Catalli, archaeologist. As first author, I wrote the manuscripts, with the contribution of all the authors.

The thesis is structured as follows:

Chapter 1 – Historical Background: in this first chapter the historical-archaeological knowledge about orichalcum is presented, as well as the current information from scientific and archaeometric studies. In particular, here is described the method used by ancient populations to produce orichalcum, starting from the deposit ores selected to the minting of coins.

Chapter 2 – Article "Microstructure and chemical composition of Roman orichalcum coins emitted after the monetary reform of Augustus (23 B.C.)", published on *Scientific Report* (doi: 10.1038/s41598-019-48941-4): here the archaeological samples were studied, using a multi-analytical approach, from the external degraded patina to the inner undegraded core. In addition, archaeometric issues about sample dating have been addressed.

Chapter 3 – Article "Solid-state electrochemical characterization of emissions and authorities producing Roman brass coins", published on *Microchemical Journal* (doi: 10.1016/j.microc.2019.104306): in this article, the compounds present in the patinas of the samples were analysed using VIMP methodology combined with ATR-FTIR and FIB-FESEM-EDX. Moreover, a grouping of the coins by emission or by authority was purposed using VIMP methodology.

Chapter 4 – Article "Structural and chemical characterization of an ancient alloy from micro to nanoscale: the case of Roman orichalcum coins.", currently under review: here is presented the characterization of the orichalcum alloy from micro to nanoscale, with the aim of exploring the processes that induced corrosion and, gradually, dealloying.

Conclusions: Here are reported the conclusions and consideration of the research project contained in this thesis.

Appendices: In this section it is possible find detailed data and images acquired via EMPA, XRF and VIMP not published in the articles mentioned above.

Chapter 1 - Historical background

The term *orichalcum* is an ancient word derived from the Greek *ὀρείχαλκος (oreichalkos)*, that means “copper from the mountain” (ὄρος, *óros*, "mountain" and χαλκός, *chalkós*, "copper"), later changed by Romans in *aurichalcum*, literally “golden copper”. This word was used since the 7th century BC in the Homeric *Hymns*: according to the Greek manuscript, for her birth the goddess Aphrodite wore jewellery made in gold and orichalcum (Omero Minore, 1925). The presence of *orichalcum* word in a religious context denote the worth and the relevance that this alloy had in ancient times, so much that it was associated to the gold.

Plato in his *Critia’s dialogues* (4th century BC) described *orichalcum* as the most precious metal known at that time, after gold, directly extracted from the ground of the fictional Island of *Atlantis*. Indeed, for its value the orichalcum was used on the Island to cover the defence wall of the *Acropolis* and to decor the inner of the Poseidon temple (Platone, 2001).

Orichalcum was considered a precious and special material, so that historical literary sources report the use of this alloy for a part of the armour worn by Hercules (Esiodo, 1929).

The use of this ancient alloy, similar to the modern brass, both for coinage and for common objects is closely related to the production of copper-based alloys and, thus, to the achievement of ever higher technological levels in metalwork.

1.1 The production and use of orichalcum

1.1.1 Ore deposits

Zinc can be found in nature as component of different ore minerals, as blende or sphalerite (ZnS), calamine or smithsonite ($ZnCO_3$) and hemimorphite ($2ZnO{\cdot}SiO_2{\cdot}H_2O$). Sometimes, zinc can be found in association with copper: it occurs in Cyprus and Ireland deposits as impurity or trace element. The low content of this element in the deposits of

origin can justify the presence of zinc in traces (with a content of less than 3%) in prehistoric or early historic artefacts (Craddock, 1978; Tylecote, 1992).

Unfortunately, there are limited historical sources reporting information about active mines in antiquity of zinc ores mining. Strabo's *Geography* is one of the most famous and used reference that describes ore deposits known in ancient times. In his work, the author talks about a stone quarried near Andeira (Phyrigia, north-west of Anatolia) that, if burned, yields drops of "false silver"; this drops mixed to copper formed a product called *oreichalkos* (Caley, 1964; Craddock, 1998). It is known that deposits of argentiferous lead/zinc pyrites are present in the Turkish region where the ancient city of Andeira was, exploited in early as in recent times. In addition, galena, sphalerite, chalcopyrite and arsenopyrite are present in the same ore deposit (Craddock, 1998; Gale et al., 1985).

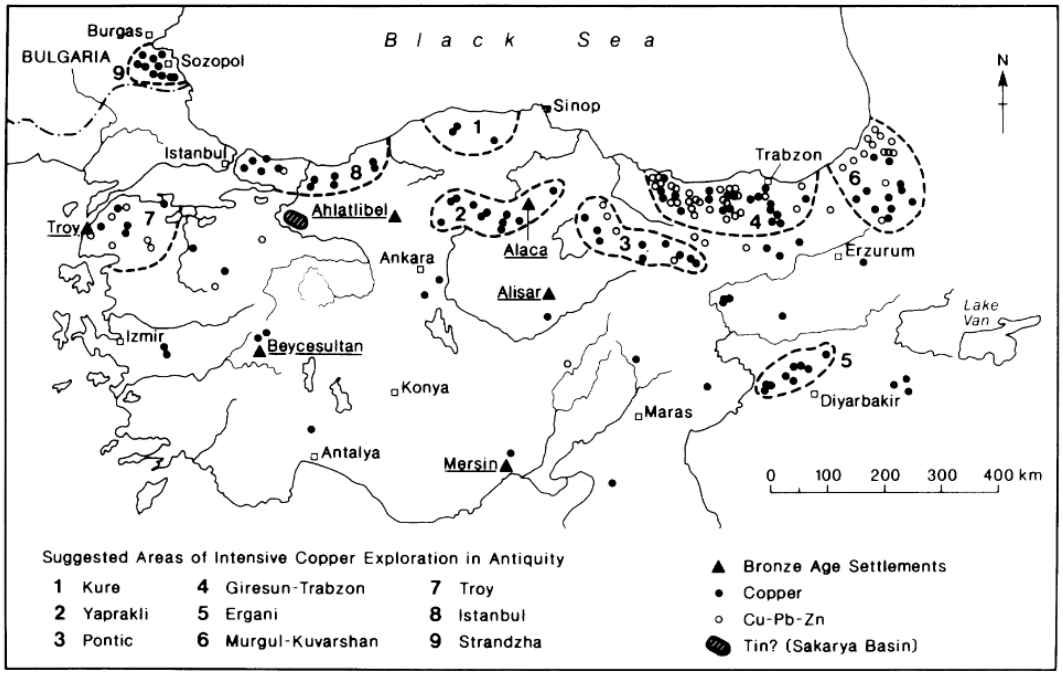

Figure 1: Map of the suggested Turkish areas of exploitation in antiquity. From *Gale et al 1985*

Another mining sites exploited in ancient times was located in the mining district of Laurion (southern Attic Peninsula). This ore is a mixture of sulphides of iron (pyrite), lead (galena) and zinc (sphalerite) (Alexakis, 2008). In particular, the Laurion ores were originally exploited to extract silver from the argentiferous galena. Probably, due to a unperfect separation system, sphalerite was included in the smelting process, producing unintentionally zinc oxide in the silver furnaces, called *lauriotis* by Plinius in his *Naturalis*

Historia (from the name of Laurion mine) (Caley, 1964). Moreover, archaeological and scientific evidences revealed the presence of an intense mining activity on the Cyprus Island (south-east of the Mediterranean sea) from the 8th century BC to the 15th century AD (Pyatt, 2001).

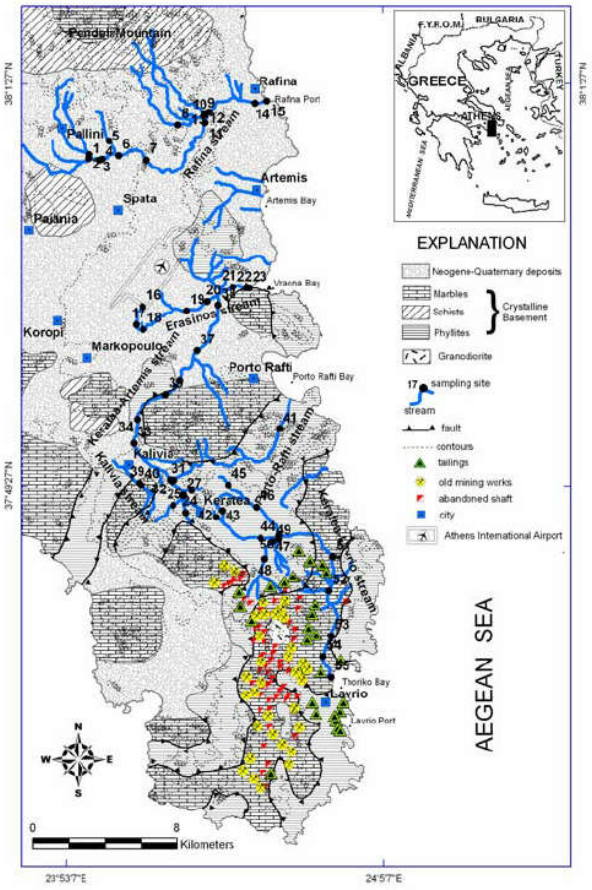

Figure 2: Simplified geological map of the East Attica region. The old mining works in the Laurion region are highlighted. From *Alexakis, 2008*

In the western area of the Mediterranean sea, ore deposits of sulphides and non-sulphides zinc are located in the historical Iglesiente region, near the City of Iglesias, south-west of Sardinia (Italy) and present pyrite, sphalerite and galena, besides calcic skarns of the Zn-Pb(-Cu) type and minerals of the calamine category (i.e. smithsonite, hydrozincite and hemimorphite as main Zn-bearing minerals) (Boni et al., 2003). These mines were exploited since the Phoenician civilization on his arrival on the Sardinian island. The Romans continued the mining activity in the region of the Iglesiente not only to extract zinc- and lead-rich minerals but, in particular, for the high content of silver in the deposits (Boni et al., 2003). Also the metalliferous regions in the Iberian Peninsula was exploited by Romans, in particular during the late Republican Era and for all the Imperial Era (Edmondson, 1989).

One of the most known and used calamine ore in north Europe was located near Aachen, Germany (the ancient *Aquisgranum*) (Dejonghe, 1998), discovered during the second half of the 1st century AD and declined in the 4th century (Bayley, 1998).

On the contrary, despites the archaeological finds of objects casted in brass, chemical analyses seems to indicate that the Slovenian zinc-bearing ores near the ancient Emona were not exploited by Romans (Giumlia-Mair, 2001).

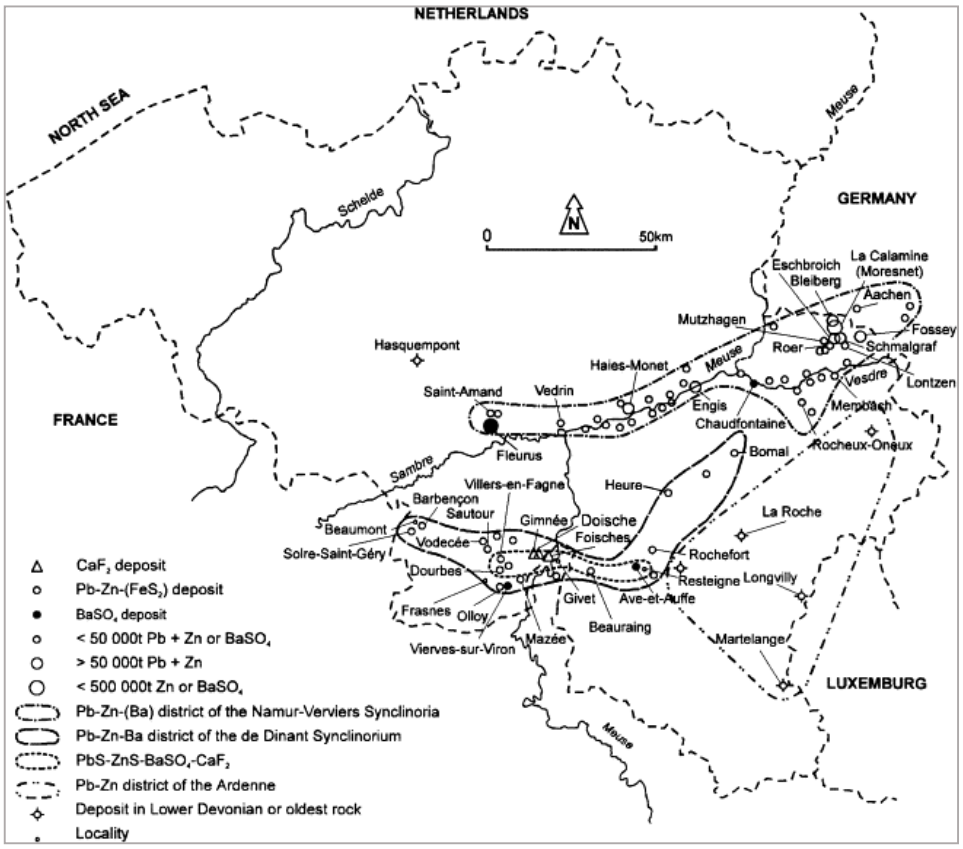

Figure 3: Map of major lead–zinc ore deposits located near the city of Aachen. From *Dejonghe, 1998*

1.1.2 The cementation process

The two main metals composing orichalcum are copper and zinc. Both these elements belong to the transition metal block of the periodic table, but present different physical properties. Indeed, the temperature required reducing zinc minerals and ores is 1000-1200 °C and, unfortunately, it is higher than the temperature of boiling point of the zinc itself (907°C). Hence, it means that in open environment, or in presence of air in general, zinc in state of vapor is rapidly transformed into its corresponding oxide. In contrast, the copper melting point is 1083°C and temperature required to reduce this element is higher than the zinc boiling point.

Therefore, the difficult to extract zinc from ores by melting prevented ancient population to produce orichalcum in open crucibles or primitive furnaces, due to the high

temperature required and the need of a reducing environment (Caley, 1964). Using carbonate ores or oxides directly, zinc could be extract with charcoal under reducing condition, whereas the sulphide ores required an initial roasting phase that, due to the high temperature needed, caused the loss of the zinc in vapour phase (Craddock, 1978).

To directly produce a zinc-based alloy from ores it should be employed a peculiar system to condense the resulting zinc vapour. For this reason, the so-called "cementation process" appeared to be the better way to produce copper-zinc alloys, probably since the prehistoric times (Caley, 1964). Despite the absence of archaeological evidences (Craddock, 1978) but according to historical sources, the cementation procedure adopted in Roman Times provided the use of ceramic crucibles, sealed with more or less accuracy, in which zinc ores were heated with charcoals and fragments of copper to a temperature between the zinc boiling point and the copper melting point (i.e. 900-1000°C); this range of temperature allowed zinc in vapour to spread in the non-complete molten (due to the low temperature) copper producing a solution that, further heated and stirred, formed the orichalcum alloy. In particular, the historical cementation involved as first step the calcination and the fine grinding of the calamine and then the mixing of the mineral with charcoal. After that, the mix was placed in a hot crucible, filled to one-sixth of its capacity. The crucible was than filled with copper and covered with other charcoal and, once the cementation reaction had completed, it was heated to the temperature necessary to melt and homogenise the vessel content (Bayley, 1998; Bayley and Rehren, 2007; Tylecote, 1992).

With this method, the percentage of the zinc in the alloy unlikely can exceed the 28-30% (Bayley, 1998; Newbury et al., 2005; Rehren, 1999; Thornton, 2007).

With the cementation method the zinc vapours are trapped in the molten copper, forming a liquid copper-zinc alloy. The cementation produces a homogeneous alloy, without structures with copper or zinc microdomains from macro to meso scale.

The first historical mention of a technical process for the extraction and the isolation of metal, zinc in particular, is in Theopompus' *Philippica* (4th century BC), used later as historical source by Strabo in his *Geography* (1st century AD). Both the manuscripts talk about a stone found in Andeira (Asia Minor) which, if burned, produced droplet of "false silver" (probably metallic zinc extracted from ores, although some

authors referred to "false silver" as arsenical copper) and, added to copper, gave a mixture called "*oreichalkos".*

The cementation process was completely abandoned in the 18th century AD, after the introduction of a new method of brass-making patented by William Champion: starting from his father's patented new method of cementation, Champion invented a new furnace for the distillation of zinc *per descensum* that reduced the loss of the zinc vapour and increased the percentage of zinc in brass alloy (Day, 1998; Dungworth and White, 2007). The Champion's system can be reconducted to the method used to smelt and distil zinc in India during the Middle-Ages (Craddock, 1978; Craddock et al., 1998; Day, 1998). Indeed, the Indian method of the zinc distillation by descending provided for the use of a retort with the neck of the condenser facing down, where a cool chamber with water was placed to collect the dripping distilled zinc; in this system, as in the Champion one, the combustion chamber with fire was placed at the top (Craddock et al., 1998; Day, 1998).

1.1.3 Orichalcum as a high value alloy

In the early 1st millennium BC copper was the main metal used, alone or alloyed with tin, antimony or silver. On contrary, zinc was not taken into account by ancient smiths for metalworking as its extraction was difficult. The first use of zinc can be considered as an experiment to replace tin. The need of metallurgical experimentation probably lies in the difficulty of supplying tin, after the collapse of the Mycenaean Empire (Craddock, 1978).

Orichalcum was considered an expensive alloy and worthy of the gods, as suggested by references found in ancient Greek literature, probably due to its golden colour.

In Asia Minor, the intentional use of zinc was attested by archaeological findings in northern Iraq, dated back to the 14th century BC. Indeed, rings with a content of zinc up to 14.4% were found, so they can be considered among the oldest brass objects intentionally produced, although using a different method of production than cementation, due to the low amount of zinc (Bayley, 1998).

Despite the belief that *orichalcum* was initially used only for coinage by the Romans, new archaeological evidences in Europe, brought to light from the end of the 20th century, revealed that this alloy was used by them since the first half of the 1st century BC to produce different kind of object, e.g. brooches (Istenič and Šmit, 2007; Šmit et al., 2005) or blinkers for military use (Barrena et al., 2008). The use of brass by European pre-Roman tribes and populations seems to be attested only after their contact with the Romans (Bayley, 1998; Fajfar et al., 2015; Istenič and Šmit, 2007).

During the 2nd and the 3rd century AD, the use of zinc in alloys was gradually reduced and a new copper-based alloy with few percent of other metals, such as tin and lead (the modern leaded gunmetal), started to be used (Craddock, 1978). This has been also confirmed by archaeological findings of brooches dated back to 1st-5th Centuries AD in Roman Britain (Bayley, 1998), by findings of vessels, statuettes, fibulae, pins and bracelets dated to 4th -5th century AD in the archaeological area of Emona (the modern Ljubljana, Slovenia) (Giumlia-Mair, 2001), by the discover of finger rings and amulet pendants dated back to 4th-7th century AD in the south-east coasts of the Mediterranean sea (modern Israel) (Ashkenazi et al., 2015), all produced in brass, leaded brass and gunmetal. With the improvement of metallurgical skills over time, metalworkers employed different compositions and quality of alloys for different classes of object and, moreover, for different parts of the same object (Giumlia-Mair, 2001).

1.1.4 Orichalcum as a coinage alloy

In general, the use of a good-quality metal to produce ingots (Caponetti et al., 2017), and thus coins, was fundamental to ensure the commercial value of the coin itself. Indeed, the use of a specific metal or alloy, in addition to a standard weight of coins, needed in ancient times as today to guarantee the authenticity and the value of each denomination in circulation (Smekalova, 2009).

The use of orichalcum as a coinage alloy started only after the use of other copper-based alloys. Probably, the first coins in orichalcum were minted in the Kingdom of Pontus and in the regions of Phrygia and Bithynia, during the reign of *Mithridates VI* (120-96 BC) (Fajfar et al., 2015; Smekalova, 2009). In particular, the issue of brass coins

started probably in the city of Pergamon, the new capital of the Kingdom of Pontus after the conquering by Mithridates VI (Smekalova, 2009).

Probably, orichalcum was adopted for the first time in Asia Minor during the first war between Rome and *Mithridates VI* and then during all the Mithridatic Wars. Indeed, according to Smekalova (Smekalova, 2009), the Anatolian issues in orichalcum were connected to the victories of the King of Pontus on Rome (starting to the First Mithridatic War, 89-85 BC) and to the military and political activities carried out by *Mithridates* himself. The reason of these new issues lies in the need to replace coins of high intrinsic value (i.e. silver-rich coins), that lacked in circulation as the preparation to the wars and the support of the further military campaigns required new economic resources; this deficiency of metallic and monetary sources was, thus, solved using orichalcum alloy to struck coins as experimentation (Smekalova, 2009).

After the death of *Mithridates VI* no more brass coins were produced in series until the new issues in orichalcum of the proconsuls C. Clovius (mint of Rome) and Q. Oppius (oriental mint) 46-44 BC (Amela Valverde, 2004; Barbato, 2015; Smekalova, 2009).

An exception can be considered the emission struck by the Celtic tribe of Arveni in 53-52 BC. In fact, a group of these coins were analysed and resulted to have from 9 to 15% of zinc. Probably, this emission was made to replace gold coins (*Vercingetorix* staters), due to the lack of gold during the Gallic Wars of *Julius Caesar* (Fajfar et al., 2015; Istenič and Šmit, 2007).

According to the current state of the studies, the Roman coin production in orichalcum is limited to the Caesarean Era and to the phase of the Julio-Claudian dynasty. In particular, the use of brass to strike coins under the reign of *Julius Caesar* can be considered as experimental issues (Crawford, 1974), that was suddenly halted due to *Caesar* death in 44 BC. *Julius Caesar's* emission in orichalcum probably derived from a meditated reform of the entire monetary system that has never been implemented (Catalli, 2003). The last phase of the Roman Republic was characterized by a remarkable monetary disorder, in which the production of coins was left to the initiative of the commanders, without control from central authority and, therefore, without respecting the characteristics of weight, dimension and alloy provided for each denomination. To solve this problem, in 23 BC the Emperor *Octavianus Augustus* carried out a complete reform of the monetary system, stabilizing the issues, establishing clear weight standards

and organizing a precise and rigorous exchange rate system between the values of all the denominations (Amela Valverde, 2004; Breglia, 1964; Catalli, 2003). In particular, according to historical sources, the denominations produced in metals or alloys different from gold and silver were: the *sestertius* (with a value of four *asses* or two *dupondii*) and the *dupondius* (with a value of two *asses)* coined in orichalcum; the *as* and the *semis* (with a value of a half *as*) in bronze; the *quadrans* (with a value of a quarter of *as*) in copper. This monetary system remained unchanged until Nero's new monetary reform, in 63-64 AD, which defined again the standards of production and introduced the issues of *semisses* and *quadrantes* in orichalcum, instead of bronze and copper, respectively (Amela Valverde, 2004; Breglia, 1964; Catalli, 2003).

The use of orichalcum coin, probably also issued in previous years, continued after the death of Nero, i.e. in the Traian Age (98-117 AD), as archaeological evidences in burial areas revealed (Aurisicchio et al., 2002).

References

Alexakis, D., 2008. Geochemistry of stream sediments as a tool for assessing contamination by Arsenic, Chromium and other toxic elements: East Attica region, Greece. European Water 21, 57–72.

Amela Valverde, L., 2004. RRC 476 y 550, dos emisiones en oricalco de C. Julio César. Nvmisma 248, 7–22.

Ashkenazi, D., Taxel, I., Tal, O., 2015. Archeometallurgical characterization of Late Roman- and Byzantine-period Samaritan magical objects and jewelry made of copper alloys. Materials Characterization 102, 195–208. https://doi.org/10.1016/j.matchar.2015.01.019

Aurisicchio, C., Ferro, D., Martinelli, G., Cesaro, S.N., Rapinesi, I.A., 2002. A study of a distaff of the second century A.D. from a necropolis of Boccone D'Aste (Rome, Italy)—tomb 75. Journal of Cultural Heritage 3, 107–116. https://doi.org/10.1016/S1296-2074(02)01168-8

Barbato, M., 2015. The Coins of Clovius and Oppius (RRC 476/1 and 550/1-3): New Evidence from Find-spots. The Numismatic Chronicle 175, 103–116.

Barrena, M.I., Gómez de Salazar, J.M., Soria, A., 2008. Corrosion of brass archaeological blinker: Characterisation of natural degradation process. Materials Letters 62, 3944–3946. https://doi.org/10.1016/j.matlet.2008.05.015

Bayley, J., 1998. The production of brass in antiquity with particular reference to Roman Britain, in: 2000 Years of Zinc and Brass, Occasional Paper. P.T. Craddock, British Museum, London.

Bayley, J., Rehren, T., 2007. Towards a functional and typological classification of crucibles, in: Metals and Mines: Studies in Archaeometallurgy. La Niece, Susan; Hook, Duncan R.; Craddock, P. T., London.

Boni, M., Gilg, H.A., Aversa, G., Balassone, G., 2003. The "Calamine" of Southwest Sardinia: Geology, Mineralogy, and Stable Isotope Geochemistry of Supergene Zn Mineralization. Economic Geology 98, 731. https://doi.org/10.2113/gsecongeo.98.4.731

Breglia, L., 1964. Numismatica antica: storia e metodologia. Feltrinelli.

Caley, E.R., 1964. Orichalcum and related ancient alloys, Numismatic notes and monograph. American Numismatic Society, New York.

Caponetti, E., Francesco, A., Martino, D.C., Saladino, M.L., Ridolfi, S., Chirco, G., Berrettoni, M., Conti, P., Bruno, N., Tusa, S., 2017. First discovery of orichalcum ingots from the remains of a 6th century BC shipwreck near gela (Sicily) seabed. Mediterranean Archaeology and Archaeometry 17, 11–18. https://doi.org/10.5281/zenodo.581716

Catalli, F., 2003. Numismatica greca e romana. Istituto Poligrafico e Zecca dello Stato, Roma.

Craddock, P.T., 1998. Zinc in classical antiquity, in: 2000 Years of Zinc and Brass, Occasional Paper. P.T. Craddock, British Museum, London.

Craddock, P.T., 1978. The composition of the copper alloys used by the Greek, Etruscan and Roman civilizations. Journal of Archaeological Science 5, 1–16. https://doi.org/10.1016/0305-4403(78)90015-8

Craddock, P.T., Freestone, I., Gurjar, L., Middleton, A., Willies, L., 1998. Zinc in India, in: 2000 Years of Zinc and Brass, Occasional Paper. P.T. Craddock, British Museum, London.

Crawford, M.H., 1974. Roman Republican Coinage. Cambridge University Press.

Day, J., 1998. Brass and zinc in Europe from the Middle Ages until the Mid-Nineteenth Century, in: 2000 Years of Zinc and Brass, Occasional Paper. P.T. Craddock, British Museum, London.

Dejonghe, L., 1998. Zinc–lead deposits of Belgium. Ore Geology Reviews 12, 329–354. https://doi.org/10.1016/S0169-1368(98)00007-9

Dungworth, D., White, H., 2007. Scientific examination of zinc-distillation remains from Warmley, Bristol. Historical Metallurgy 41, 77–83.

Edmondson, J.C., 1989. Mining in the Later Roman Empire and beyond: Continuity or Disruption? The Journal of Roman Studies 79, 84–102. https://doi.org/10.2307/301182

Esiodo, 1929. Lo Scudo di Ercole, in: I Poemi. Le Opere e i Giorni, La Teogonia, Lo Scudo Di Ercole, Frammenti. Nicola Zanichelli, Bologna.

Fajfar, H., Rupnik, Z., Šmit, Ž., 2015. Analysis of metals with luster: Roman brass and silver. Nuclear Instruments and Methods in Physics Research Section B: Beam

Interactions with Materials and Atoms 362, 194–201. https://doi.org/10.1016/j.nimb.2015.09.081

Gale, N.H., Stos-Gale, Z.A., Gilmore, G.R., 1985. Alloy Types and Copper Sources of Anatolian Copper Alloy Artifacts. Anatolian Studies 35, 143–173. https://doi.org/10.2307/3642880

Giumlia-Mair, A., 2001. Technical studies on the Roman copper-based finds from Emona. Berliner Beiträge zur Archäometrie 18, 5–42.

Istenič, J., Šmit, Ž., 2007. The beginning of the use of brass in Europe with particular reference to the southeastern Alpine region, in: Metals and Mines: Studies in Archaeometallurgy. La Niece, Susan; Hook, Duncan R.; Craddock, P. T., London, pp. 140–147.

Newbury, B.D., Notis, M.R., Newbury, D.E., 2005. Revisiting the zinc composition limit of cementation brass. Historical metallurgy 39, 75–81.

Omero Minore, 1925. Inni minori - Ad Afrodite, in: Omero Minore. Inni, Batracomiomachia, Epigrammi, Margite. Nicola Zanichelli, Bologna.

Platone, 2001. Crizia, in: Tutti Gli Scritti. A Cura Di Giovanni Reale, Il Pensiero Occidentale. Bompiani, Milano, pp. 1418–1433.

Pyatt, F.B., 2001. Copper and Lead Bioaccumulation by Acacia retinoides and Eucalyptus torquata in Sites Contaminated as a Consequence of Extensive Ancient Mining Activities in Cyprus. Ecotoxicology and Environmental Safety 50, 60–64. https://doi.org/10.1006/eesa.2001.2087

Rehren, T., 1999. Small Size, Large Scale Roman Brass Production in Germania Inferior. Journal of Archaeological Science 26, 1083–1087. https://doi.org/10.1006/jasc.1999.0402

Smekalova, T.N., 2009. The earliest application of brass and “pure” copper in the Hellenistic coinages of Asia Minor and the northern Black Sea coast. Mithridates VI and the Pontic Kingdom 233–48.

Šmit, Ž., Istenič, J., Gerdun, V., Milić, Z., Mladenovič, A., 2005. Archaeometric analysis of Alesia group brooches from sites in Slovenia, in: Slovenska Akademija Znanosti in Umetnosti.

Thornton, C.P., 2007. Of brass and bronze in prehistoric southwest Asia, in: Metals and Mines: Studies in Archaeometallurgy. La Niece, Susan; Hook, Duncan R.; Craddock, P. T., London.

Tylecote, R.F., 1992. A history of metallurgy, 2nd edition. ed, Matsci Series. Institute of Materials.

Chapter 2 - Microstructure and chemical composition of Roman orichalcum coins emitted after the monetary reform of *Augustus* (23 B.C.)

Abstract

A collection of ancient Roman orichalcum coins, *i.e.*, a copper-zinc alloy, minted under the reigns from *Caesar* to *Domitianus*, have been characterised using scanning electron microscopy (SEM-EDS) and electron microprobe analysis (EMPA). We studied, for the first time, coins emitted by Romans after the reforms of *Augustus* (23 B.C.) and *Nero* (63-64 A.D). These coins, consisting of *asses*, *sestertii*, *dupondii* and *semisses*, were analysed using non- and invasive analysis, aiming to explore microstructure, corrosive process and to acquire quantitative chemical analysis. The results revealed that the coins are characterized by porous external layer, which are affected by dezincification and decuprification process. As pictured by the X-ray maps, the elemental distribution of Cu and Zn shows pattern of depletion that in some cases penetrate in deep up to 1mm. The composition of the un-corroded nucleus is a Cu-Zn alloy containing up to 30% of Zn, typical of coins produced *via* cementation process.

2.1 Introduction

The term *Orichalcum* is a classical ancient word used to describe a Cu-Zn-based alloy with a discrete percentage of Zn (5-28%) (Caley, 1964; Craddock, 1978), and similar in appearance to the modern brass. Higher in value than the bronze, this alloy was melted in the form of ingots (Caponetti et al., 2017) and then used to obtain different kind of objects both in the ancient (Ashkenazi et al., 2015; Barrena et al., 2008; Martini et al., 2013) and modern times (Ashkenazi et al., 2016).

Orichalcum was rarely used for coinage in the Hellenistic world (Smekalova, 2009) and was experimentally used by Romans under the reigns of *Caesar* and *Marcus Antonius*.

The scope of the monetary reform of *Augustus* (23 B.C.) was reducing the disorder of the Republican Roman coinage, introducing *sestertii* and *dupondii* in Cu-Zn alloy, rather than silver and bronze. Lately, a new monetary reform was made by *Nero* during the 63-64 A.D., introducing *asses*, *semisses* and *quadrantes* in orichalcum (Amela Valverde, 2004; Catalli, 2003).

The *cementation* process, used to produce the Cu-Zn alloy, was improved and developed by ancient Romans for coinage and production of different kind of artefacts (Bayley, 1998; Bourgarit and Bauchau, 2010; Caley, 1964; Craddock, 1978). This process consisted of using crucibles with specific size and shape to reach thermodynamic requirements for orichalcum production. The diffusion of the vapours of zinc into the copper melt produced a Cu-Zn based alloy with a maximum content of Zn near 30%. The maximum content of zinc present in orichalcum was mainly controlled by temperature, partial pressure of Zn_{vapour} and the redox conditions (Bayley, 1998). The transformation of zinc oxide into metal required (strongly) reducing conditions, with a minimum temperature of about 900°C. This temperature threshold represents the boiling point of zinc, necessary to produce the vapour phase of zinc (Craddock, 1978; Rehren, 1999). The re-oxidation process and the suitable partial pressure of zinc were provided during *cementation* process by the use of closed crucibles (Bayley and Rehren, 2007; Rehren, 1999).

Similar processes and similar techniques of that of Roman *cementation* were applied and diffused in Middle East (Ashkenazi et al., 2015), India (Craddock et al., 1998),

China (Luo et al., 2016; Zhou et al., 2014), Northern Europe (Bayley, 1998; Dungworth, 1997; Rehren, 1999).

The corrosion of orichalcum coins as well as that of archaeological artefacts is one of the most important problems linked to the conservation and the preservation of Cultural Heritage materials (Ashkenazi et al., 2016, 2015; Barrena et al., 2008; Chiavari et al., 2015; Papadopoulou et al., 2016).

The corrosion of orichalcum is associated with dezincification and decuprification processes (Campanella et al., 2009; Marshakov, 2005; Mattsson, 1980), which can occur for several micron in depth; therefore to evaluate the degree of corrosion it is necessary to analyse cross section of samples "from rim-core-to-rim" (Corsi et al., 2016; Doménech-Carbó et al., 2018).

A very limited number of studies about orichalcum coins (Barrena et al., 2008; Marshakov, 2005; Mattsson, 1980; Papadopoulou et al., 2016) and their corrosion are reported and, above all, these contributions are based on the use of qualitative data or semi-quantitative data on dezincification process.

Nowadays, the most common techniques applied to investigate ancient alloys are Scanning Electron Microscope (Barrena et al., 2008; Calliari et al., 1999; Giumlia-Mair, 2005) and X-Ray Fluorescence (Campanella et al., 2009; Scuotto et al., 2014).

A multi-analytical approach (Di Fazio et al., 2019; Fabrizi et al., 2019) based on μRaman (Ospitali et al., 2012), X-Ray Diffraction, X-ray Photoelectron Spectroscopy (Mezzi et al., 2014) or micro-PIXE (Ager et al., 2013) was applied to investigate the external layers of metal object. Electrochemical analyses as Voltammetry of Immobilized Micro Particle and Electrochemical Impedance Spectroscopy (Cepriá et al., 2001; Di Turo et al., 2018, 2017; Di Turo et al., 2018; Doménech-Carbó et al., 2017a, 2017b) are also used to explore the state of conservation of the patina and to identify the corrosion products.

Some authors applied superficial techniques to investigate both corroded and uncorroded alloy composing samples (Vadrucci et al., 2019). However, the error related to major and minor elements is too high to help answer to archaeological issues.

Nowadays, the most suitable way to investigate the depth of the dezincification process is to analyse cross sections obtained from samples in study (with the authorisation of the owners of the coins). Destructive analysis should be preferred, when possible, to evaluate the "real" composition of orichalcum, because the small amount of

sample removed from the patina of the coins could not be representative of uncorroded alloy (Caley, 1964). Cross-section analysis allows comparing the real quantity of major elements, which compose orichalcum produced in different ages and, thus, giving information about the development of the *cementation* process during the Roman Era.

Recently, EMPA technique was used obtaining quantitative chemical analysis of Roman alloys used for coinage (Doménech-Carbó et al., 2018).

The aim of this study is to investigate the composition of the orichalcum coins in the un-corroded nucleus and the corrosion phenomena that affected these coins, acquiring qualitative and quantitative chemical data from the external layers to the unaltered core.

We use SEM and EMP analyses to reconstruct the nature of the original alloy and to explore the mechanisms which induced corrosion (Barrena et al., 2008). The patterns of corrosion are explored using SEM-EDS and X-ray imaging of the elements of the alloy. In addition, a deep investigation of the microstructure is made.

A set of 13 Roman orichalcum coins (Figure 1 and Table 1) were selected for this study from about 60 coins from *Private Collections*. Numismatic examination, considering the weight, the size, the legend and the engraved type of each coin (Crawford, 1974; Sutherland, 1984), revealed that they are *asses*, *sestertii*, *dupondii* and *semisses* minted from *Julius Caesar* to *Domitianus*. The majority of coins were minted after the two important monetary reform of Augustus (23 B.C.) and Nero (63-64 A.D).

Three samples turned out to be interesting cases of study: the two *asses* coined by *Caligula* and *Claudius* before the introduction of *asses* in orichalcum with the *Nero* reform, and the *sestertius* coined by *Tiberius* with a Cu-based alloy, contrary to historical information that describes *Tiberius sestertii* as denominations in orichalcum. Indeed, one of the false certainty of the numismatists is the belief that orichalcum was used by *Mithridates VI* (120-96 B.C.) for a short time of his coinage (Smekalova, 2009), lately experimental emissions by *Caesar* and *Marcus Antonio* occurs. Finally , under the Julio-Claudian dynasty (from *Augustus* to *Nero*), a limited number of denominations (*sestertii, dupondii* and under *Nero* also *semisses* and *quadrantes*) (Barello, 2006) were emitted in orichalcum.

This research attempts to fill the scientific gap existing in the Roman orichalcum coinage, contributing to characterize this ancient alloy, to better understand the

dezincification process and to highlight possible differences among samples minted in different years.

Figure 1 Orichalcum coins emitted in different period of Roman Era, representative of different denomination, from private collections. Numismatic information is reported in Table1.

Sample	Value (denomination)	Authorithy	Emission authority	Year	Mint	Numismatic reference
A1	As	-	Q. Oppius	88 B.C.	Laodicea (Turkey)	RRC 550/1-2
A2	As	G. Iulius Caesar (100 B.C.-44 B.C.)	C. Clovius	45 B.C.	Uncertain	RRC 476/1-2
A3	Dupondius	Augustus (63 B.C. -14 A.D.)	C. Cassius Celer	16 B.C.	Rome	RIC I, 2 Augustus 375
5#	Sestertius	Tiberius (42 B.C.-37 A.D.)	-	22-23 A.D.	Rome	RIC I, 2 Tiberius 42
6#	Sestertius	Tiberius (42 B.C.-37 A.D.)	-	21-22	Rome	RIC I, 2 Tiberius 48 var.
B4	Dupondius	Caligula (12-41 A.D.)	-	37-41 A.D.	Rome	RIC I, 2 Gaius/Caligula 56
C9	As	Caligula (12-41 A.D.)	-	37-38 A.D.	Rome	RIC I, 2 Gaius/Caligula 35
A9	As	Claudius (10-54 A.D.)	-	41-50 A.D.	Rome	RIC I, 2 Claudius 100
10#	Sestertius	Claudius (10-54 A.D.)	-	41-50 A.D.	Rome	RIC I, 2 Claudius 99 (?)
A	Sestertius	Claudius (10-54 A.D.)		50-54 A.D.	Rome	RIC I, 2 Claudius 112
B5	Sestertius	Claudius (10-54 A.D.)	-	50-54 A.D.	Rome	RIC I, 2 Claudius 115
B14	Semis	Nero (37-68 A.D.)	-	62-68 A.D.	Rome	RIC I, 2 Nero 78
20#	Sestertius	Domitianus (51-96 A.D.)	-	-	-	-

Table 1 Numismatic characterization of the coins. Samples highlighted in grey are considered exotic samples, because minted with a different alloy compared to the rules of the monetary reform of Augustus (23 B.C.).

2.2 Methods

All the information on samples, concerning year and place of coinage, emission authority and numismatic references, is reported in Table1.

Preliminarily, qualitative elemental analyses on the patinas were carried out by energy-dispersive X-ray fluorescence spectroscopy (EDXRF) (Department of Basic and Applied Sciences for Engineering, Sapienza University of Rome, Italy). The spectrometer

consists of an X-ray generator (Amptek MiniX) with an anode target of rhodium and a beryllium window of 127 μm of thickness. The detector is a Peltier cooled silicon drift with integrated amplifier and multi-channel analyzer (Amptek 123-SDD). The detector has a surface of 25 mm^2, a thickness of 450 μm, a beryllium window of 12.5 μm of thickness and its energy resolution is 140 eV, full width half maximum at 5.9 keV. The incident and the revealed beams form an angle of 45° with respect to the surface of the sample. The analysed surface is distant 3 cm from the X-ray generator anode and 3.5 cm from the detector surface. The X-ray generator was equipped with a 2 mm diameter collimator and was powered with an accelerating potential difference of 35 kV and an electronic current of 15 μA. For each sample, three measures were obtained, with an acquisition time of 200 s each.

SEM investigation on cross section from rim to core of samples was performed using a FEI-Quanta 400 (SEM-EDS) instrument, operating at 30 kV, equipped with X-ray energy-dispersive spectroscopy (Department of Earth Sciences, Sapienza University of Rome, Italy). X-ray maps and SE/BSE imaging were carried out to investigate microstructure of the alloy, to estimate the depth of the corrosion and the elemental distribution from the external rim to core.

EMPA data for quantitative chemical analyses were performed using a Cameca SX50 electron microprobe equipped with five wavelength-dispersive spectrometers (CNR–IGAG, Rome, c/o Department of Earth Sciences, Sapienza University of Rome). The operating conditions were: accelerating voltage 15 kV, beam current 15 nA. Element peaks and background were measured with counting times of 20 and 10s respectively. Metallic Cu and metallic Zn were used respectively as a reference standard for Cu and Zn (LIF), galena for Pb (PET), cassiterite for Sn (PET), metallic Ni and metallic Co respectively for Ni and Co (LIF), synthetic GaAs for As (TAP), rhodonite and metallic Mn for Mn (PET), olivine and synthetic magnetite for Fe (LIF). Matrix corrections were calculated by the PAP method (Pouchou and Pichior, 1985), with software supplied by Microbeams Services. The detection limits under the specified working condition vary from 0.05 to 0.1 wt% with standard deviations from 0.02 to 0.04 wt%. The analytical error was ∼1% rel. for the major elements.

2.3 Results and discussion

2.3.1 XRF investigation for preliminary discrimination of the coins

A preliminary XRF analysis allows confirming that the majority of samples are in orichalcum; although those affected by important dezincification process can be erroneously consider Cu-based alloys. This investigation is useful to test the presence of Zn in the surfaces even at low percentage, avoiding unnecessary cutting of the sample that are not in orichalcum. Indeed, deep corroded orichalcum coins are similar in appearance to that in bronze alloy.

Despite numismatic references, the screening by XRF on orichalcum *sestertius*, minted under *Tiberius*, did not reveal the presence of zinc (sample 6#, RIC I, 2 48 var.). In addition, two *asses*, theoretically in bronze and minted during *Caligula* and *Claudius* empires, seemed also to be composed of orichalcum (sample C9, RIC I, 2 Caligula 35, sample A9, RIC I, 2 48)(Sutherland, 1984).

The surface analysis by XRF revealed the presence of Cu and Zn as two main alloy components, followed by Fe and Pb. Tin is present in all samples, with higher peaks particularly in A2, A and B14 samples than others. Chlorine occurs in all samples (Fig. 1S), but in low amounts as highlighted by the low-intensity of its characteristic peaks. Exogenous elements, such as Ca, S, Si, Al, P and Mn are also present (Papadopoulou et al., 2016) and represent a contaminants from soils through porosity of the external layer.

2.3.2 SEM investigation of the microstructure, qualitative chemical composition and elemental distribution

The results on cross-sections of all the coins allowed studying microstructure and compositional variations along cross section of the coins. The microstructure of the alloy presents (SE image at high magnification) the typical α grains structure, clearly visible near the external rim of the sample A3 (Fig. 2b). This is the result of an efficient casting-cooling practice, suggesting a well-controlled *cementation* process (Scott, 1991). The grains size varies from ~50µm to ~200µm, suggesting a non-rapid cooling speed. Moreover, some grains present deformed borders with thin strain lines inside (Fig. 2a, sample B4 and Fig.

2b, sample A3), due to heavy cold-working, which causes of the slip of crystal planes with the result of a series of parallel movements that produced fine lines (Giardino, 1998; Scott, 1991). In addition, the twin lines do not present further deformation, suggesting that coins were struck only once. The dendritic structures are not observed.

We present and discuss here in detail the results of samples 5# and B14 (Fig. 2c,d), from the external corroded layers to the inner core, having high and low degree of corrosion, respectively. In addition, the chemical composition of the unaltered area gives information about the ratio of the two main metals in the alloy.

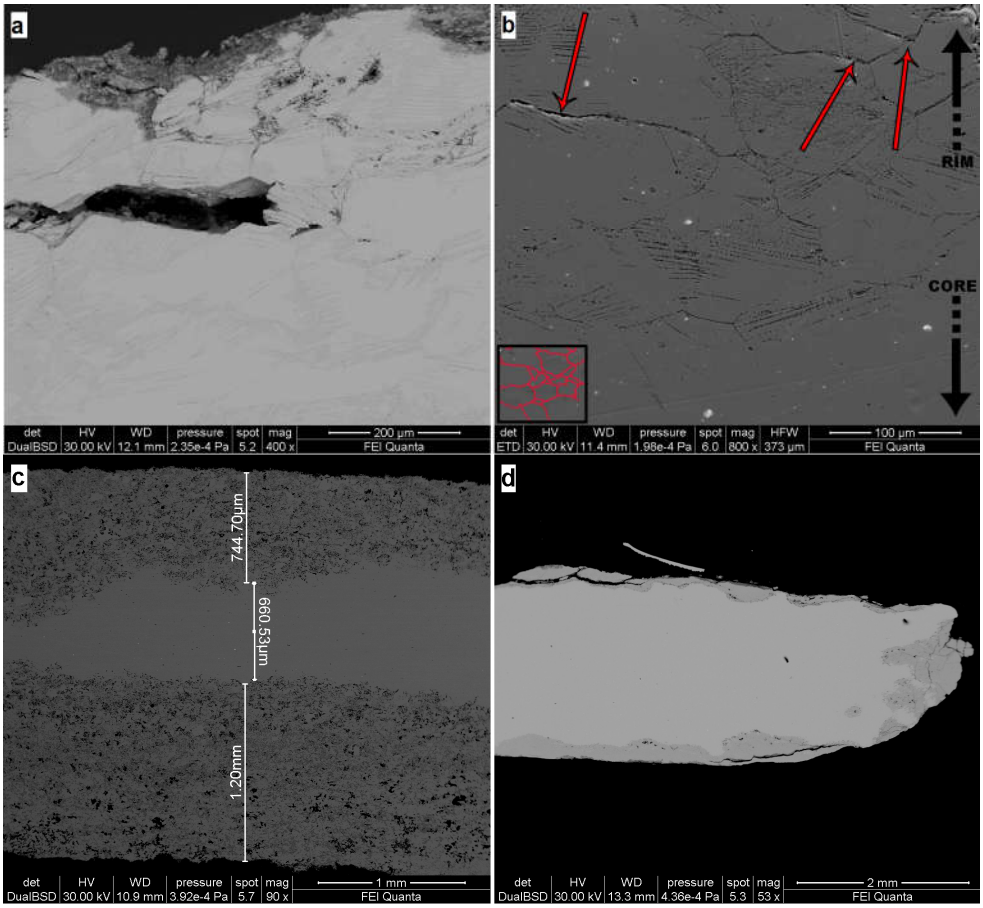

Figure 2 BSE images of coins B4(a), 5#(c) and B14(d) and SE image of coin A3(b). The α-grains structure and the strain lines are evident in (a) and (b). The process of dezincification is showed in (c) and (d), reaching 1.2 mm as the maximum depth of corrosion (c). The red arrows in (b) indicate the trans-granular stress corrosion.

The corroded patina has an irregular thickness with different degree of dezincification, followed by high porosity in the external areas. Sample B14 (Fig. 2d) has two different layers of patina, *i.e.,* the external one (darker grey) has a thickness of few

microns with partial detachments from the sample; the second layer (medium grey) is more coherent with the un-corroded core (lighter grey). On the contrary, the patina of the sample 5# (Fig. 2c) has one layer with an irregular surface in shape. In this sample an important dezincification process occurs, extending up to 1.2 mm in depth. The corrosion proceeds from the rim to the inner core with micro-areas of selective corrosion (Fig. 3, BSE image), driven by grain boundaries of the α-grain structure (Barrena et al., 2008) of the alloy. This selective corrosion is evident in sample 5# (Figure 3), where the content of Zn in corroded micro-domains (darker grey) is below the 20%; whereas in the lighter grey micro-domains Zn content is similar to that of un-corroded nucleus (Table 2). The selective dealloying can be attribute to the trans-granular stress corrosion, usually observed in alloys with content of Zn between 20% and 30% (Sieradzki et al., 1987) and can be clearly observed at the contact of the border zones of the sample A3 (Figure 2b, red arrows). With the evolution of the dezincification process in the external layer is formed a sponge-type structure, typical of brass with low content of Sn, as observed by

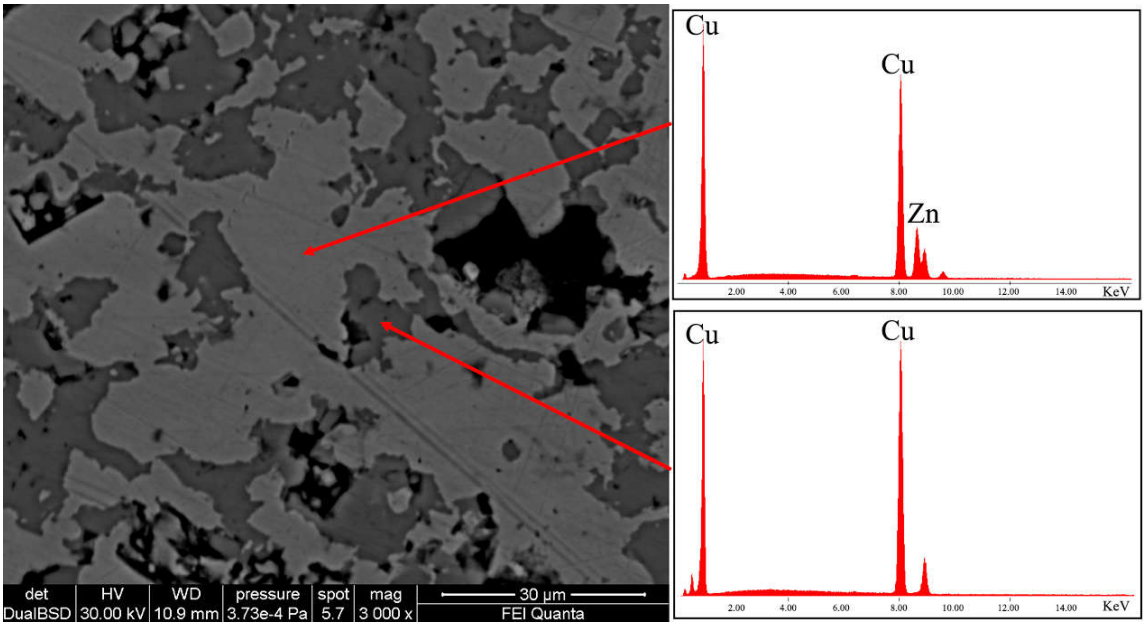

Figure 3 BSE image of the external patina of sample 5# in cross section. ESD spectrum acquired on the lighter area shows a Cu-Zn alloy and that of the darker areas shows only Cu, due to the loss of Zn

Constantinides et al.(2002) in standard sample representative of archaeological brass. Moreover, in the most corroded areas of this layer porous microstructure was found as reported also in previous studies (Carter et al., 1978; Marshakov, 2005) mainly made by copper oxides.

Element (w.t. %)	Upper corroded layer		Un-corroded core		Lower corroded layer	
	Darker grey	Lighter grey	Upper point	Lower point	Darker grey	Lighter grey
Cu	91.78	86.41	77.17	77.28	99.05	93.63
Zn	6.98	12.42	23.49	23.38	0.60	5.42

Table 2 Quantitative EMP analyses of major element of the sample 5#. Data of darker and lighter grey areas are referred to BSE image of Figure 4

In addition, qualitative EDS analyses (Fig. 3, EDS spectra) were carried out to evaluate the chemical composition of the unaltered core of the coins. EDS spectra confirmed Cu and Zn as two major elements composing the alloy. Lead is present in samples A1, A2, B5 and 20#, whereas Sn in samples A3, 20#, occurring these elements as minor and/or trace. Iron occurs in A1, A2, A, B4, 5#, 20#.

X-ray maps of the elements composing the alloy provide information about their distribution along rim-core-rim cross-sections. The maps of samples 5# and B5 (Fig. 4 and Fig. 5) illustrate two different degrees of dezincification, revealed studying the whole coin set: a high level of corrosion, for example in sample #5 (Fig. 4) and a medium level of corrosion, as in sample B5 (Fig. 5). The core of almost all the samples, as shown in the X-ray maps (Fig. 4 and Fig.5), presents a homogeneous distribution of Cu, Zn and, where present, also of Sn. These patterns indicate an expertise in *cementation* process by Romans and a well-controlled procedure during the melting-cooling phase of the alloys in the Roman mint, with a diffusion of Zn at nanoscale level along with the absence of micro-domains of Cu and Zn. Lead, when present in the alloy, forms droplets of different size throughout the coin, due to the low solubility of these two metallic elements, which at low temperature do not give solid solution (Dungworth, 1997). The homogeneous presence of Fe (Fig. 4) suggests the use of chalcopyrite rich-ore for the extraction of Cu. However, the superficial Fe-enrichment can be explained with the contribution of exogenous Fe from the soils. The occurrence of Pb suggests the use of raw materials composed of a mix of base-metals, such as chalcopyrite, galena and sphalerite or the use of calamine from carbonate-hosted Zn(Pb) ore deposits (Boni et al., 2003). As previously

revealed by XRF analysis, the occurrence of exogenous Cl probably induced corrosion processes, producing pitting on the surface of the coins, due to the high pitting potential of the Cu-Zn alloy attributed to the presence of Cu_2O and ZnO on the coins' patina (Alfantazi et al., 2009).

The rim of all the coins, as showed in the X-ray maps (Fig. 4 and Fig. 5), presents evidence of dezincification process, involving Cu enrichment in the external surfaces.

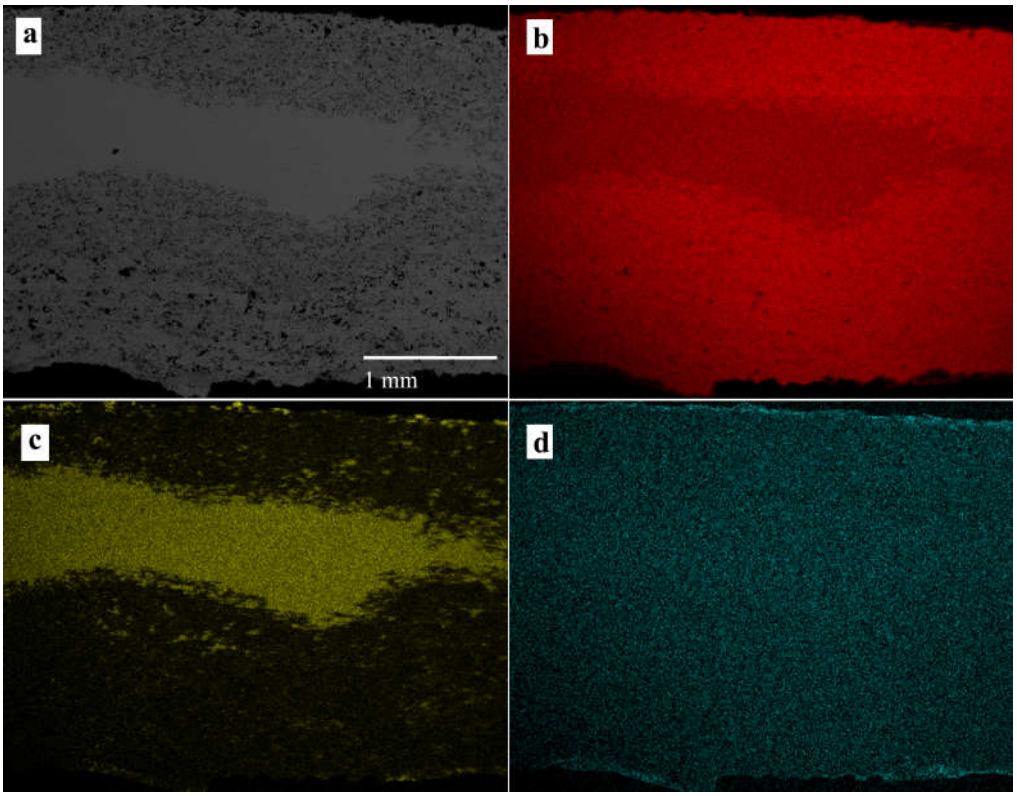

Figure 4 BSE image of sample 5# (a) and X-ray maps of Cu (b), Zn (c) and Fe (d).

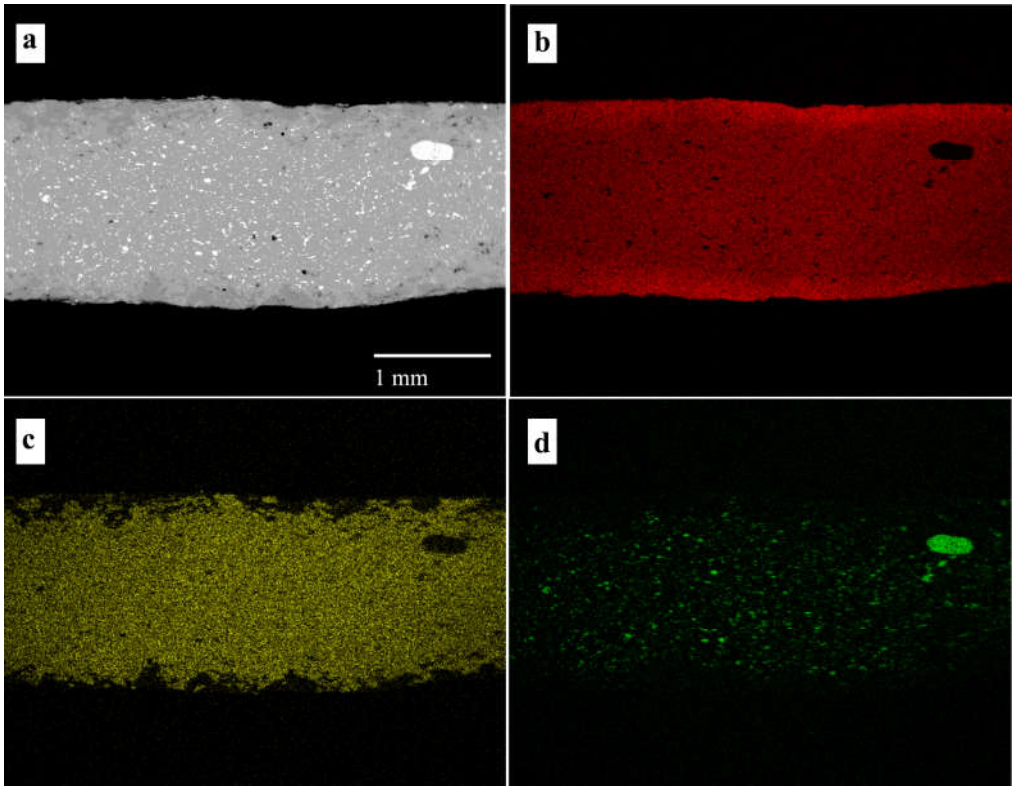

Figure 5 BSE image of sample B5 (a) and X-ray maps of Cu (b), Zn (c) and Pb (d).

2.3.3 SEM investigation of the exotic samples

The three exotic samples, *asses* C9, *asses* A9 and *sestertius* 6#, were also investigated using SEM technique.

As other orichalcum samples, C9 presents a corroded patina extended up to ~400µm in depth, with a medium degree of porosity (Fig. 6a). Also in this case, the corroded area is characterized by micro-domains with different amount of Zn, due to a selective de-alloying. However, the distribution of the corroded micro-domains follows a banded structure (Fig. 6a,b) in which high dezinced areas (darker grey) are alternated to low dezincificated areas (lighter grey). Qualitative EDS analysis confirms the presence of the corroded bands if compared to the one of the uncorroded area. Indeed, the unaltered alloy presents the typical Cu-Zn composition of the orichalcum (Fig. 6d, EDS spectrum corresponding to point 1 in Fig. 6b), whereas the corroded bands are Zn depleted (Fig. 6e,h EDS spectra corresponding respectively to points 2 and 4 in Fig. 6b) and the bands

with a low degree of dezincification (Fig. 6b, point 3) present an intermediate composition between the unaltered alloy and the corroded areas (Fig. 6g EDS spectrum).

Sample A9 presents a remarkable detachment of the patina from the sample (Fig. 6c). The patina is composed of two different layers, where the external one presents a higher degree of corrosion than the inner layer. EDS analysis shows the presence of exogenous elements, such as C, O, Al, Si, Ca, P, S, Ti and Fe as contaminants from soils, on the external surface and inside the empty space derived from the detachment of the patina (Fig. 6i, EDS spectrum corresponding to point 2 in Fig. 6c). The presence of Zn showed by EDS spectrum of the inner layer (Fig. 6f, EDS spectrum corresponding to point 1 in Fig. 6c), suggests a lower degree of corrosion, and a less presence of contaminants elements, probably due to the protective effect induced by the outer passive layer.

Also Cl occurs in both the corroded layers of the patina (Fig 6f,i), inducing the corrosion process and in turn the detachment of the layers from the sample.

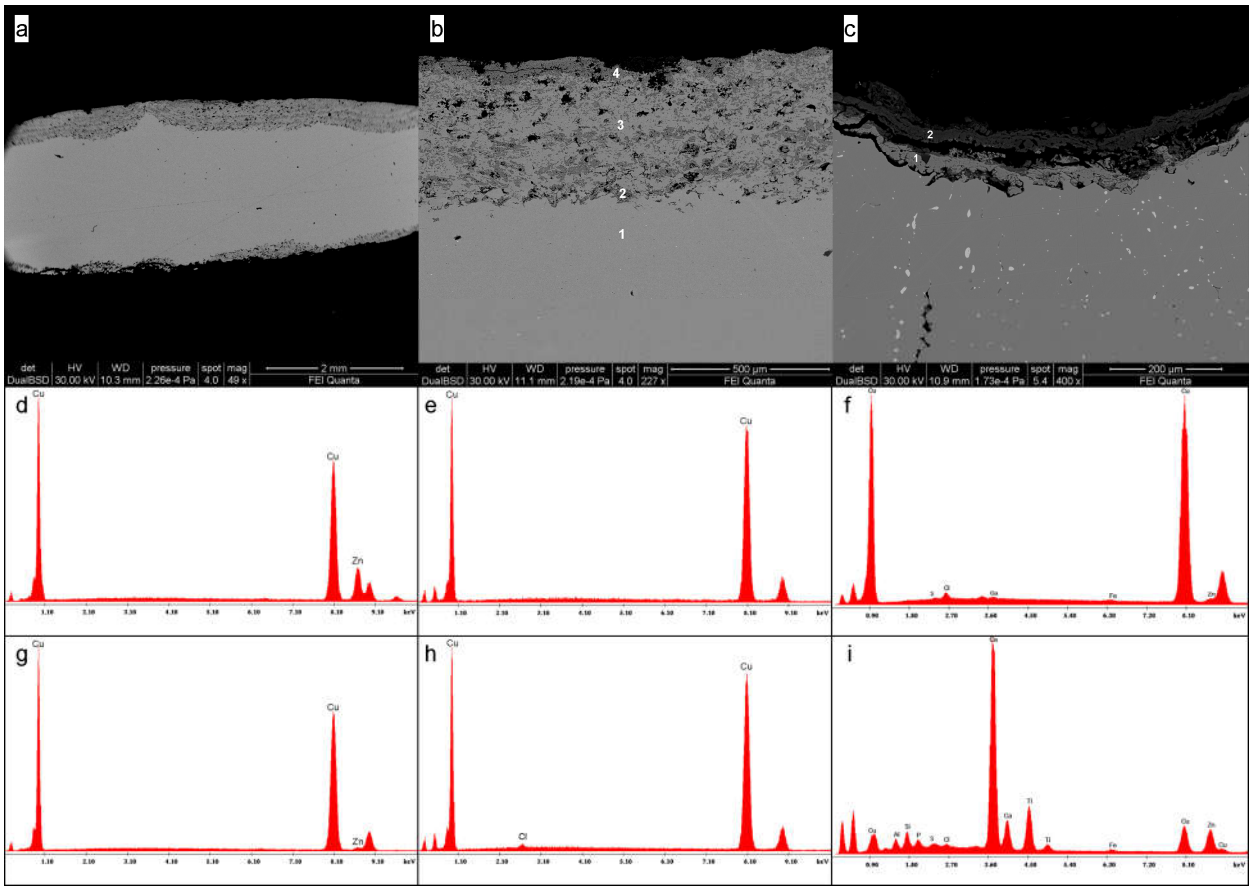

Figure 6 BSE images of exotic samples C9 (**a**,**b**) and A9 (**c**). The EDS spectra of sample C9 in points 1, 2, 3 and 4 (**d**–**h**) were acquired in spot analyses as highlighted in (**b**). The EDS spectra of sample A9 were acquired in points 1 and 2 (**f**,**i**) as highlighted in (**c**).

Sample 6# is one of the two *sestertii* minted during the reign of *Tiberius* here studied (the other one is sample 5#). The alloy of this sample is a Cu-Sn-based alloy (bronze), contrary to the rules of the monetary reform of Augustus (23 B.C.), and presents a homogeneous pattern through the section (rim-core-rim analysis with SEM-EDS). The Cu depleted patina is extended up to ~120 µm in depth and results particularly corroded in the intergranular zone. Chlorine is present in the areas where Cu occurs, and an high porosity characterizes the patina.

2.3.4 EMP analysis of the un-corroded nucleus

EMP analysis of the un-corroded nucleus allows obtaining quantitative chemical compositions of the coins and along with SEM imaging and X-ray maps permits to reconstruct the dezincification and decuprification pattern through the section (rim-core-to-rim). This analysis was necessary to determinate the composition of the orichalcum alloy without the influence of the corroded external surfaces and to highlight differences among alloys casted under different Emperors.

Samples with a low degree of corrosion show homogeneous distribution of Cu% and Zn% throughout the section (*i.e.*, sample A), whereas in the corroded samples the percentage of Zn varies from 1.33% to 23.49% (sample 5#, Fig. 7a). The exotic coin C9 presents trend of values of the two main elements, from one rim to the other, comparable to samples with high degree of corrosion (Fig. 7c). Indeed, the first 4 points of measurements (400µm ca.) have 98-99% of Cu and values of Zn < 0.5%. This confirms the high degree of dezincification of the sample. In the uncorroded core of the coin, the alloy is composed mainly of 77% ca. of Cu and 20% ca. of Zn, whereas in the last 100 µm of the cross section the values of the major elements return to have the values of the other side patina. The exotic coin A9 does not presents compositional variation of Cu and Zn in the whole section, confirming the low degree of corrosion of such sample. Moreover, A9 is composed of the alloy with the maximum average value of Zn (30.64%) of the whole collection.

Minor and trace elements such as Sn, As and Fe, present homogenous values in un-corroded areas of the alloy (Fig. 7b), whereas Pb is often heterogeneous as in some

samples it occurs as exsolution domains from ~400 microns to ~5 microns resulting in Pb-rich areas (Fig. 5). The low content of Fe and their trend from rim to rim inside the samples can suggest the use of chalcopyrite to extract Cu (Tab. 3).

2.4 Conclusions

EMPA data acquired in the uncorroded core of each coin are compared with the average values of Caley (1955), from this comparison our data show an irregular fluctuation of Cu and Zn through 100 years of minting of orichalcum coins (Fig. 7d). Therefore, the fluctuations of Cu and Zn seem to suggest difficulties in the supply of raw materials as well as not regular control of the *cementation* process to produce orichalcum ingots.

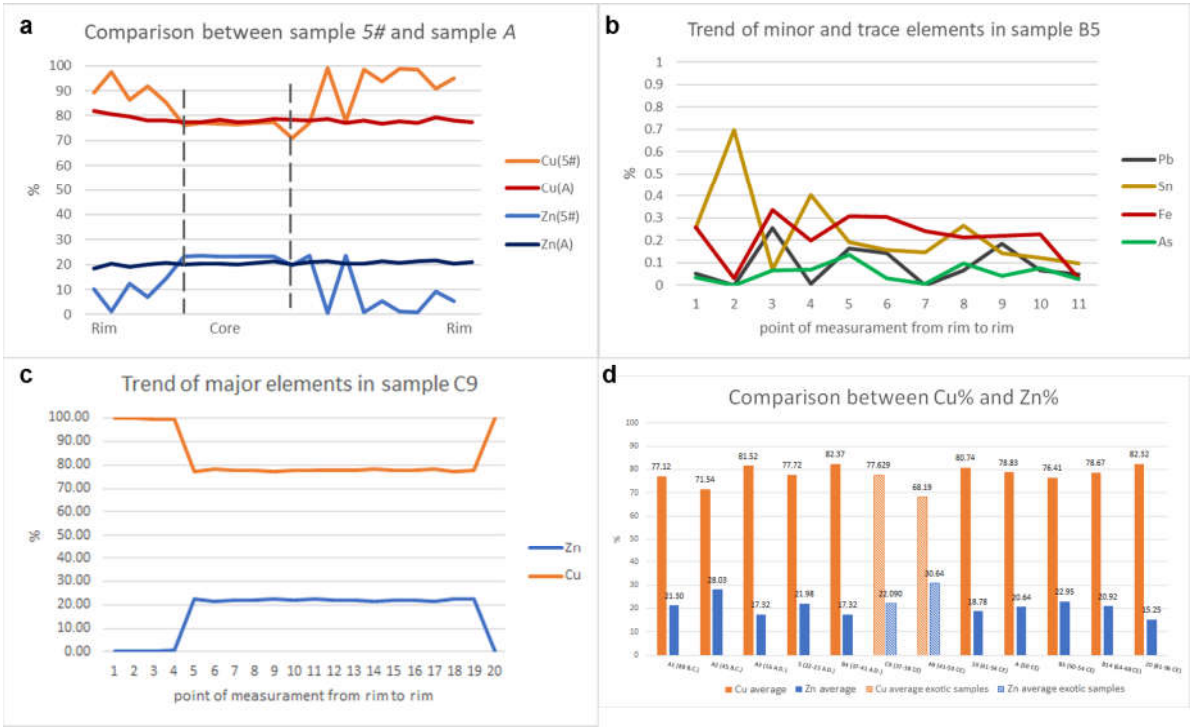

Figure 7 Patterns of EMP analysis on cross section and chronological comparison among samples. (a) The line-graph represent the comparison between the pattern of Cu and Zn in samples 5# and A. Dashed lines describe the area of the uncorroded core of sample 5#; (b) line-graph representing the trend of minor and trace elements (Pb, Sn, Fe and As) in sample B5; (c) line-graph representing the trend of Cu and Zn in sample C9; (d) bar-plot of chronological comparison of the average of major elements in orichalcum coins. The bars with a line pattern represent the average Cu or Zn values of the exotic samples. Data were obtained considering the uncorroded core of each sample, using a minimum of 8 to 22 spot analyses.

Previous studies (Caley, 1955) suggested the possibility to approximately date coins, and other orichalcum objects, comparing the content of Zn in the alloy with that of a series of dated coins. Caley described a decrease of the Zn that corresponded to a regular increase in the average proportion of Sn and Pb, from the oldest to the most recent coins (23 B.C.- 162 A.D.). He justified the chronological decrease of the Zn with the necessity of recasting of metals. However, comparing the private collection analysed in the present study with the results of Caley (1955), the chronology by Cu and Zn percentages results different. Indeed, the average value of Zn, from 88 B.C. to 96 A.D., results extremely variable and fluctuating (Fig. 7d), exceeding sometimes the value of 28% considered as the maximum limit possible in ancient brasses by some authors (Scott, 1991).

Element (w.t.%)	A1			A2			A3			5#			B4			C9		
	Max.	Min.	Avg. n=13	Max.	Min.	Avg. n=15	Max.	Min.	Avg. n=10	Max.	Min.	Avg. n=8	Max.	Min.	Avg. n=8	Max.	Min.	Avg. n=15
Cu	79.42	72.52	77.12	72.01	71.27	71.54	82.12	81.14	81.52	85.30	76.21	77.72	82.87	82.05	82.37	78.30	77.12	77.63
Zn	22.34	19.75	21.30	28.28	27.59	28.03	17.82	16.73	17.32	23.49	14.46	21.98	17.65	16.89	17.32	22.56	21.40	22.09
Pb	5.49	0.00	0.45	0.20	0.00	0.06	0.09	0.00	0.03	0.09	0.00	0.03	0.11	0.00	0.04	0.07	0.00	0.02
Fe	0.47	0.21	0.32	0.29	0.19	0.24	0.40	0.25	0.34	0.17	0.03	0.13	0.11	0.03	0.07	0.21	0.12	0.18
Sn	1.14	0.35	0.73	0.09	0.00	0.06	0.84	0.61	0.72	0.13	0.04	0.09	0.18	0.09	0.02	0.11	0.00	0.02
As	0.09	0.00	0.03	0.09	0.00	0.04	0.04	0.00	0.01	0.06	0.00	0.02	0.10	0.00	0.05	0.06	0.00	0.02

Element (w.t.%)	A9			10#			A			B5			B14			20#		
	Max.	Min.	Avg. n=18	Max.	Min.	Avg. n=14	Max.	Min.	Avg. n=22	Max.	Min.	Avg. n=8	Max.	Min.	Avg. n=9	Max.	Min.	Avg. n=11
Cu	69.75	67.61	68.19	81.19	80.22	80.74	81.01	77.72	78.83	76.98	75.55	76.41	79.00	78.44	78.67	83.47	81.99	82.32
Zn	31.25	29.29	30.64	19.03	18.45	18.78	21.68	18.38	20.64	23.73	22.40	22.95	21.41	20.65	20.92	15.02	15.41	15.25
Pb	0.10	0.00	0.02	0.77	0.00	0.12	0.17	0.00	0.06	0.25	0.00	0.11	0.10	0.00	0.03	0.06	0.00	0.03
Fe	0.05	0.00	0.01	0.24	0.17	0.21	0.38	0.27	0.34	0.34	0.20	0.25	0.31	0.20	0.24	0.32	0.34	0.28
Sn	1.36	0.68	1.08	0.13	0.02	0.06	0.15	0.01	0.07	0.40	0.07	0.19	0.07	0.00	0.04	2.27	1.00	2.03
As	0.10	0.00	0.01	0.10	0.02	0.06	0.05	0.00	0.01	0.13	0.01	0.06	0.15	0.00	0.07	0.05	0.00	0.01

Table 3 Maximum (Max.), minimum (Min.) and average (Avg.) EMP analyses of major, minor and trace

Acknowledgements

Financial support was provided by Sapienza University of Rome (Ateneo funding, 2017-18). PhD grants of the Department of Earth Sciences, Sapienza University of Rome, are gratefully acknowledged. The authors are indebted to *Private Collectors* for generously providing the coins which were sacrificed for the study.

Supplementary material

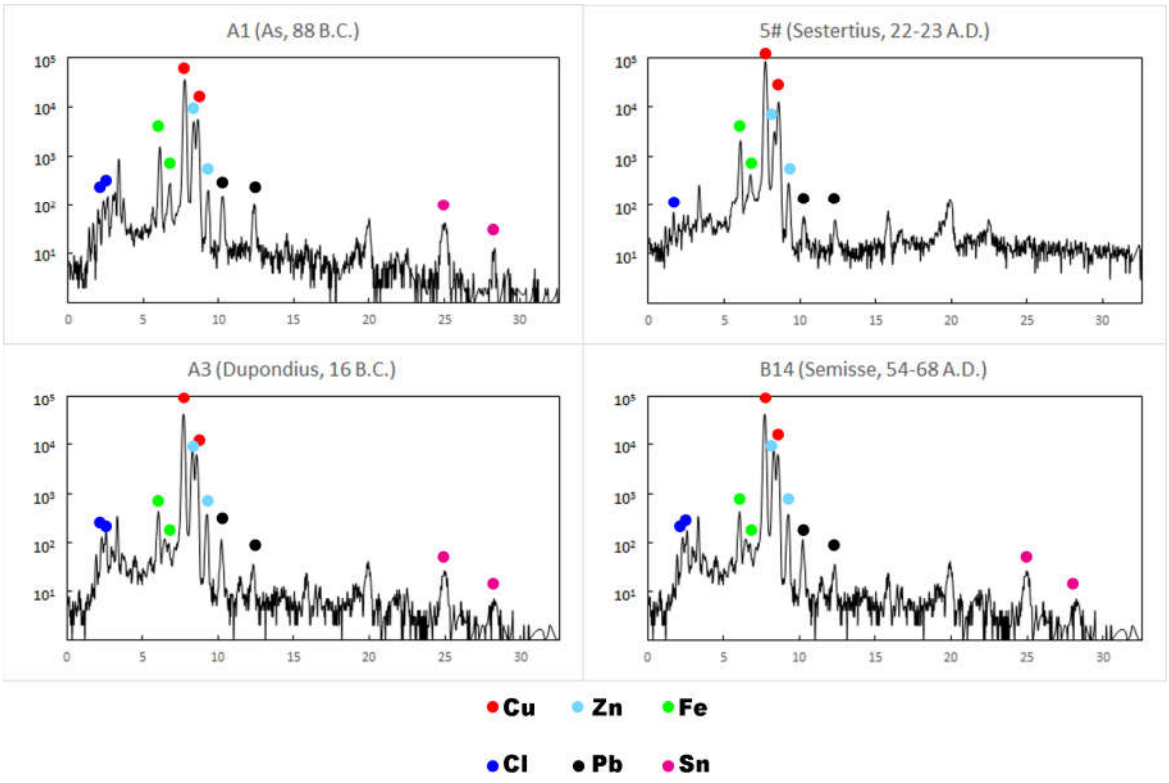

Figure 1S XRF spectra of samples A1, A3, 5# and B14.

References

Ager, F.J., Moreno-Suárez, A.I., Scrivano, S., Ortega-Feliu, I., Gómez-Tubío, B., Respaldiza, M.A., 2013. Silver surface enrichment in ancient coins studied by micro-PIXE. Nuclear Instruments and Methods in Physics Research Section B: Beam Interactions with Materials and Atoms 306, 241–244. https://doi.org/10.1016/j.nimb.2012.12.037

Alfantazi, A.M., Ahmed, T.M., Tromans, D., 2009. Corrosion behavior of copper alloys in chloride media. Materials & Design 30, 2425–2430. https://doi.org/10.1016/j.matdes.2008.10.015

Amela Valverde, L., 2004. RRC 476 y 550, dos emisiones en oricalco de C. Julio César. Nvmisma 248, 7–22.

Ashkenazi, D., Inberg, A., Langgut, D., Hendler, N., Cvikel, D., 2016. Brass–iron couple and brass–iron–wood ternary system of metal objects from the Akko 1 shipwreck (Israel). Corrosion Science 110, 228–241. https://doi.org/10.1016/j.corsci.2016.04.003

Ashkenazi, D., Taxel, I., Tal, O., 2015. Archeometallurgical characterization of Late Roman- and Byzantine-period Samaritan magical objects and jewelry made of copper alloys. Materials Characterization 102, 195–208. https://doi.org/10.1016/j.matchar.2015.01.019

Barello, F., 2006. Archeologia della moneta: produzione e utilizzo nell'antichità. Carocci, Roma.

Barrena, M.I., Gómez de Salazar, J.M., Soria, A., 2008. Corrosion of brass archaeological blinker: Characterisation of natural degradation process. Materials Letters 62, 3944–3946. https://doi.org/10.1016/j.matlet.2008.05.015

Bayley, J., 1998. The production of brass in antiquity with particular reference to Roman Britain, in: 2000 Years of Zinc and Brass, Occasional Paper. P.T. Craddock, British Museum, London.

Bayley, J., Rehren, T., 2007. Towards a functional and typological classification of crucibles, in: Metals and Mines: Studies in Archaeometallurgy. La Niece, Susan; Hook, Duncan R.; Craddock, P. T., London.

Boni, M., Gilg, H.A., Aversa, G., Balassone, G., 2003. The "Calamine" of Southwest Sardinia: Geology, Mineralogy, and Stable Isotope Geochemistry of Supergene Zn Mineralization. Economic Geology 98, 731. https://doi.org/10.2113/gsecongeo.98.4.731

Bourgarit, D., Bauchau, F., 2010. The ancient brass cementation processes revisited by extensive experimental simulation. JOM 62, 27–33. https://doi.org/10.1007/s11837-010-0045-3

Caley, E.R., 1964. Orichalcum and related ancient alloys, Numismatic notes and monograph. American Numismatic Society, New York.

Caley, E.R., 1955. On the existence of chronological variations in the composition of Roman brass. The Ohio journal of science 55, 137–140.

Calliari, I., Magrini, M., Zambon, A., Guerriero, P., Martini, R., 1999. Microstructural and compositional characterization of Roman coins. X-Ray Spectrom. 28, 86–90. https://doi.org/10.1002/(SICI)1097-4539(199903/04)28:2<86::AID-XRS313>3.0.CO;2-B

Campanella, L., Alessandri, O.C., Ferretti, M., Plattner, S.H., 2009. The effect of tin on dezincification of archaeological copper alloys. Corrosion Science 51, 2183–2191. https://doi.org/10.1016/j.corsci.2009.05.047

Caponetti, E., Francesco, A., Martino, D.C., Saladino, M.L., Ridolfi, S., Chirco, G., Berrettoni, M., Conti, P., Bruno, N., Tusa, S., 2017. First discovery of orichalcum ingots from the remains of a 6th century BC shipwreck near gela (Sicily) seabed. Mediterranean Archaeology and Archaeometry 17, 11–18. https://doi.org/10.5281/zenodo.581716

Carter, G.F., Kimiatek, M.H., Klupacs, F.J., Giard, J.-B., 1978. Chemical Compositions of Copper-Based Roman Coins. V. Imitations of Caligula, Claudius and Nero. Revue numismatique 69–88.

Catalli, F., 2003. Numismatica greca e romana. Istituto Poligrafico e Zecca dello Stato, Roma.

Cepriá, G., Aranda, C., Pérez-Arantegui, J., Lacueva, F., Castillo, J.R., 2001. Voltammetry of immobilised microparticles: a powerful analytical technique to study the physical and chemical composition of brass. Journal of Electroanalytical Chemistry 513, 52–58. https://doi.org/10.1016/S0022-0728(01)00599-X

Chiavari, C., Bernardi, E., Balbo, A., Monticelli, C., Raffo, S., Bignozzi, M.C., Martini, C., 2015. Atmospheric corrosion of fire-gilded bronze: corrosion and corrosion protection during accelerated ageing tests. Corrosion Science 100, 435–447. https://doi.org/10.1016/j.corsci.2015.08.013

Constantinides, I., Adriaens, A., Adams, F., 2002. Surface characterization of artificial corrosion layers on copper alloy reference materials. Applied Surface Science 189, 90–101. https://doi.org/10.1016/S0169-4332(02)00005-3

Corsi, J., Grazzi, F., Lo Giudice, A., Re, A., Scherillo, A., Angelici, D., Allegretti, S., Barello, F., 2016. Compositional and microstructural characterization of Celtic silver coins from northern Italy using neutron diffraction analysis. Microchemical Journal 126, 501–508. https://doi.org/10.1016/j.microc.2016.01.006

Craddock, P.T., 1978. The composition of the copper alloys used by the Greek, Etruscan and Roman civilizations. Journal of Archaeological Science 5, 1–16. https://doi.org/10.1016/0305-4403(78)90015-8

Craddock, P.T., Freestone, I., Gurjar, L., Middleton, A., Willies, L., 1998. Zinc in India, in: 2000 Years of Zinc and Brass, Occasional Paper. P.T. Craddock, British Museum, London.

Crawford, M.H., 1974. Roman Republican Coinage. Cambridge University Press.

Di Fazio, M., Di Turo, F., Medeghini, L., Fabrizi, L., Catalli, F., De Vito, C., 2019. New insights on medieval Provisini silver coins by a combination of non-destructive and micro-invasive techniques. Microchemical Journal 144, 309–318. https://doi.org/10.1016/j.microc.2018.09.016

Di Turo, F., Montoya, N., Piquero-Cilla, J., De Vito, C., Coletti, F., Favero, G., Doménech-Carbó, A., 2017. Archaeometric analysis of Roman bronze coins from the Magna Mater temple using solid-state voltammetry and electrochemical impedance spectroscopy. Analytica Chimica Acta 955, 36–47. https://doi.org/10.1016/j.aca.2016.12.007

Di Turo, F., Parra, R., Piquero-Cilla, J., Favero, G., Doménech-Carbó, A., 2018. Crossing VIMP and EIS for studying heterogeneous sets of copper/bronze coins. Journal of Solid State Electrochemistry. https://doi.org/10.1007/s10008-018-04182-5

Di Turo, F., Montoya, N., Piquero-Cilla, J., De Vito, C., Coletti, F., Favero, G., Doménech-Carbó, T.M., Doménech-Carbó, A., 2018. Dating Archaeological Strata in the Magna Mater Temple Using Solid-state Voltammetric Analysis of Leaded

Bronze Coins. Electroanalysis 30, 361–370. https://doi.org/10.1002/elan.201700724

Doménech-Carbó, A., del Hoyo-Meléndez, J.M., Doménech-Carbó, M.T., Piquero-Cilla, J., 2017a. Electrochemical analysis of the first Polish coins using voltammetry of immobilized particles. Microchemical Journal 130, 47–55. https://doi.org/10.1016/j.microc.2016.07.020

Doménech-Carbó, A., Doménech-Carbó, M.T., Álvarez-Romero, C., Montoya, N., Pasíes-Oviedo, T., Buendía, M., 2017b. Electrochemical Characterization of Coinage Techniques the 17th Century: The maravedís Case. Electroanalysis 29, 2008–2018. https://doi.org/10.1002/elan.201700326

Doménech-Carbó, M.T., Di Turo, F., Montoya, N., Catalli, F., Doménech-Carbó, A., De Vito, C., 2018. FIB-FESEM and EMPA results on Antoninianus silver coins for manufacturing and corrosion processes. Scientific Reports 8, 10676. https://doi.org/10.1038/s41598-018-28990-x

Dungworth, D., 1997. Roman Copper Alloys: Analysis of Artefacts from Northern Britain. Journal of Archaeological Science 24, 901–910. https://doi.org/10.1006/jasc.1996.0169

Fabrizi, L., Di Turo, F., Medeghini, L., Di Fazio, M., Catalli, F., De Vito, C., 2019. The application of non-destructive techniques for the study of corrosion patinas of ten Roman silver coins: The case of the medieval Grosso Romanino. Microchemical Journal 145, 419–427. https://doi.org/10.1016/j.microc.2018.10.056

Giardino, C., 1998. I metalli nel mondo antico. Introduzione all'archeometallurgia. Editori Laterza, Bari.

Giumlia-Mair, A., 2005. On surface analysis and archaeometallurgy. Nuclear Instruments and Methods in Physics Research Section B: Beam Interactions with Materials and Atoms 239, 35–43. https://doi.org/10.1016/j.nimb.2005.06.178

Luo, W., Li, D., Mu, D., Bai, J., Xiao, B., 2016. Preliminary study on zinc smelting relics from the Linjiangerdui site in Zhongxian County, Chongqing City, southwest China. Microchemical Journal 127, 133–141. https://doi.org/10.1016/j.microc.2016.02.015

Marshakov, I.K., 2005. Corrosion Resistance and Dezincing of Brasses. Protection of Metals 41, 205–210. https://doi.org/10.1007/s11124-005-0031-2

Martini, C., Chiavari, C., Ospitali, F., Grazzi, F., Scherillo, A., Soffritti, C., Garagnani, G.L., 2013. Investigations on a brass armour: Authentic or forgery? Materials Chemistry and Physics 142, 229–237. https://doi.org/10.1016/j.matchemphys.2013.07.010

Mattsson, E., 1980. Corrosion of Copper and Brass: Practical Experience in relation to Basic Data. British Corrosion Journal 15, 6–13. https://doi.org/10.1179/000705980798318708

Mezzi, A., Riccucci, C., de Caro, T., Angelini, E., Faraldi, F., Grassini, S., Gouda, V.K., 2014. Combined use of SA-XPS, XRD and SEM + EDS for the micro-chemical characterisation of Ag-based archaeological artefacts. Surf. Interface Anal. 46, 801–806. https://doi.org/10.1002/sia.5385

Ospitali, F., Chiavari, C., Martini, C., Bernardi, E., Passarini, F., Robbiola, L., 2012. The characterization of Sn-based corrosion products in ancient bronzes: a Raman approach. J. Raman Spectrosc. 43, 1596–1603. https://doi.org/10.1002/jrs.4037

Papadopoulou, O., Alessandri, O.C., Vassiliou, P., Grassini, S., Angelini, E., Gouda, V., 2016. Soil-induced corrosion of ancient Roman brass - A case study. Materials and Corrosion 67, 160–169. https://doi.org/10.1002/maco.201408115

Pouchou, J., Pichior, F., 1985. “PAP” f(rZ) procedure for improved quantitative analysis, in: Microbeam Analysis. Armstrong J.T. (Ed.), San Francisco, California, pp. 104–106.

Rehren, T., 1999. Small Size, Large Scale Roman Brass Production in Germania Inferior. Journal of Archaeological Science 26, 1083–1087. https://doi.org/10.1006/jasc.1999.0402

Scott, D.A., 1991. Metallography and microstructure of ancient and historic metals. Getty Conservation Institute in association with Archetype Books, [Marina del Rey, CA].

Scuotto, M., Bassi, C., Lezzerini, M., Grifoni, E., Legnaioli, S., Lorenzetti, G., Pagnotta, S., Palleschi, V., 2014. X-ray fluorescence analysis on a group of coins from the ancient roman city of Tridentum (Trento, Italy). X-Ray Spectrom. 43, 370–374. https://doi.org/10.1002/xrs.2567

Sieradzki, K., Kim, J.S., Cole, A.T., Newman, R.C., 1987. The Relationship Between Dealloying and Transgranular Stress-Corrosion Cracking of Cu-Zn and Cu-Al Alloys. Journal of The Electrochemical Society 134, 1635–1639. https://doi.org/10.1149/1.2100726

Smekalova, T.N., 2009. The earliest application of brass and “pure” copper in the Hellenistic coinages of Asia Minor and the northern Black Sea coast. Mithridates VI and the Pontic Kingdom 233–48.

Sutherland, C.H.V., 1984. The Roman Imperial Coinage: From 31 BC to AD 69: with introd. to the mints. Spink, London.

Vadrucci, M., Mazzinghi, A., Gorghinian, A., Picardi, L., Ronsivalle, C., Ruberto, C., Chiari, M., 2019. Analysis of Roman Imperial coins by combined PIXE, HE-PIXE and μ-XRF. Applied Radiation and Isotopes 143, 35–40. https://doi.org/10.1016/j.apradiso.2018.10.016

Zhou, W., Martinón-Torres, M., Chen, J., Li, Y., 2014. Not so efficient, but still distilled: the technology of Qing Dynasty zinc production at Dafengmen, Chongqing, southwest China. Journal of Archaeological Science 43, 278–288. https://doi.org/10.1016/j.jas.2014.01.009

Chapter 3 - Solid-state electrochemical characterization of emissions and authorities producing Roman brass coins

Abstract

The voltammetry of immobilized particles (VIMP) is applied to describe the solid state electrochemistry of brass. This methodology, which involves sampling at the nanogram level, is applied to discriminate mints/authorities producing different Roman monetary emissions covering since the Republic (88 BCE) to Domitianus (55-96 CE). Upon attachment to graphite electrodes in contact with aqueous acetate buffer at pH 4.75, well defined voltammetric responses were obtained centered on Cu- and Zn-localized signals whose intensity can be correlated to EMP data, being sensitive to the contents of Zn (15-30 %wt) and Sn (0.01-1.1 %wt). Voltammetric data, combined with ATR-FTIR and FIB-FESEM/EDS, yield information on the structure of the metal patina and permit to characterize different monetary emissions being able, in the case of Augustus' *sestertii*, to discriminate between the productions from different monetary authorities.

3.1 Introduction

Brass is a binary Cu-Zn alloy widely used for producing coins since the antiquity (Caponetti et al., 2017). The term Orichalcum is a classical ancient word to describe a Cu-based alloy with discrete percentage of Zn (5-28% wt) (Craddock, 1978; Rehren, 1999), similar to the modern brass. Higher in value than the bronze, this alloy was melted in the form of ingots (Caponetti et al., 2017) and then used to obtain different kinds of objects (Barrena et al., 2008; Martini et al., 2013). Orichalcum was rarely exploited to mint coins in the ancient Hellenistic world and, experimentally, was used by *Caesar* and *Marcus Antonius*. During the monetary reform of *Augustus* between 15 BCE and 20-23 CE, there was some uncontrolled emission of *sestertii*, *dupondii* and *semisses*. Orichalcum was regularly used to mint coins, particularly during the monetary reform of *Nero* (63-65 CE) (Catalli, 2003), but this practice decayed at the end of the *Iulio-Claudia* age. The cementation technique was the usual manufacturing procedure (Bourgarit and Bauchau, 2010; Craddock, 1978).

Given the importance of coins as archaeological remains, the characterization of their composition and manufacturing technique are analytical targets of interest usually achieved via chemical and metallographic analysis (Constantinides et al., 2002; Scott, 1991) accompanied by electron microscopy, diffraction, different spectroscopic techniques (Agresti et al., 2016; Carl and Young, 2016; del Hoyo-Meléndez et al., 2015; Ferrer-Eres et al., 2010; Lutterotti et al., 2016; Peris-Vicente et al., 2008) and isotope analysis (Gomes et al., 2016). Direct analysis of the metal requires more or less invasive sampling through cross-sections with the concomitant limitations (Scott, 1994) prompting an increasingly growing interest in techniques that extract archaeometric information from the physico-chemical analysis of the metal patina (Robbiola et al., 1998; Robbiola and Portier, 2006).

The corrosion of brass is a complex problem. Under corrosion, brass usually suffers dezincification, a process which is believed to proceed via a) dissolution of both Cu and Zn followed by Cu re-deposition, or, b) selective dissolution of Zn (Mattsson, 1980). Interestingly, dezincing reduces the corrosion resistance of brass due to the formation of a copper metal layer but, in the absence of dezincing, the accumulation of copper corrosion products enhances the corrosion through an autocatalytic effect (Marshakov,

2005). The presence of low amounts of Sn (and Pb) prevents to some extent the selective corrosion of zinc, as studied in modern (Karpagavalli and Balasubramaniam, 2007; Sohn and Kang, 2002) and archaeological brasses (Campanella et al., 2009). Here, the soil-induced corrosion can produce complicated corrosion patterns (Barrena et al., 2008; Papadopoulou et al., 2016).

In this context, the voltammetry of immobilized particles (VIMP), a solid-state electrochemical methodology developed by Scholz et al. (Doménech-Carbó Antonio et al., 2012; Scholz et al., 2005; Scholz and Meyer, 1998), has been used for the analysis of metals and metal corrosion patinas (Arjmand and Adriaens, 2012; Costa et al., 2009; Doménech-Carbó et al., 2013, 2008; Šatović et al., 2010; Serghini-Idrissi et al., 2005), including brass(Cepriá et al., 2001). The inherent high sensitivity of VIMP, needing amounts of sample at the nanogram level, has prompted its use in the archaeometric domain(Doménech-Carbó, 2010; Doménech-Carbó et al., 2009; Doménech-Carbó Antonio and Doménech-Carbó María Teresa, 2018), in particular for tracing, mapping and dating metals (Doménech-Carbo, 2017; Doménech-Carbó et al., 2014, 2011; Doménech-Carbó and Scholz, 2019).

Studies on metal coins are focused on the determination of the composition and microstructure of the base alloy and the identification of the corrosion products using multi-technique approaches some of which require some destructive sampling (Di Fazio et al., 2019; M. T. Doménech-Carbó et al., 2019; Inberg et al., 2018). In this context, we applied the VIMP methodology in order to acquire archaeometric information based on a minimally invasive (at the nanogram level) sampling on the metal patina. Application to the discrimination of different monetary series was described for silver (Doménech-Carbó et al., 2017a), bronze (Di Turo et al., 2017; Di Turo et al., 2018; A. Doménech-Carbó et al., 2019; Doménech-Carbó et al., 2017b) and copper (Doménech-Carbó et al., 2017c) coins, but no studies on *orichalcum* materials have been done. This is based on the assumption that, under conditions of similar 'corrosion history', subtle differences in the composition and metallographic structure of the coins result in detectable features of the voltammetric response of the corrosion patina. As a result, electrochemical grouping of different sets of coins was obtained without disposal of information on the chemical composition of the metal alloy used in their minting.

The current study was aimed to: i) describe the solid state electrochemistry of *orichalcum*; ii) establish discrimination criteria for characterizing different monetary emissions made of brass; iii) correlate electrochemical with composition data, and iv) test the possible influence of the degree of corrosion. The question to be elucidated is if it is possible to distinguish different mints and/or authorities producing brass coins from the minimally invasive VIMP sampling. The established electrochemical discrimination criteria have been applied to the study of a set of twenty-five Roman brass coins from private collections, minted between 88 BCE (late Republic) and 96 CE (Domitianus Emperor). They include five denominations (*As, Sestertius, Dupondius, Semis* and *Quadrans*) and include three coins without definite ascription, presenting different degree of corrosion, with a non-homogeneous patina. Figure 1 shows the obverse and reverse images of the studied coins.

Figure 1 The orichalcum coins studied in this work. For samples A1, A2, A3, B4, B5, B14, C9, 5, 10, and 20 see Di Fazio et al. [44]. Numismatic and historic information is reported in

A sub-set of 11 coins was submitted to partially destructive sampling to determine the composition by EMP analysis in order to gain more information concerning the corrosion process. Such data have been complemented by attenuated total reflectance – Fourier transform infrared spectroscopy (ATR-FTIR) and focusing ion beam-field emission scanning electron microscopy (FIB-FESEM-EDS) for the characterization of the corrosion layers of the coins.

3.2 Materials and Experimental

3.2.1 Materials

The characteristics of the studied coins from a numismatic point of view are summarized in Table 1. The coins come originally from different burial environments with no documented cleaning. Examination at the optical microscope does not show erosion features denoting sandblasting, nor smoothing associated to intense chemical cleaning. As shown in Figure 1, the obverse and reverse legends are readable, as they allowed a good numismatic examination, identifying in some cases both the reigning authority and the issuers responsible for minting operations (*Tresviri Monetales*).

Sample	Denomination (Authority)	Issuer	Year	Mint	Numismatic ref.	Conservation state
A1	As (-)	Q. Oppius	88 BCE	Laodicea	RRC 550/1-2	xxxxx
A2	As (Julius Caesar)	C. Clovius	45 BCE	Uncertain	RRC 476/1-2	xxxxx
1	As (Julius Caesar)	-	45 BCE	-	-	xxxxx
2	As (Julius Caesar)	-	45 BCE	-	-	xxxxx
A3	Dupondius (Augustus)	C. Cassius Celer	16 BCE	Rome	RIC I Augustus 375	xxxxx
228	Sestertius (Augustus)	C. Gallius Lupercus	16 BCE	Rome	RIC I Augustus 377	xxxxx
213	Sestertius (Augustus)	C. Gallius Lupercus	16 BCE	Rome	RIC I Augustus 377	xxxxx
235	Sestertius (Augustus)	G. Asinio Gallo	16 BCE	Rome	RIC I Augustus 370	xxxxx
236	Sestertius (Augustus)	G. Asinio Gallo	16 BCE	Rome	RIC I Augustus 370	xxxxx

234	Sestertius (Augustus)	Gnaeus Calpurnius Piso	15 BCE	Rome	RIC I Augustus 380	xxxxx
227	Sestertius (Augustus)	L. Naevius Surdinus	15 BCE	Rome	RIC I Augustus 383	xxxxx
226	Sestertius (Augustus)	C. Plotius Rufus	15 BCE	Rome	RIC I Augustus 387	xxxxx
232	Sestertius (Augustus)	C. Plotius Rufus	15 BCE	Rome	RIC I Augustus 387	xxxxx
240	Sestertius (Augustus)	C. Plotius Rufus	15 BCE	Rome	RIC I Augustus 387	xxxxx
5	Sestertius (Tiberius)	-	22-23 CE	Rome	RIC I Tiberius 42	xxxxx
E5	Sestertius (Tiberius)	-	-	-	-	xxxxx
B15	Sestertius (Tiberius)	-	22-23 CE	Rome	RIC I Tiberius 48	xxxxx
B4	Dupondius (Caligula)	-	37-41 CE	Rome	RIC I Gaius/Caligula 56	xxxxx
C9	As (Caligula)	-	37-38 CE	Rome	RIC I Gaius/Caligula 35	xxxxx
A9	As (Claudius)	-	41-50 CE	Rome	RIC I Claudius 100	xxxxx
10	Sestertius (Claudius)	-	41-50 CE	Rome	RIC I Claudius 99 (?)	xxxxx
B5	Sestertius (Claudius)	-	50-54 CE	Rome	RIC I Claudius 115	xxxxx
E6	Quadrans (Claudius)	-	-	-	-	xxxxx
B14	Semis (Nero)	-	62-68 CE	Rome	RIC I, 2 Nero 78	xxxxx
20	Sestertius (Domitianus)	-	-	-	-	xxxxx

Table 1 Historic and numismatic information of the coin samples in this study. The conservation state is provided from visual test.

3.2.2 Instrumentation and experimental methods

ATR-FTIR spectra were obtained to determine the composition of the corrosion products on microsamples of the corrosion layer of the coins using a Vertex 70 Fourier-transform infrared spectrometer with an FR-DTGS (fast recovery deuterated triglycine sulphate) temperature-stabilised coated detector and a MKII Golden Gate ATR accessory.

A total of 32 scans were collected at a resolution of 4 cm^{-1} and the spectra were processed using the OPUS/IR software.

In order to study the structure and elemental composition of the metal patina, FIB-FESEM experiments were carried out with Zeiss (Orsay Physics Kleindiek Oxford Instruments) model Auriga compact equipment. Such experiments permit to perform a square trench of 10 × 10 μm in the coins surface that enabled the characterization of the microtexture and mineral phases in the superficial corrosion layer. For generating the focused beam of Ga ions the operating conditions were voltage, 30 kV and current intensity, 500 μA and 20 nA in the FIB. A voltage of 3 kV was used in the FESEM for photographs. X-ray linescans were performed in the trench operating with an Oxford-X Max X-ray microanalysis system coupled to the FESEM controlled by Aztec software. A voltage of 20 kV and a working distance of 6 -7 mm was used. SEM investigation on cross sections from the corroded rim to the un-corroded core was performed using a FEI-Quanta 400 (SEM-EDS) instrument, operating at 30 kV, equipped with X-ray energy-dispersive spectroscopy (Department of Earth Sciences, Sapienza University of Rome, Italy).

To determine the composition of the metal core of 11 of the studied coins, EMP for quantitative chemical analyses were performed using a Cameca SX50 electron microprobe equipped with five wavelength-dispersive spectrometers (CNR–IGAG, Rome, c/o Department of Earth Sciences, Sapienza University of Rome). The operating conditions were: accelerating voltage 15 kV, beam current 15 nA. Element peaks and background were measured with counting times of 20 and 10s respectively. Metallic Cu and metallic Zn were used respectively as a reference standard for Cu and Zn (LIF), galena for Pb (PET), cassiterite for Sn (PET), metallic Ni and metallic Co respectively for Ni and Co (LIF), synthetic GaAs for As (TAP), rhodonite and metallic Mn for Mn (PET), olivine and synthetic magnetite for Fe (LIF). Matrix corrections were calculated by the PAP method (Pouchou and Pichior, 1985), with software supplied by Microbeams Services. The detection limits under the specified work conditions vary from 0.05 to 0.1 wt% with standard deviations from 0.02 to 0.04 wt%. The analytical error was ≈ 1% rel. for the major elements, and it increases as the concentration decreases up to 10% for trace elements.

Voltammetry of Microparticles were performed at 298 K in a three-electrode cell using a CH I660C device (Cambria Scientific, Llwynhendy, Llanelli UK) using air-saturated

aqueous 0.25 M HAc/NaAc aqueous buffer solution (Panreac) at pH 4.75. A sample-modified graphite bar (Alpino, HB type, 3 mm diameter) was used as a working electrode, the three-electrode arrangement being completed by a platinum wire auxiliary electrode and an Ag/AgCl (3 M NaCl) reference electrode. The analysis of coins was carried out by pressing a graphite bar onto selected spots of the coin surface (regions where no pit corrosion of green products exists) as already described (Di Turo et al., 2017; Di Turo et al., 2018; A. Doménech-Carbó et al., 2019; Doménech-Carbó et al., 2017a, 2017b, 2017c). Depending on the number and extension of such spots 3-5 replicate measurements were performed on each coin. Square wave voltammetry (SWV) was used as a detection mode determining successively the negative- and the positive-going potential scans using as parameters: potential step increment 4 mV; square wave amplitude 25 mV; frequency 5 Hz.

3.3 Results and Discussion

3.3.1 Composition of patina and corrosion products

The study involves balancing the information on the chemical composition of the coin's patina, to be acquired from ATR-FTIR spectra, the elemental composition of the base alloy provided by EMP analysis and the structure and composition of the subsurface corrosion layers from FIB-FESEM in order to combine it with VIMP analysis.

The ATR-FTIR measurements were acquired on the patinas of a limited number of coins (*i.e.*, A1, A2, A3, A9, 1, 2, 5, 10, B4, B15, C9, E5, E6, 213, 226, 232), due to the low quantity of collectable material. Figure 2 shows the IR absorption spectra of samples 1, 10, 213 and 232, representative of the entire set of the coins. Some spectra revealed the presence of atacamite/clinoatacamite ($Cu_2(OH)_3Cl$) in the patina (bands at 3436, 3330, 3310, 890, 840, 949 and 985 cm-1 in Fig. 2a and 2d) and malachite $Cu(CO_3).Cu(OH)_2$ (bands at 3400, 3309, 1486, 1395, 1039, 864, 743 and 704 cm^{-1} in Figure 2a-c). Furthermore, specific absorption bands can be assigned to different components of the patina. The band at ~3571 cm^{-1} in sample 1 (Figure 2a) can indicate the presence of clay materials in the patina, probably as a burial contaminant. The presence of a band at 1584 cm^{-1} can be attributed to the presence of copper carboxylates. One possibility is the

presence of copper(II) acetate resulting of the corrosion process due to old cleaning treatments, but the presence in the spectra of bands of organic compounds resulting from the contact with the human skin oils and their alteration products oxalate type (vide infra), denotes the significant maintenance of the original coin surface.

Bands at ~2962 cm^{-1}, ~2923 cm^{-1}, ~2852 cm^{-1} and ~2807 cm^{-1} for the sample 1 (Figure 2a), ~2924 cm^{-1} and ~2855 cm^{-1} for the sample 10 (Figure 2b), ~2916 cm^{-1} and ~2848 cm^{-1} for the sample 232 can represent the organic compounds of the patina. The band at ~1738 cm^{-1} for the sample 10, well visible in Figure 2b, can be assigned to the C=O group, that indicate the presence of lipids. The occurrence of lipids in the corrosion layer is the result of the contact of the coin with the human skin oils, present on the hands of the ancient users of these coins when were in circulation (A. Doménech-Carbó et al., 2019). Moreover, the presence of bands at 1584 and 1541 cm^{-1} (Figure 2c), typical of the copper and zinc stearates or zinc palmitates, is an evidence of the reactions of free fatty acids hydrolized from lipids with Cu(II) and Zn(II) metal ions released from the coin during corrosion processes. Finally, the bands at ~1378 cm^{-1} (Figure 2a) and at ~1319 cm^{-1} (Figure 2c) can be assigned to the copper and calcium oxalates. These compounds are the result

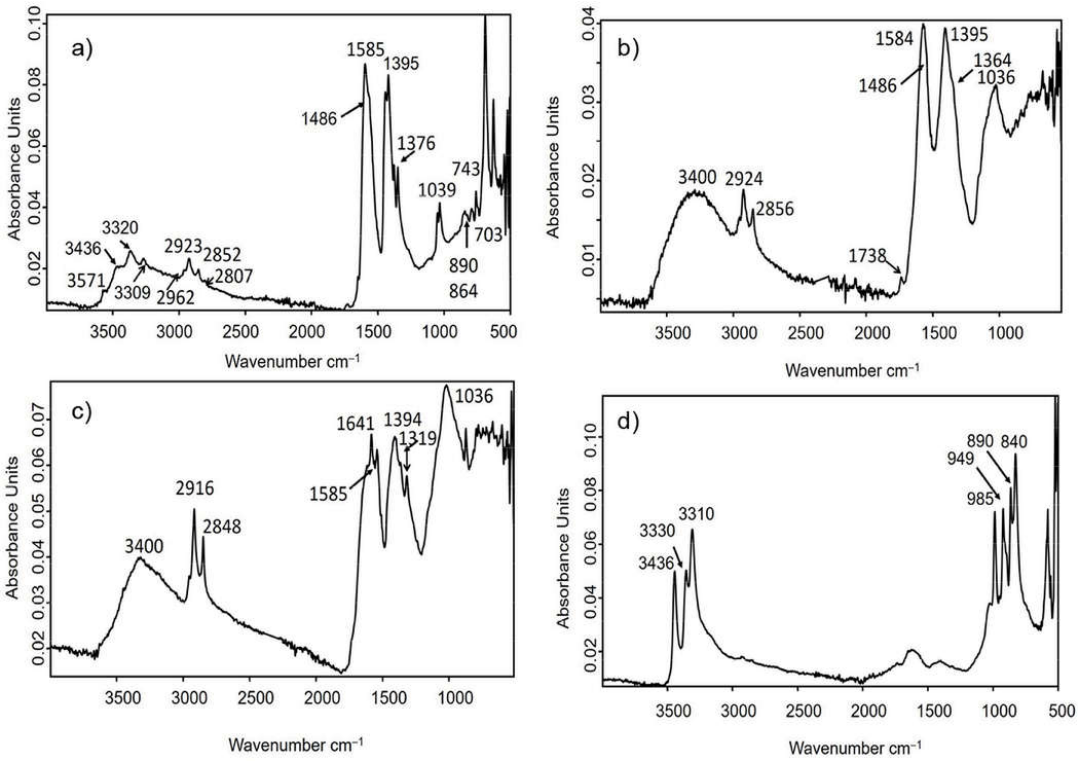

Figure 2 ATR-FTIR Spectra of sample1 1 (a), 10 (b), 213 (c), 232 (d) compared with the spectra of reference materials.

of the degradation of lipids to oxalates and further complexation with metal ions (A. Doménech-Carbó et al., 2019; Inberg et al., 2018).

A group of selected samples (*i.e.*, 2, 236, B14, B15, E5) were analysed using FIB-FESEM, a nano-invasive technique, aiming to investigate the corrosion pattern occurring in the first ~10µm in depth of the patina. Figure 3 shows secondary electron images of the trenches obtained with the Ga ion beam for two representative coins, illustrating different corrosion patterns and semi-quantitative elemental composition of the patina. Coin 236 (Figure 3a,c) presents a high degree of corrosion in the external layer. Indeed, the first 3 µm of the patina are characterized by micro-domains with low amount of Zn, due to a selective de-alloying.

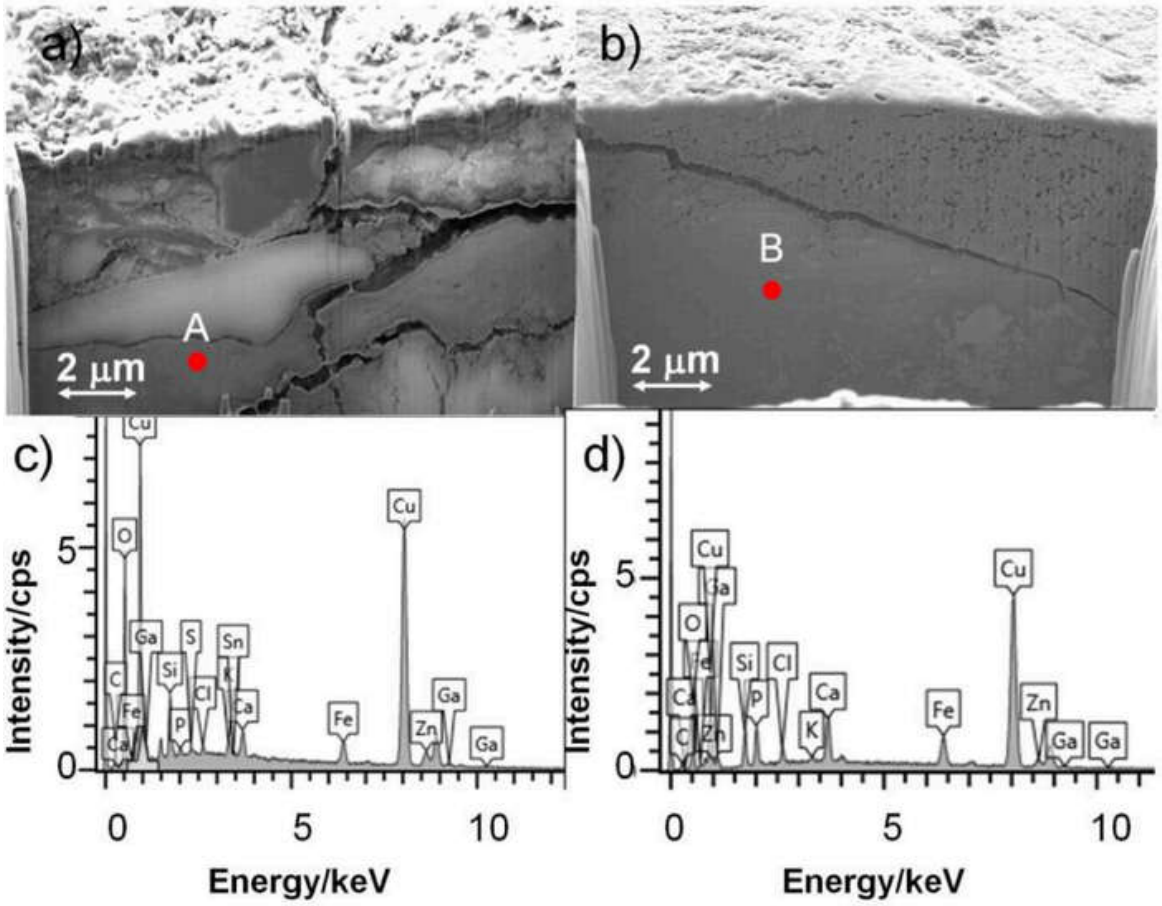

Figure 3 Secondary electron images acquired at 3kV of the trenches on coins 236 (a,c) and B14 (b,d). Representative X-ray microanalysis carried out in points A (Fig. 3a) and B (Fig. 3b) are reported. Trench image width 15µm, trench image depth 10µm. Spectrum A (Fig 3c): 75.5 wt.% Cu and 5.5 wt.% content ; spectrum B (Fig. 3d): 76.3 wt.% Cu and 3.6 wt.% content .Working conditions: voltage 20kV; working distance: 6mm.

The more porous external layer of coin B14 (Figure 3b,d) extends up to 4 µm in deep, due to the dezincification process in the Zn-rich micro-domains of the alloy. The segregation areas of Cu and Zn are well visible in the deeper region of the analysed patina. Moreover, all the samples present small pores and cracks lines, due both to mechanical stress and corrosion process. The patterns are comparable to the one previously described (Di Fazio et al., 2019), especially for the samples 2, 236, B15 and E5 that cannot be analysed using destructive techniques, *e.g.* EMP analysis on cross sections.

EMP analyses (Table 2) were acquired in the un-corroded metallic nucleus of a sub-set of 11 sacrificed coins, *i.e.*, sectioned as already reported (Di Fazio et al., 2019). The content of Zn ranges between 15% and 30% with the concomitant variation in the percentage of Cu, as can be seen in Figure 4. It is possible to notice a regular variation between the two main component of the alloy, considering their average values in the un-corroded core of each sample. Nevertheless, taking into account different periods of minting, Zn and Cu contents in the alloy have an irregular fluctuation of values, making impossible a grouping of samples. In contrast, the representation of the Sn content vs. the Zn content (inset in Figure 4), permits to separate the coins in three groups. The first one includes coins A2, 5, B4, 10, A, B14, and 20, having Sn content below 0.15%; B5 coin has 0.25% of Sn and coins A1, A3, A9 with content of Sn ranging from 0.7 to 1.1 %.

Sample	Authority	Year	%Cu	%Zn	%Sn	%Fe
A1	Republica	88 BCE	77.12	21.3	0.73	0.32
A2	Cesar	45 BCE	71.54	28.03	0.06	0.24
A3	Augustus	16 CE	81.52	17.32	0.72	0.34
5	Tiberius	22-23 CE	77.72	21.98	0.09	0.13
B4	Caligula	37-41 CE	82.37	17.32	0.13	0.07
10	Claudius	41-50 CE	80.74	18.78	0.06	0.21
A9	Claudius	40-50 CE	68.19	30.64	1.08	0.01
A	Claudius	50 CE	78.83	20.64	0.07	0.34
B5	Claudius	50-54 CE	67.92	20.40	0.19	0.25
B14	Nero	54-68 CE	78.67	20.92	0.04	0.24
20	Domitianus	81-96 CE	82.32	15.25	2.05	0.28

Table 2 Averaged composition of the metallic nucleus of a sub-set of the studied coins determined

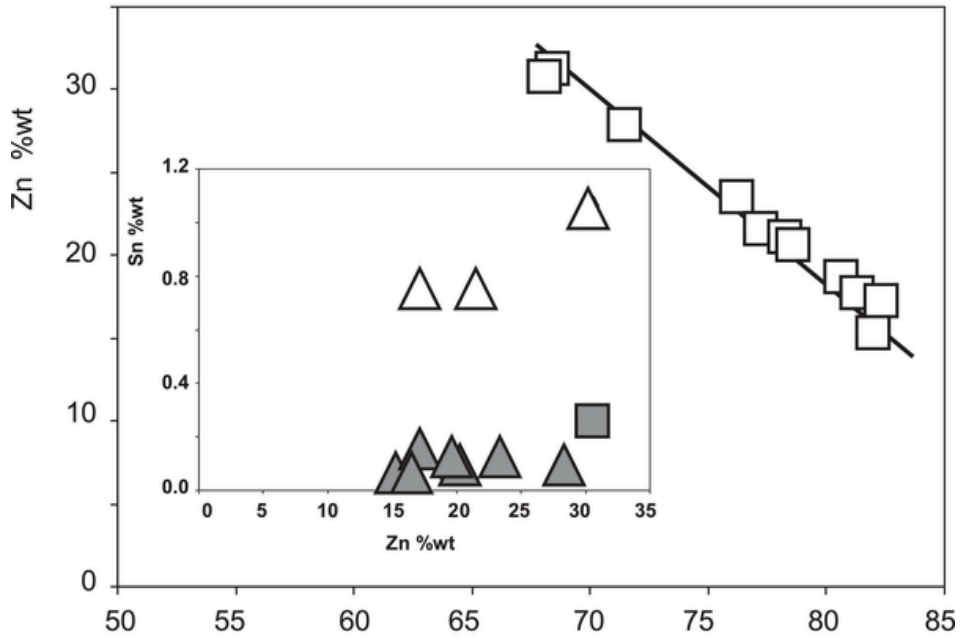

Figure 4 Relationship between the averaged percentages (% wt) of Zn and Cu determined by means of EMP of the nucleus of a sub-set of the studied coins. Inset: percentages of Sn and Zn.

3.3.2 Voltammetric pattern

The voltammetric response of coin samples on graphite electrodes was recorded in contact with air-saturated aqueous 0.25 M HAc/NaAc aqueous buffer solution at pH 4.75. Three replicates were performed for each coin sampling in three different areas of the same. Figure 5 illustrates the typical negative- and positive-going potential scan voltammograms for a,b) coin 1, a Caesar's *As* produced in 44 BCE and c,d) coin B15, a Tiberius' *Sestertius* minted in 22-23 CE. In the initial negative-going potential scan (Figures 5a,c), cathodic peaks at ca. 0.0 and −0.60 V vs. Ag/AgCl appear, followed by a prominent rising current at ca. −1.0 V. This last can be attributed to the hydrogen evolution reaction (HER) whereas the signal at 0.0 V (C1) can be assigned to the reduction of cuprite and other corrosion products (malachite-, brochantite-, atacamite-type minerals) to copper metal. The reduction of tenorite (CuO) occurs between −0.4 and −0.5 V (Di Turo et al., 2017; Di Turo et al., 2018; A. Doménech-Carbó et al., 2019; Doménech-Carbó et al., 2017a, 2017b, 2017c), here appearing as an ill-defined shoulder (C2). The cathodic wave at −0.60 V (C3) can be mainly attributed to the reduction of dissolved oxygen (oxygen

reduction reaction, ORR) but it is more or less peaked due to the superposition of the reduction of lead corrosion products (Doménech-Carbó et al., 2018, 2016). In turn, the reduction of zinc corrosion products will occur at more negative potentials, being indistinguishable from the HER process under our experimental conditions.

In the positive-going potential scan voltammograms (Figure 5b,d) anodic signals appear between 0.0 and +0.20 V (A1) and at ca. −0.80 V (A2). These signals can in principle be attributed to the oxidative dissolution (anodic stripping) of the metal deposits (Cu and Zn, respectively) formed at negative potentials as a result of the reduction of corrosion products. Minor signals at ca. −0.60 V can be assigned to the presence of Pb (and Sn) corrosion products (Doménech-Carbó et al., 2018, 2016).

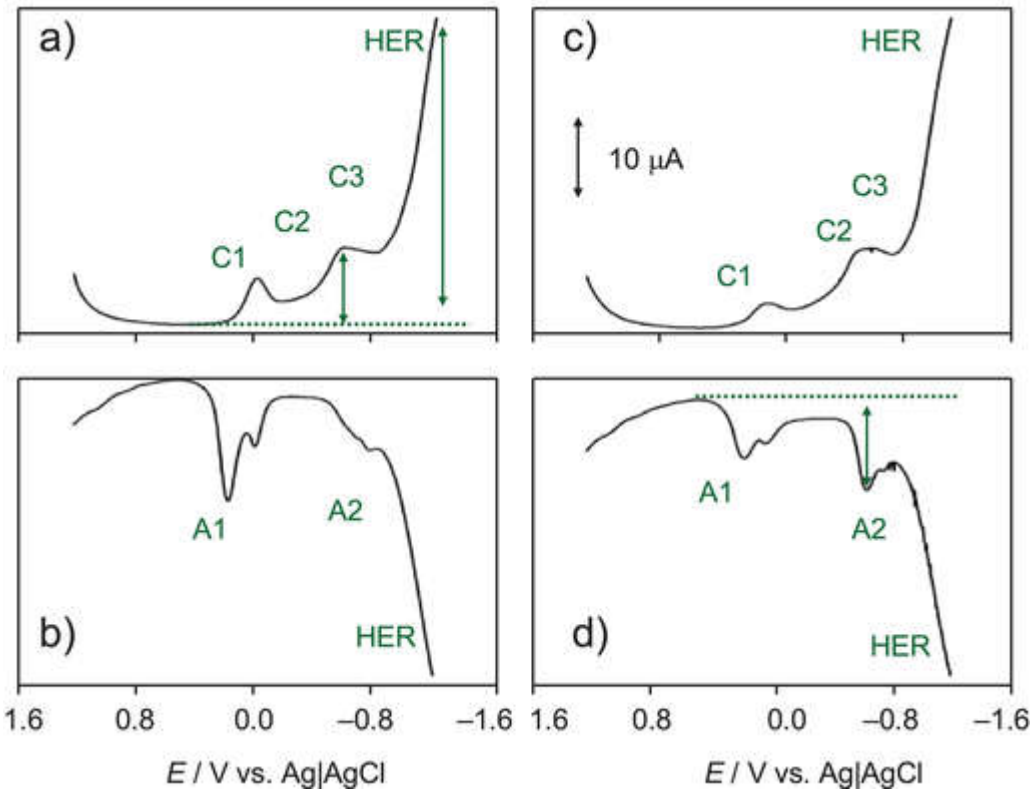

Figure 5 Square wave voltammograms of samples (a, b) 1 (As, Caesar, 45 BCE) and (c, d) B15 (Sestertius, Tiberius, 22–23 CE) attached to graphite electrode in contact with air-saturated 0.25M HAc/NaAc, pH 4.75. Potential scan initiated at (a, c) +1.25V in the negative direction; (b, d) −1.25V in the positive direction; potential step increment 4mV; square wave amplitude 25mV; frequency 5Hz.

Interestingly, replicate measurements in different spots of the same coin produced quite similar voltammetric profiles. Given the relatively large area of sampling (ca. 7 mm^2), the sampling compensate the local differences in roughness (surface features below the μm level, see Figure 2) between different regions of the same coin and between different coins. The relevant point to emphasize is that the relative height of the different voltammetric signals exhibits small but significant variations from one sample to another. This can be seen on comparing the series of replicate voltammograms for coins A9 (*As*, Claudius, 10-54 CE) and 213 (*Sestertius*, Augustus, 16 BCE). Although displaying common general profiles, the ratio between the intensities of different pairs of signals exhibits significant variations.

The above differences result from i) differences in the composition and metallographic treatment of the base metal alloy and ii) differences in the 'corrosion history' of the coin. Assuming that, sampling in regions of moderate corrosion of the coins, there is possibility of assuming reasonably uniform conditions of corrosion, we can attempt to group the coins on the basis of the variation of selected pairs of currents.

3.3.3 VIMP grouping

For grouping purposes, the intensities of the different voltammetric peaks can be used (Di Turo et al., 2017; Di Turo et al., 2018; A. Doménech-Carbó et al., 2019; Doménech-Carbó et al., 2017a, 2017b). As a preliminary requirement for grouping purposes, the self-consistency of voltammetric data has to be tested. Figure 6 depicts the representation of the peak current for the signals A1 and A2, *i*(A1), *i*(A2), vs. the peak current for the process C1, *i*(C1), for coin samples in this study (3 replicate measurements are presented as separate data points for each sample) using peak current measured in square wave voltammograms such as in Figure 5. Since, as previously described, the signals C1 and A1 (sum of the two resolved peaks) correspond to copper-centered signals recorded for the same sample, their peak currents should be proportional. Consistently, the plot of *i*(A1) vs. *i*(C1), although with some data dispersion, defines a straight line passing by the origin. In contrast, the plot of of *i*(A2) vs. *i*(C1) does not show a comparable

variation. Here, the values of the signal A2, attributed previously to the stripping of Zn, appear as independent on the copper-localized signal C1.

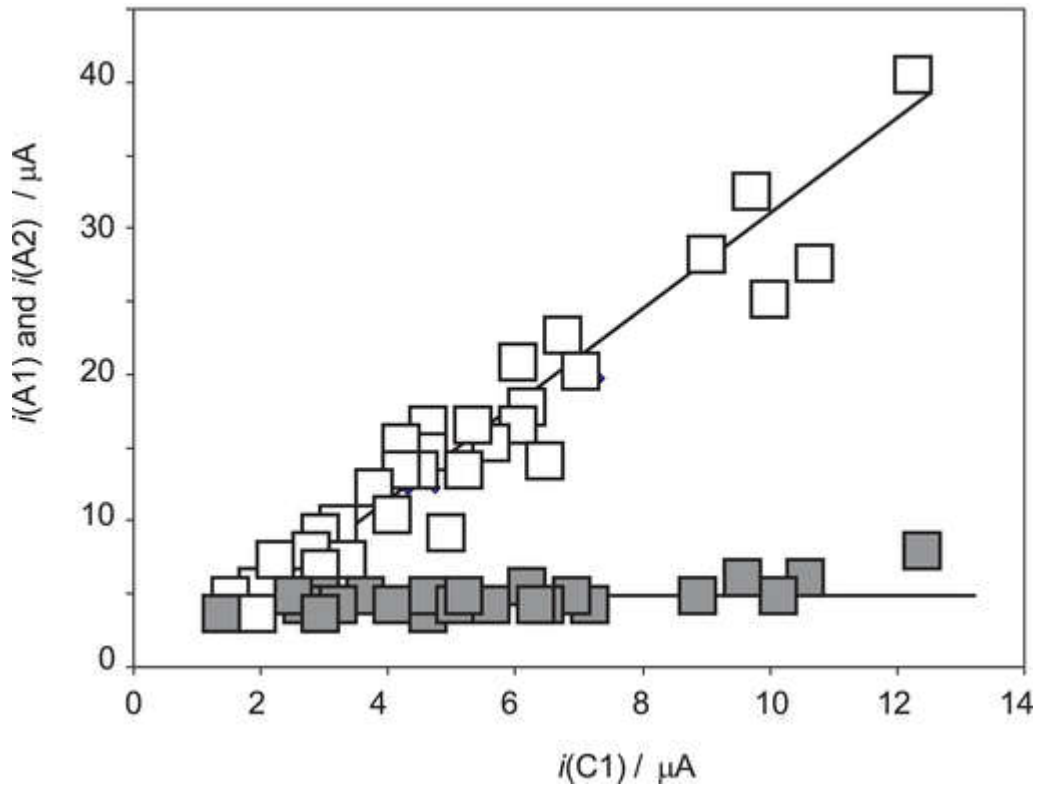

Figure 6 Plots of: i(A1) vs. i(C1) (squares) and b) i(A2) vs. i(C1) (solid squares) for samples in this study. From square wave voltammograms in the conditions such as those in Fig. 5.

In principle, the voltammetric response appears to be directly related to the composition of the base metal. Figure 7a depicts the plots of *i*(A2) vs. *i*(A1) for samples A9, 5, and 10, corresponding, respectively, to a Claudius' *as*, a Tiberius' *Sestertius*, and a Claudius' *Sestertius*. The data points for five replicate experiments on each coin fall in a common tendency curve so that the values of *i*(A2) relative to those of *i*(A1) increase on increasing the Zn content on the base metal determined from EMP analysis (EMPA) of coins cross sections (30.6, 23.3, 18.8 % wt, respectively). This result can be rationalized on considering that, even after dezincification, the composition of the corrosion layer of the coins should be representative of the composition of the base metal alloy so that the stripping peaks for zinc and copper will reflect the relative abundances of such metals in the coin core.

There is, however, a more complicated situation because the proportion of Sn also plays a significant role in the electrochemical response. This can be seen in Figure 7b, where the *i*(A2) vs. *i*(A1) plots for samples A9 and B5, this last a Claudius' *as*, both containing a 30% wt Zn but clearly different Sn contents (1.08 and 0.25 %wt), can be compared. One can see in this figure that the curve for the coin containing the highest Sn content reinforces the overall *i*(A2)/*i*(A1) ratio relative to the other. This is, in principle, consistent with the inhibiting effect exerted by tin on dezincification of brass (Campanella et al., 2009): the coin containing the higher Sn content presents a corrosion layer enriched in Zn. Data in Figure 7 are consistent with the foregoing set of considerations taking into account that the percentage of Zn of the coins A1 and A2 is similar (21.30 and 28.03 %wt, respectively), but their Sn content is clearly different (0.73 %wt for A1 and 0.06 %wt for A2).

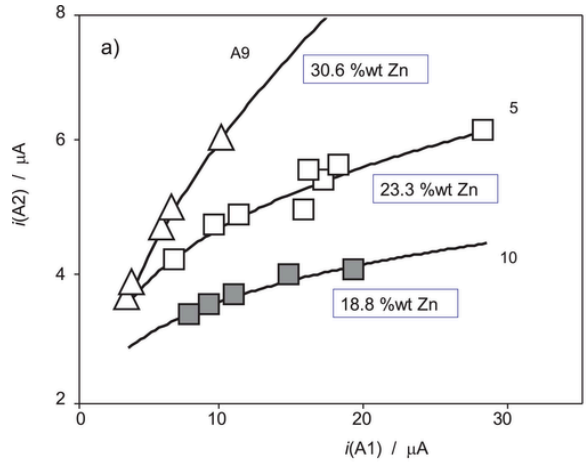

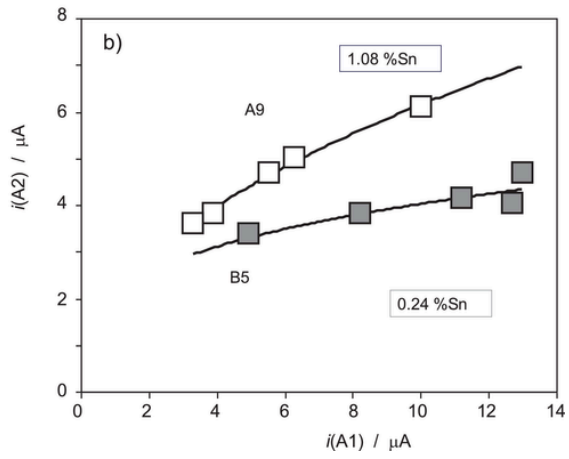

Figure 7 Plots of i(A2) vs. i(A1) for: a) samples A9, 5, and 10; b) samples A9 and B5. Data points for five independent replicate measurements on each coin using square wave voltammograms such as in Figure 5b. Continuous lines correspond to the fit of experimental data points to a potential function.

The same representation of the ln(*i*(A2)) vs. ln(*i*(A1)) for Augustus' *Sestertii* reveals systematic differences depending on the emission authority. As can be seen in Figure 8, coins from Asinio Gallo (235, 236) and Plotius Rufus (226, 232, 240), define two tendency lines which differ from the line defined by *Sestertii* from Casius Celler (A3), Gallius Lupercus (213, 228), Gnaeus Calpurnius Piso (234), and Naevius Surdinus (227) corresponding, apparently, to lower Zn and/or Sn contents.

In the series of Augustus' *Sestertii* there is only disposal of composition data for sample A3, characterized by a low zinc content (17.32 %wt) and a high tin content (0.72 %wt). Accordingly, and taking into account the previously described results, it appears reasonable to attribute the Augustus' *Sestertii* minted under the authority of Asinio Gallo and Plotius Rufus to a production with relatively high Zn and/or Sn contents whereas the production under the authority of Naevius Surdinus, and Gnaeus Calpurnius Piso, Cassius Celler and Gallius Lupercus, would be characterized by lower Zn and/or Sn contents. Conjointly considered these results illustrate the capability of VIMP measurements to discriminate between monetary emissions.

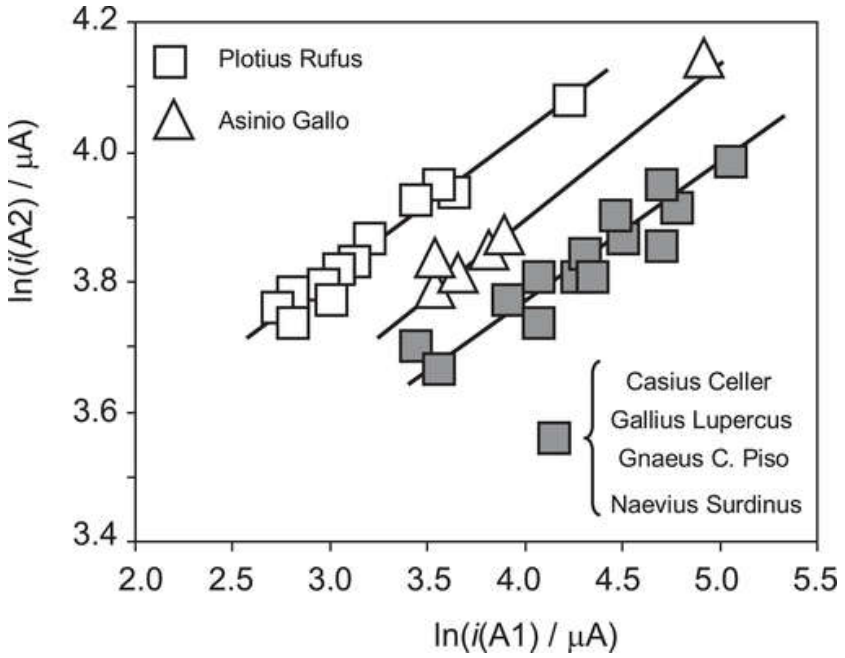

Figure 8 Plots of ln(*i*(A2)) vs. ln(*i*(A1)) for Augustus' *Sestertii* grouped from the emission authority (coins A3 from Casius Celler, 213 and 228 from Gallius Lupercus, 234 from Gnaeus Calpurnius Piso, and 227 from Naevius Surdinus (solid squares), coins 235, 236 from Asinio Gallo (triangles) and coins 226, 232, 240 from Plotius Rufus (squares). From positive-going potential scan voltammograms such as in Figure 5b. Continuous lines correspond to the fit of experimental data points to a straight line.

Although studies on copper coins are focused on elemental analysis and microstructure (Caponetti et al., 2017; Craddock, 1978; Di Fazio et al., 2019; M. T. Doménech-Carbó et al., 2019; Griesser et al., 2016; Inberg et al., 2018; Klein et al., 2004; Lönnqvist, 2003; Rehren, 1999), prompting the characterization of provenances and ateliers preparing forgeries (Deraisme and Barrandon, 2008). Recently, Caponetti et al. concluded that Cd, Ag, Zn, Bi, As, ans Sn are the elements with more discriminant capacity in regard to grouping orichalcum ingots from the underwater Gela's archaeological site (Caponetti et al., 2017), whereas Griesser et al. (Griesser et al., 2016) have underlined the importance of the casting technique in the corrosion of leaded copper coins. Conjointly considered, these results can be seen as consistent with the electrochemical data presented here underlining the importance of the composition, but also of variations in the minting technique, in the composition and structure of the metal patina and hence on the voltammetric response which in turn constitutes the basis for the electrochemical grouping described here for orichalcum coins.

3.4 Conclusions

All coins displayed a relatively similar corrosion pattern, with prevalence of copper corrosion products and more or less extensive dezincification, as denoted by FIB-FESEM/EDS data. Indeed, FESEM analysis shows a high degree corroded patina, characterized by micro-domains with low amount of Zn and a porous structure due to the progressive de-alloying process. To have a multi-analytic point of view, a low amount of patina from selected coins was analysed by ATR-FTIR. Data acquired confirm the prevalence of copper corrosion products compared to zinc products, confirming the dezincification of the external layers of the samples.

The voltammetric response of submicro-samples from the patina of a series of orichalcum Roman coins covering from the late Republic to Domitianus in contact with aqueous acetate buffer at pH 4.75 provides distinctive signals for copper corrosion products accompanied by anodic signals corresponding to the stripping of copper and zinc. The intensity of the later signals can be correlated to the averaged elemental compositions of the metallic nucleus known for a sub-set of the studied coins.

Quantitative data obtained by EMP analysis allow to evaluate the real composition of the alloy in the un-altered core of sample. Here, the ratio Zn/Cu was found to be sensitive to the Zn content (between 15 and 30 %wt), but also to the Sn content (between 0.01 and 1.08 %wt). Replicate voltammetric measurements on different points of the studied coins permit to obtain tendency curves which permit the grouping of coins by emissions and, in the case of Augustus' *Sestertius*, even discriminate between coins emitted under different authorities.

Acknowledgments: Financial support is gratefully acknowledged from the Spanish "R+D+I" project CTQ2017-85317-C2-1-P, CTQ2014-53736-C3-1-P and CTQ2014-53736-C3-2-P, which are supported by the *Ministerio de Ciencia, Innovación y Universidades*, *Fondo Europeo de Desarrollo Regional* (ERDF) funds and *Agencia Estatal de Investigación* (AEI). The authors wish to thank Mr. Manuel Planes, Dr. José Luis Moya and Mrs. Alicia Nuez Inbernón, technical supervisors of the Electron Microscopy Service of the Universitat Politècnica de València.

References

Agresti, J., Osticioli, I., Guidotti, M.C., Kardjilov, N., Siano, S., 2016. Non-invasive archaeometallurgical approach to the investigations of bronze figurines using neutron, laser, and X-ray techniques. Microchem. J. 124, 765–774. https://doi.org/10.1016/j.microc.2015.10.030

Arjmand, F., Adriaens, A., 2012. Electrochemical quantification of copper-based alloys using voltammetry of microparticles: optimization of the experimental conditions. J. Solid State Electrochem. 16, 535–543. https://doi.org/10.1007/s10008-011-1365-0

Barrena, M.I., Gómez de Salazar, J.M., Soria, A., 2008. Corrosion of brass archaeological blinker: Characterisation of natural degradation process. Mater. Lett. 62, 3944–3946. https://doi.org/10.1016/j.matlet.2008.05.015

Bourgarit, D., Bauchau, F., 2010. The ancient brass cementation processes revisited by extensive experimental simulation. JOM 62, 27–33. https://doi.org/10.1007/s11837-010-0045-3

Campanella, L., Alessandri, O.C., Ferretti, M., Plattner, S.H., 2009. The effect of tin on dezincification of archaeological copper alloys. Corros. Sci. 51, 2183–2191. https://doi.org/10.1016/j.corsci.2009.05.047

Caponetti, E., Armetta, F., Brusca, L., Chillura Martino, D., Saladino, M.L., Ridolfi, S., Chirco, G., Berrettoni, M., Conti, P., Bruno, N., Tusa, S., 2017. A multivariate approach to the study of orichalcum ingots from the underwater Gela's archaeological site. Microchem. J. 135, 163–170. https://doi.org/10.1016/j.microc.2017.09.003

Carl, M., Young, M.L., 2016. Complementary analytical methods for analysis of Ag-plated cultural heritage objects. Microchem. J. 126, 307–315. https://doi.org/10.1016/j.microc.2015.12.019

Catalli, F., 2003. Numismatica Greca e Romana. Istituto poligrafico e Zecca dello Stato, Roma.

Cepriá, G., Aranda, C., Pérez-Arantegui, J., Lacueva, F., Castillo, J.R., 2001. Voltammetry of immobilised microparticles: a powerful analytical technique to study the physical and chemical composition of brass. J. Electroanal. Chem. 513, 52–58. https://doi.org/10.1016/S0022-0728(01)00599-X

Constantinides, I., Adriaens, A., Adams, F., 2002. Surface characterization of artificial corrosion layers on copper alloy reference materials. Appl. Surf. Sci. 189, 90–101. https://doi.org/10.1016/S0169-4332(02)00005-3

Costa, V., Leyssens, K., Adriaens, A., Richard, N., Scholz, F., 2009. Electrochemistry reveals archaeological materials. J. Solid State Electrochem. 14, 449. https://doi.org/10.1007/s10008-009-0864-8

Craddock, P.T., 1978. The composition of the copper alloys used by the Greek, Etruscan and Roman civilizations. J. Archaeol. Sci. 5, 1–16. https://doi.org/10.1016/0305-4403(78)90015-8

del Hoyo-Meléndez, J.M., Świt, P., Matosz, M., Woźniak, M., Klisińska-Kopacz, A., Bratasz, Ł., 2015. Micro-XRF analysis of silver coins from medieval Poland. Nucl. Instrum. Methods Phys. Res. Sect. B Beam Interact. Mater. At. 349, 6–16. https://doi.org/10.1016/j.nimb.2015.02.018

Deraisme, A., Barrandon, J.-N., 2008. Unofficial Coinage in the Third Century Ad in the Gallo-Roman World: Chemical and Physical Analyses for Determining the Localization of the Workshop*. Archaeometry 50, 835–854. https://doi.org/10.1111/j.1475-4754.2007.00366.x

Di Fazio, M., Felici, A.C., Catalli, F., De Vito, C., 2019. Microstructure and chemical composition of Roman orichalcum coins emitted after the monetary reform of Augustus (23 B.C.). Sci. Rep. 9, 12668. https://doi.org/10.1038/s41598-019-48941-4

Di Turo, F., Montoya, N., Piquero-Cilla, J., De Vito, C., Coletti, F., Favero, G., Doménech-Carbó, A., 2017. Archaeometric analysis of Roman bronze coins from the Magna Mater temple using solid-state voltammetry and electrochemical impedance spectroscopy. Anal. Chim. Acta 955, 36–47. https://doi.org/10.1016/j.aca.2016.12.007

Di Turo, F., Montoya, N., Piquero-Cilla, J., De Vito, C., Coletti, F., Favero, G., Doménech-Carbó, T.M., Doménech-Carbó, A., 2018. Dating Archaeological Strata in the Magna Mater Temple Using Solid-state Voltammetric Analysis of Leaded Bronze Coins. Electroanalysis 30, 361–370. https://doi.org/10.1002/elan.201700724

Doménech-Carbo, A., 2017. Electrochemical dating: a review. J. Solid State Electrochem. 21, 1987–1998. https://doi.org/10.1007/s10008-017-3620-5

Doménech-Carbó, A., 2010. Voltammetric methods applied to identification, speciation, and quantification of analytes from works of art: an overview. J. Solid State Electrochem. 14, 363–379. https://doi.org/10.1007/s10008-009-0858-6

Doménech-Carbó, A., del Hoyo-Meléndez, J.M., Doménech-Carbó, M.T., Piquero-Cilla, J., 2017a. Electrochemical analysis of the first Polish coins using voltammetry of immobilized particles. Microchem. J. 130, 47–55. https://doi.org/10.1016/j.microc.2016.07.020

Doménech-Carbó, A., Doménech-Carbó, M.T., Álvarez-Romero, C., Montoya, N., Pasíes-Oviedo, T., Buendía, M., 2017b. Electrochemical Characterization of Coinage Techniques the 17th Century: The maravedís Case. Electroanalysis 29, 2008–2018. https://doi.org/10.1002/elan.201700326

Doménech-Carbó, A., Doménech-Carbó, M.T., Álvarez-Romero, C., Pasíes, T., Buendía, M., 2019. Screening of Iberian Coinage in the 2th-1th BCE Period Using the Voltammetry of Immobilized Particles. Electroanalysis 31, 1164–1173. https://doi.org/10.1002/elan.201900090

Doménech-Carbó, A., Doménech-Carbó, M.T., Capelo, S., Pasíes, T., Martínez-Lázaro, I., 2014. Dating Archaeological Copper/Bronze Artifacts by Using the Voltammetry of Microparticles. Angew. Chem. Int. Ed. 53, 9262–9266. https://doi.org/10.1002/anie.201404522

Doménech-Carbó, A., Doménech-Carbó, M.T., Costa, V., 2009. Electrochemical Methods in Archaeometry, Conservation and Restoration, Monographs in Electrochemistry. Springer-Verlag, Berlin Heidelberg.

Doménech-Carbó, A., Doménech-Carbó, M.T., Martínez-Lázaro, I., 2008. Electrochemical identification of bronze corrosion products in archaeological artefacts. A case study. Microchim. Acta 162, 351–359. https://doi.org/10.1007/s00604-007-0839-3

Doménech-Carbó, A., Doménech-Carbó, M.T., Montagna, E., Álvarez-Romero, C., Lee, Y., 2017c. Electrochemical discrimination of mints: The last Chinese emperors Kuang Hsü and Hsüan T'ung monetary unification. Talanta 169, 50–56. https://doi.org/10.1016/j.talanta.2017.03.025

Doménech-Carbó, A., Doménech-Carbó, M.T., Peiró-Ronda, M.A., 2011. Dating Archeological Lead Artifacts from Measurement of the Corrosion Content Using the Voltammetry of Microparticles. Anal. Chem. 83, 5639–5644. https://doi.org/10.1021/ac200731q

Doménech-Carbó, A., Doménech-Carbó, M.T., Redondo-Marugán, J., Osete-Cortina, L., Barrio, J., Fuentes, A., Vivancos-Ramón, M.V., Al Sekhaneh, W., Martínez, B., Martínez-Lázaro, I., Pasíes, T., 2018. Electrochemical Characterization and Dating of Archaeological Leaded Bronze Objects Using the Voltammetry of Immobilized Particles. Archaeometry 60, 308–324. https://doi.org/10.1111/arcm.12308

Doménech-Carbó, A., Doménech-Carbó, M.T., Redondo-Marugán, J., Osete-Cortina, L., Vivancos-Ramón, M.V., 2016. Electrochemical Characterization of Corrosion Products in Leaded Bronze Sculptures Considering Ohmic Drop Effects on Tafel Analysis. Electroanalysis 28, 833–845. https://doi.org/10.1002/elan.201500613

Doménech-Carbó, A., Lastras, M., Rodríguez, F., Osete, L., 2013. Mapping of corrosion products of highly altered archeological iron using voltammetry of microparticles. Microchem. J. 106, 41–50. https://doi.org/10.1016/j.microc.2012.05.002

Doménech-Carbó, A., Scholz, F., 2019. Electrochemical Age Determinations of Metallic Specimens—Utilization of the Corrosion Clock. Acc. Chem. Res. 52, 400–406. https://doi.org/10.1021/acs.accounts.8b00472

Doménech-Carbó Antonio, Doménech-Carbó María Teresa, 2018. Electroanalytical techniques in archaeological and art conservation. Pure Appl. Chem. 90, 447. https://doi.org/10.1515/pac-2017-0508

Doménech-Carbó Antonio, Labuda Jan, Scholz Fritz, 2012. Electroanalytical chemistry for the analysis of solids: Characterization and classification (IUPAC Technical Report). Pure Appl. Chem. 85, 609. https://doi.org/10.1351/PAC-REP-11-11-13

Doménech-Carbó, M.T., Álvarez-Romero, C., Doménech-Carbó, A., Osete-Cortina, L., Martínez-Bazán, M.L., 2019. Microchemical surface analysis of historic copper-based coins by the combined use of FIB-FESEM-EDX, OM, FTIR

spectroscopy and solid-state electrochemical techniques. Microchem. J. 148, 573–581. https://doi.org/10.1016/j.microc.2019.05.039

Ferrer-Eres, M.A., Peris-Vicente, J., Valle-Algarra, F.M., Gimeno-Adelantado, J.V., Sánchez-Ramos, S., Soriano-Piñol, M.D., 2010. Archaeopolymetallurgical study of materials from an Iberian culture site in Spain by scanning electron microscopy with X-ray microanalysis, chemometrics and image analysis. Microchem. J. 95, 298–305. https://doi.org/10.1016/j.microc.2010.01.003

Gomes, S.S., Soares, A.M., Araújo, M.F., Correia, V.H., 2016. Lead isotopes and elemental composition of Roman fistulae plumbeae aquariae from Conimbriga (Portugal) using Quadrupole ICP-MS. Microchem. J. 129, 184–193. https://doi.org/10.1016/j.microc.2016.06.027

Griesser, M., Kockelmann, W., Hradil, K., Traum, R., 2016. New insights into the manufacturing technique and corrosion of high leaded antique bronze coins. Microchem. J. 126, 181–193. https://doi.org/10.1016/j.microc.2015.12.002

Inberg, A., Ashkenazi, D., Cohen, M., Iddan, N., Cvikel, D., 2018. Corrosion products and microstructure of copper alloy coins from the Byzantine-period Ma'agan Mikhael B shipwreck, Israel. Microchem. J. 143, 400–409. https://doi.org/10.1016/j.microc.2018.08.033

Karpagavalli, R., Balasubramaniam, R., 2007. Development of novel brasses to resist dezincification. Corros. Sci. 49, 963–979. https://doi.org/10.1016/j.corsci.2006.06.024

Klein, S., Lahaye, Y., Brey, G.P., Von Kaenel, H.-M., 2004. The early roman imperial AES coinage II: Tracing the copper sources by analysis of lead and copper isotopes—copper coins of Augustus and Tiberius*. Archaeometry 46, 469–480. https://doi.org/10.1111/j.1475-4754.2004.00168.x

Lönnqvist, K.K.A., 2003. A Second Investigation into the Chemical Composition of the Roman Provincial (Procuratorial) Coinage of Judaea, AD 6–66*. Archaeometry 45, 45–60. https://doi.org/10.1111/1475-4754.00096

Lutterotti, L., Dell'Amore, F., Angelucci, D.E., Carrer, F., Gialanella, S., 2016. Combined X-ray diffraction and fluorescence analysis in the cultural heritage field. Microchem. J. 126, 423–430. https://doi.org/10.1016/j.microc.2015.12.031

Marshakov, I.K., 2005. Corrosion Resistance and Dezincing of Brasses. Prot. Met. 41, 205–210. https://doi.org/10.1007/s11124-005-0031-2

Martini, C., Chiavari, C., Ospitali, F., Grazzi, F., Scherillo, A., Soffritti, C., Garagnani, G.L., 2013. Investigations on a brass armour: Authentic or forgery? Mater. Chem. Phys. 142, 229–237. https://doi.org/10.1016/j.matchemphys.2013.07.010

Mattsson, E., 1980. Corrosion of Copper and Brass: Practical Experience in relation to Basic Data. Br. Corros. J. 15, 6–13. https://doi.org/10.1179/000705980798318708

Papadopoulou, O., Alessandri, O.C., Vassiliou, P., Grassini, S., Angelini, E., Gouda, V., 2016. Soil-induced corrosion of ancient Roman brass - A case study. Mater. Corros. 67, 160–169. https://doi.org/10.1002/maco.201408115

Peris-Vicente, J., Valle-Algarra, F.M., Ferrer-Eres, M.A., Gimeno-Adelantado, J.V., Mateo-Castro, R., Soriano-Piñol, M.D., 2008. Archaeometrical study of paleometallurgical materials from the archaeological site "Cerro de las Balsas — Chinchorro" (La Albufereta, Alacant, Spain). Microchem. J. 90, 142–146. https://doi.org/10.1016/j.microc.2008.05.003

Pouchou, J., Pichior, F., 1985. "PAP" f(rZ) procedure for improved quantitative analysis, in: J.T. Armstrong (Ed.), Microbeam Analysis. San Francisco, pp. 104–106.

Rehren, T., 1999. Small Size, Large Scale Roman Brass Production in Germania Inferior. J. Archaeol. Sci. 26, 1083–1087. https://doi.org/10.1006/jasc.1999.0402

Robbiola, L., Blengino, J.-M., Fiaud, C., 1998. Morphology and mechanisms of formation of natural patinas on archaeological Cu–Sn alloys. Corros. Sci. 40, 2083–2111. https://doi.org/10.1016/S0010-938X(98)00096-1

Robbiola, L., Portier, R., 2006. A global approach to the authentication of ancient bronzes based on the characterization of the alloy–patina–environment system. J. Cult. Herit. 7, 1–12. https://doi.org/10.1016/j.culher.2005.11.001

Šatović, D., Martinez, S., Bobrowski, A., 2010. Electrochemical identification of corrosion products on historical and archaeological bronzes using the voltammetry of micro-particles attached to a carbon paste electrode. Talanta 81, 1760–1765. https://doi.org/10.1016/j.talanta.2010.03.037

Scholz, F., Meyer, B., 1998. Voltammetry of solid microparticles immobilized on electrode surfaces. Electroanal. Chem. 20, 1–86.

Scholz, F., Schröder, U., Gulaboski, R., 2005. Electrochemistry of immobilized particles and droplets. Springer.

Scott, D.A., 1994. An Examination of the Patina and Corrosion Morphology of some Roman Bronzes. J. Am. Inst. Conserv. 33, 1–23. https://doi.org/10.1179/019713694806066419

Scott, D.A., 1991. Metallography and microstructure of ancient and historic metals. Getty Conservation Institute in association with Archetype Books, [Marina del Rey, CA].

Serghini-Idrissi, M., Bernard, M.C., Harrif, F.Z., Joiret, S., Rahmouni, K., Srhiri, A., Takenouti, H., Vivier, V., Ziani, M., 2005. Electrochemical and spectroscopic characterizations of patinas formed on an archaeological bronze coin. Electrochimica Acta 50, 4699–4709. https://doi.org/10.1016/j.electacta.2005.01.050

Sohn, S., Kang, T., 2002. The effects of tin and nickel on the corrosion behavior of 60Cu–40Zn alloys. J. Alloys Compd. 335, 281–289. https://doi.org/10.1016/S0925-8388(01)01839-4

Chapter 4 - Structural and chemical characterization of an ancient alloy from micro to nanoscale: the case of Roman orichalcum coins.

Abstract

A representative set of orichalcum (Cu-Zn alloy) coins, emitted during the Roman Empire, was analysed using micro and nanoscale techniques. Cross-sections of the samples were realized to investigate both the patinas and the unaltered inner core of the samples. In particular, SEM-EDS and HR-FESEM-EDS techniques were used to investigate the nature of the alloy, the micro and nanostructures and the pattern of corrosion of the patinas. Moreover, X-ray maps allowed to appreciate the distribution of the major element composing the alloy inside the samples and, consequently, to understand the evolution of the corrosion processes. The nanoscale investigation highlighted a great heterogeneity in composition within the strain lines structures, induced by selective dezincification.

4.1 Introduction

The archaeometric study of ancient coins (Ager et al., 2016; Corsi et al., 2016; Di Fazio et al., 2019a; Di Turo et al., 2018; Doménech-Carbó et al., 2018; Fabrizi et al., 2019; Ingo et al., 2017) is a powerful tool to enhance the knowledge on processing and use of metals, on coinage methods developments and on economic circulation in different historical periods. In particular, the study of the alloys addressed to coinage can give information about the minting techniques (Di Fazio et al., 2019b; Doménech-Carbó et al., 2018) and the technological background reached by ancient populations.

Concerning the materials, the study of ancient alloys allows to evaluate metal behaviour and corrosion in different burial environments (Ashkenazi et al., 2016; Barrena et al., 2008; Ingo et al., 2018; Papadopoulou et al., 2016; Pronti et al., 2015). All the information obtained by archaeometric investigations can give useful suggestions for the conservation and preservation of metal finds in the future (Ashkenazi et al., 2017).

During the Roman Era the most common alloys used to produce coins were bronze (Di Turo et al., 2017; Finetti, 1987), Ag-Cu based alloy (Doménech-Carbó et al., 2018) and orichalcum (Amela Valverde, 2004; Caponetti et al., 2017; Di Fazio et al., 2019b). Differences in use of alloys were strictly related to the value of each denomination issued. However, the compositions of the alloys changed over times, both for political and economic reasons (Catalli, 2003; Di Fazio et al., 2019b).

The aim of this study is to characterize the structure of the orichalcum alloy used to mint coins during the Roman Empire and to explore the parameters that induced corrosion and, gradually, dealloying. With this aim, high resolution scanning electron microscope (HR-FESEM-EDS) combined with X-ray elemental mapping give information about the chemical composition of the unaltered alloy at micro and nanoscale, determining also the degree of corrosion of the samples and, consequently, their state of conservation. The specific objectives are: investigation of (i) changes in morphology, (ii) changes in composition for corrosive process, (iii) pore system of the alloy by high resolution - field emission scanning electron microscopy (HR-FESEM-EDS).

Furthermore, the investigation of the nanostructures of the orichalcum allows a better understanding of the cementation process, *i.e.* the metallurgical process adopted and improved by Romans (Caley, 1964; Craddock, 1978). Indeed, Roman coins can suffer

of high degree of degradation, not only on superficial patina, but also into the inner layers (Di Fazio et al., 2019b). Therefore, the examination of the nanostructures allows understanding where corrosive processes started in the ancient Cu-Zn alloy.

4.2 Historical context

During the Roman Empire different monetary reforms were promulgated, in order to bring common rules to produce ingots with the same ratio of metals and to mint standard coins. The standardization of each denomination allowed an easier circulation of money through the Roman Empire and, thus, a recognition of the values of each denomination (Catalli, 2003; Finetti, 1987). In particular, a *dupondius* had the value of two *asses*, whereas a *sestertius* had the value of four *asses* (and, more or less, the value of two contemporary *euros*). *Quadrantes* were a low value coins, commonly used in daily purchases.

The monetary reform of Augustus (23 BCE) introduced two orichalcum denominations, *i.e. dupondii* and *sestertii*. Nero introduced a new monetary reform during the 63-64 CE, adding *asses*, *semisses* and *quadrantes* as new denominations in orichalcum (Amela Valverde, 2004; Catalli, 2003).

4.3 Materials and methods

4.3.1 Materials

A set of coins (A3, F1, F13, F14) were selected for this study, from private collections (Figure 1 and Table 1), to investigate the microstructures of the orichalcum alloy and the degradation of the patina, with a characteristic pattern.

Numismatic examination (Sutherland, 1984) revealed that they were one *dupondius*, one *sestertius* and two *quadrantes* issued under the reign of Augustus (27 BCE – 14 CE), Caius (37-41 CE) and Nero (54-68 CE). In particular, the samples A3 and F1 were minted during Augustus and Caius Empire, respectively, following the rules of the

Augustus monetary reform (23 BCE), whereas the samples F13 and F14 were produced under Nero, after his monetary reform of 63-64 CE (Catalli, 2003).

Figure 1 Images of samples (reverse and obverse), from private collection, analysed during this study. Numismatic information is reported in Table 1.

Sample	**Value** (denomination)	**Emperor (emission authority)**	**year**	**Mint**	**Numismatic reference**
A3	*Dupondius*	Augustus (C. Cassius Celer.)	16 BCE	Rome	RIC I, 2 Augustus 375
F1	*Sestertius*	Caligula (-)	37-38 CE	Rome	RIC I, 2 Gaius/Caligula 32
F13	*Quadrantes*	Nero	62-38 CE	Rome	RIC I, 2 Nero 258
F14	*Quadrantes*	Nero	62-38 CE	Rome	RIC I, 2 318

Table 1 Numismatic features of the coins.

4.3.2 Methods

To explore and characterize the nature of the alloy and the patina, it was necessary to prepare cross sections of the samples, cutting the coins from rim to rim. Then, the sections were coated in epoxy resins, using appropriate moulds.

Scanning electron microscope investigations (SEM-EDS) were performed on cross section (from rim-core-to-rim), using a FEI-Quanta 400 instrument with an EDAX Genesis Microanalysis system (Department of Earth Sciences, Sapienza University of Rome, Italy). SE and BSE imaging along with X-ray maps were carried out to study the microstructure of the alloy and to evaluate the evolution of the corrosion process inside archaeological samples.

The investigation at nanoscale was performed on the same cross section by means of an AURIGA Zeiss high resolution Field Emission Scanning Electron Microscope (HR-FESEM) equipped with a Bruker EDS system (SNN-lab at Center for Nanotechnology for Engineering - CNIS, Sapienza University of Rome).

4.4 Results

4.4.1 Coins F1 and A3

SEM imaging analysis allows highlighting the microstructures of the alloy and the potential presence of corrosion layers, besides to evaluate the degree of corrosion of the samples.

The *sestertius* F1 shows a complex pattern of degradation (Figure 2). Indeed, considering an average thickness of the sample of ~2mm, the uncorroded nucleus has a maximum breadth of ~1,2mm and a minimum of ~200µm, whereas the corroded layer varies from ~400µm up to ~1mm in depth (Figure 2a). As previously reported (Constantinides et al., 2002; Di Fazio et al., 2019b), the corroded external layer is formed by a porous microstructure, increasing from the inner nucleus to the external rim.

Back-scattered images show the presence of fine and parallel strain lines, especially in proximity of the external corroded layer of the sample (Fig 2b). As suggested by the occurrence of at least two shades of grey, the parallel lines (in darker grey) are

different in chemical composition than the surrounding alloy (lighter grey) as they are depleted in Zn.

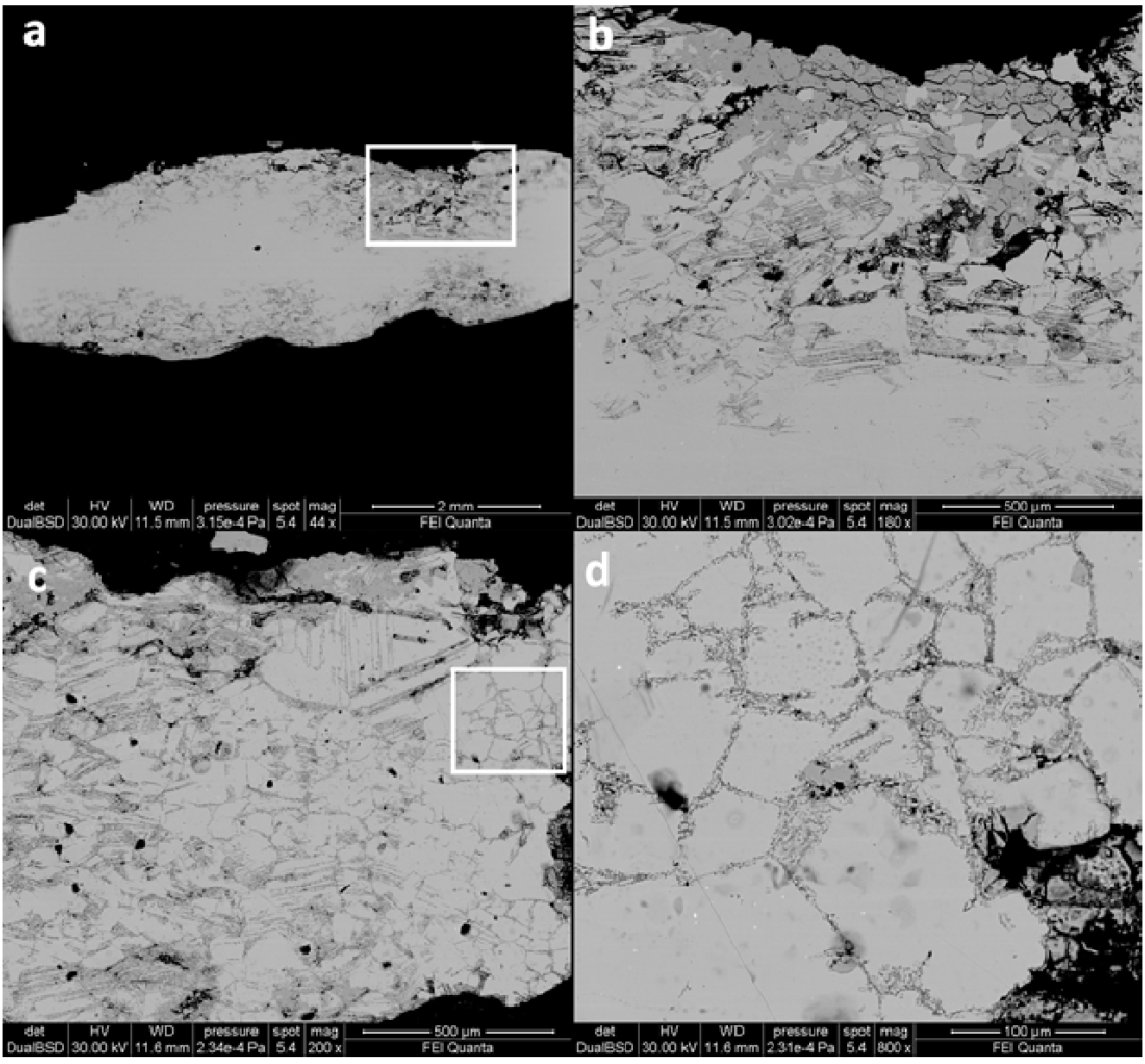

Figure 2 BSE image of cross section of sample F1. From (a) to (d) the magnification is increased: the highlighted area in (a) is expanded in (b) and (c), the highlighted area in (c) is expanded in (d).

HR-FESEM-EDS analysis was performed at different optical magnifications, aiming to investigate the morphological and structural characteristics of non- and corroded alloy.

HR-FESEM images of these structures at nanoscale (Figure 3c, d), previously analysed at microscale, show that the parallel lines are not continuous, unlike what is seen in microscale images (Fig 3a). Indeed, they are composed by Cu nanodomains structures followed by nanodomains depleted in Zn. Each nanodomain presents homogeneous composition. The presence of the microdomains and nanodomains structures denotes the preferential dezincification of strain areas. At the perpendicular intersections of two bundles of parallel lines, a single cross-shaped nanodomains with a homogeneous composition are formed (Figure 3d). Small areas with a different chemical composition can be minor than 1 μm in diameter (Figure 3). In addition, sample F1 shows evidences of a corrosion process and consequent dezincification, following the grain boundary (Figure 2c, d). Indeed, Figure 2d shows microdomains of Cu around the grain composing the alloy, highlighting the typical orichalcum microstructure produced by cementation process (Scott, 1991). Differences in the chemical composition of the microstructures observed in the section at high magnification are also confirmed by X-ray elements maps as showed by samples A3 and F1 (Figure 4 and Figure 5). The elemental distribution map shows a Zn depletion in the external part of the patina, near the grain boundaries and in correspondence with the strain lines. The distribution of Cu is homogeneous, excluding the areas where porosity is present due to the leaching of such element. Concerning sample A3 and F1, chlorine is concentrated in the area of the map corresponding to the patina-core interface. In addition, in sample F1 (Figure 5) Cl matches with the Cu-depleted areas, suggesting the occurrence of basic copper (II) chloride of stoichiometry $Cu_2Cl(OH)$ as botallacktite, atacamite, paratacamite and clinoatacamite (Doménech-Carbó et al., 2008).

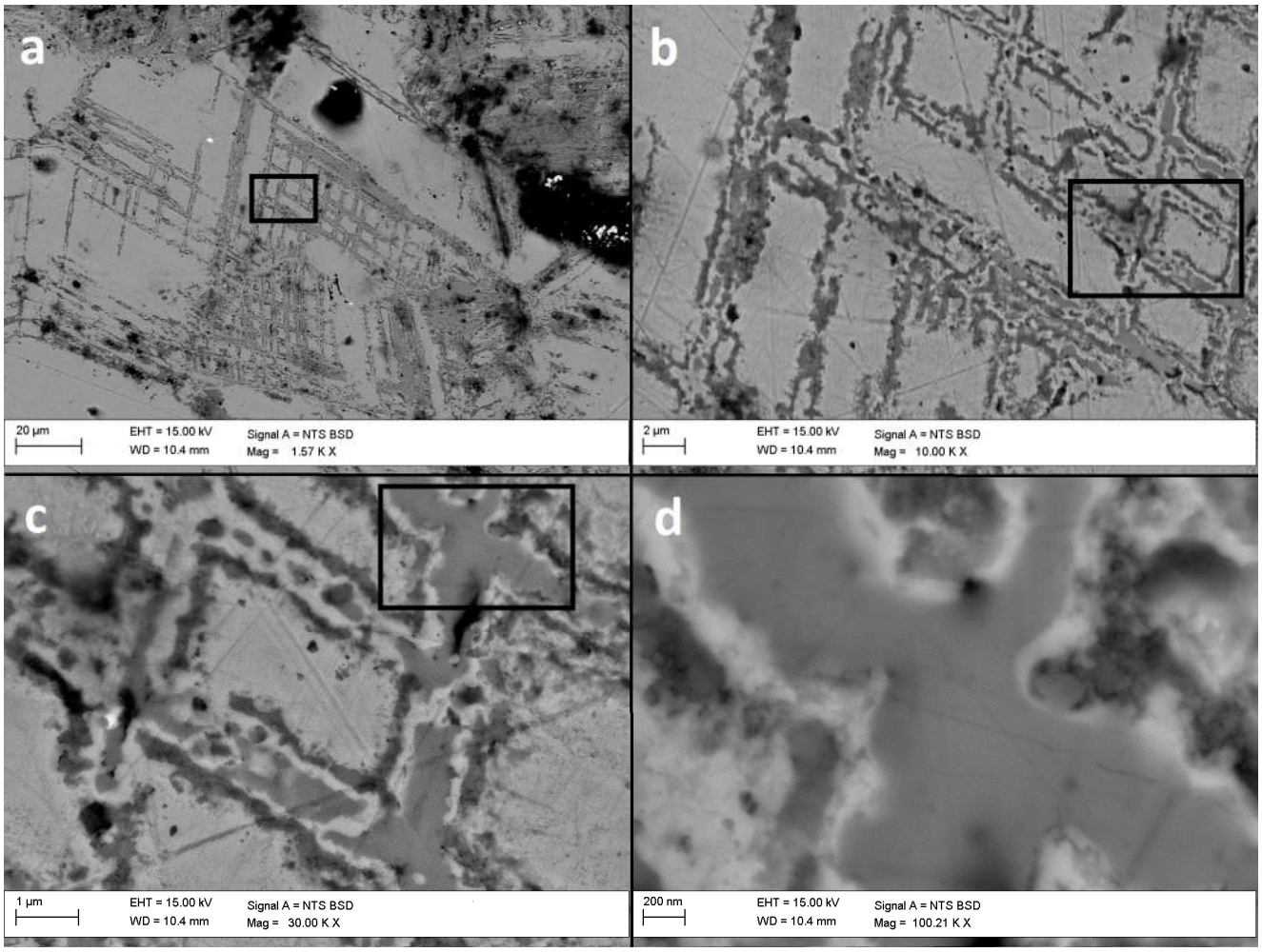

Figure 3 : BSE image at nanoscale of cross section of sample F1. From (a) to (d) the magnification is increased: the highlighted area in (a) is expanded in (b), the highlighted area in (b) is expanded in (c), the highlighted area in (c) is expanded in (d).

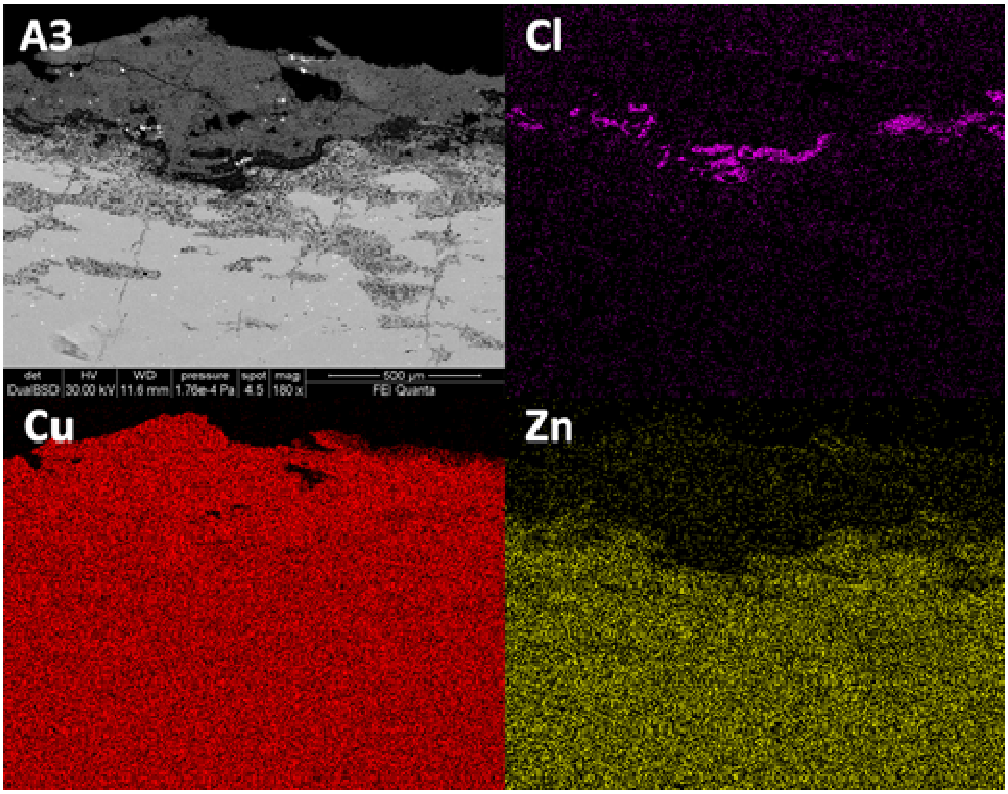

Figure 5 BSE cross section image of sample A3 and related X-ray maps of Cl, Cu and Zn.

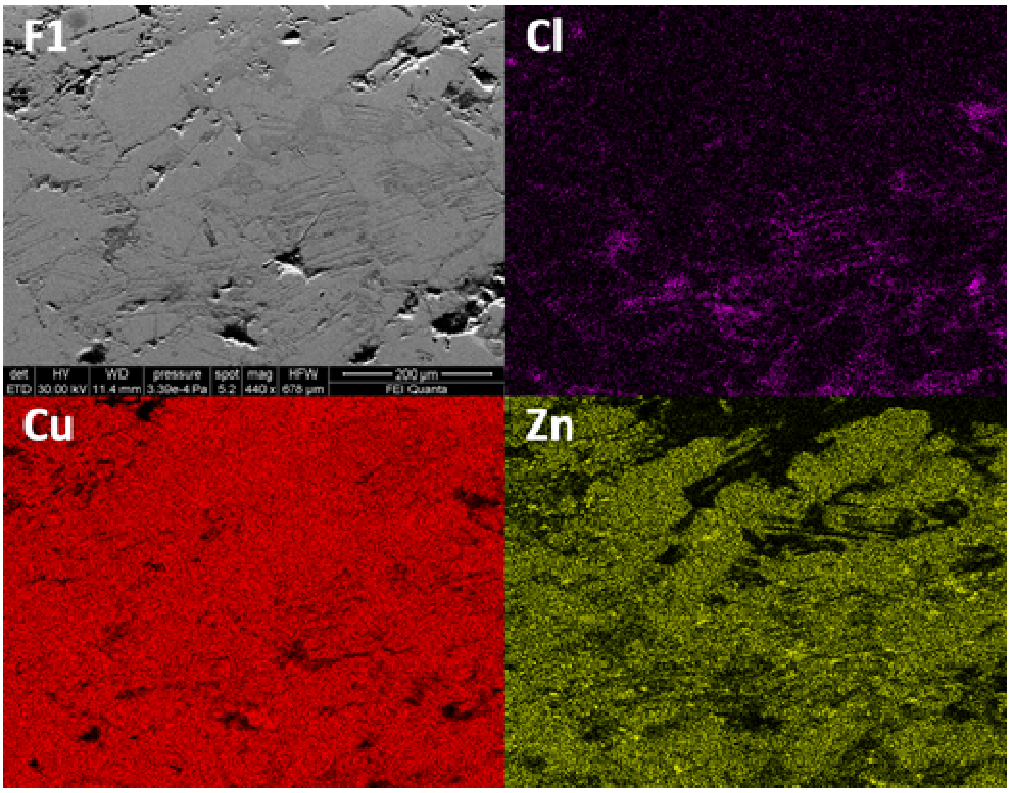

Figure 4 SE cross section image of sample F1 and related X-ray maps of Cl, Cu and Zn.

4.4.2 Coins F13 and F14

The *quadrantes* F13 and F14 have a dezincified patina, as the *sestertius* and the *dupondius*. EDS analyses (Figure 6) and X-ray maps of the elements (Figure 7) show a low presence of Zn in the external layer of these coins. In particular, in the sample F13 a homogeneous patina of ~60 µm occurs (Figure 6a, b), whereas the patina of sample F14 has an average thickness of ~100 µm (Figure 7). At high magnification, SEM imaging shows a detachment between the uncorroded core and the patina of the sample (Figure 6a, b). Despite this, the patinas appear to be compact and with a very low degree of porosity. EDS analyses on the patinas (Figure 6c-e) reveal that a dezincification process has occurred on the external area, whereas in the inner area Zn is still present (Figure 6b, e). In addition, the patina of sample F13 shows an intense EDS signal for Si (Figure 6c, d), as shown in the patina of sample F14 by Si X-ray map (Figure 7). Both EDS and X-ray map analyses do not reveal the presence of Cl.

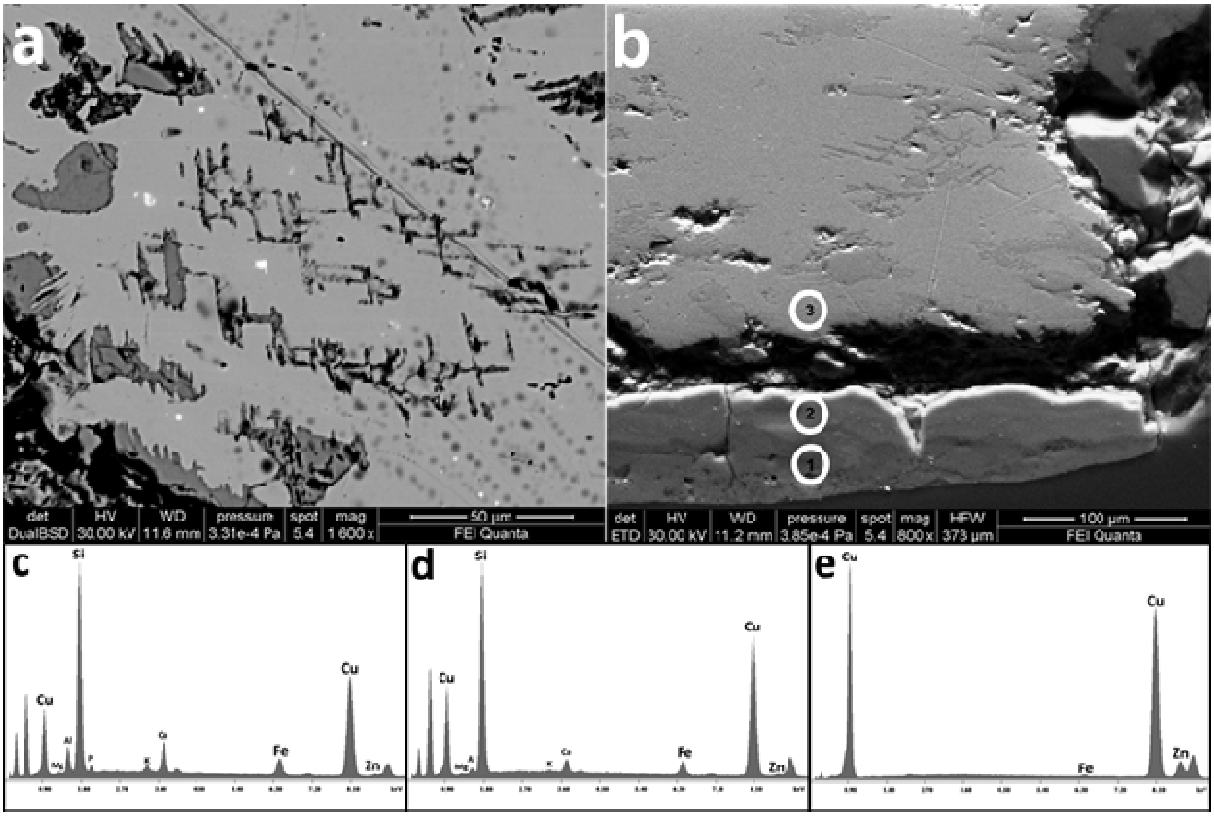

Figure 6 BSE (a) and SE (b) high magnification images of sample F13; c) EDS spectrum of point "1" in image (b); d) EDS spectrum of point "2" in image (b); e) EDS spectrum of point "3" in image (b)

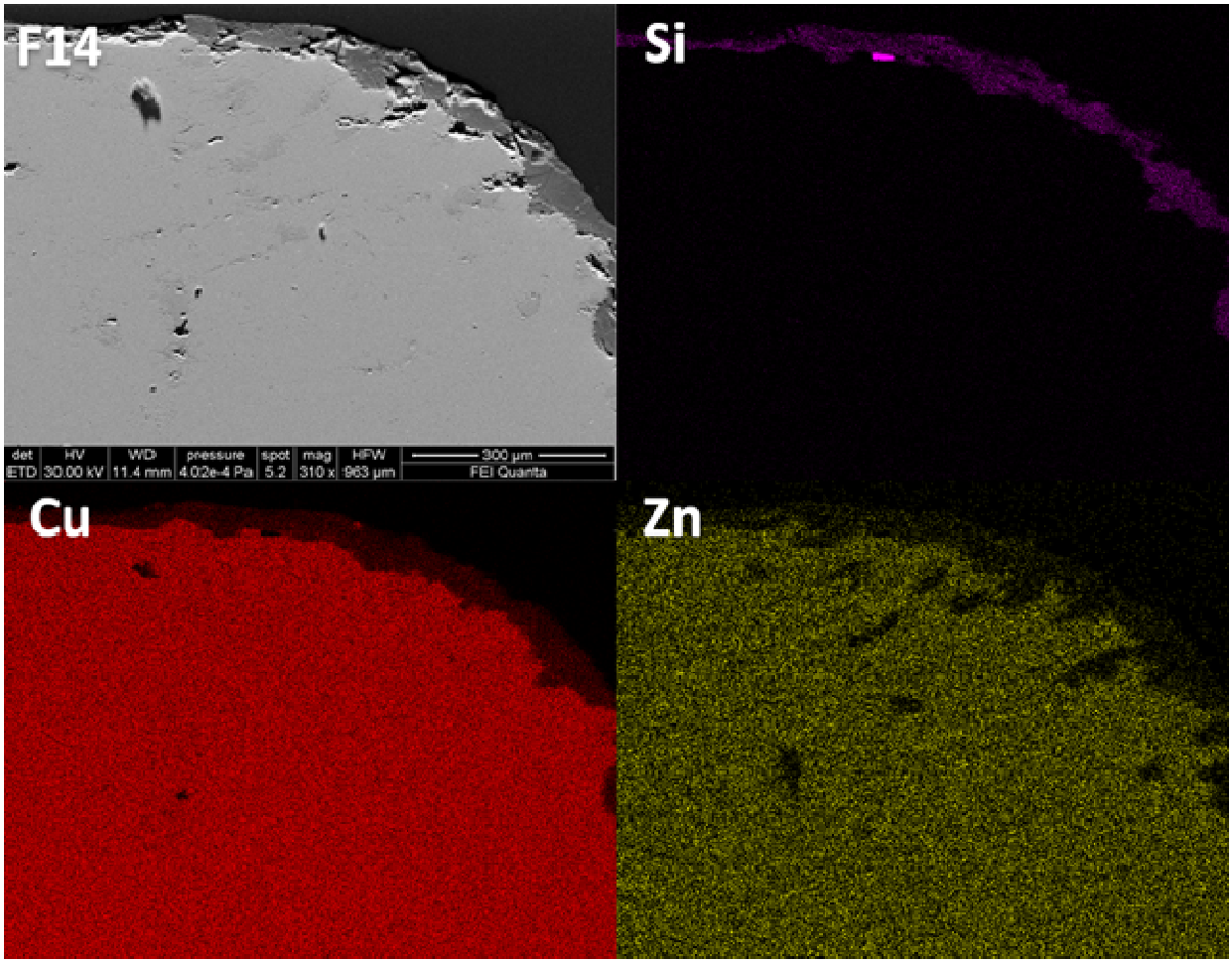

Figure 7 SE cross section image of sample F14 and related X-ray maps of Si, Cu and Zn.

BSE images of *quadrantes* F13 and F14 show the presence of fine and parallel strain lines near the external corroded layer (Figure 6a), which are darker grey than the light colour of the surrounding alloy indicating, as for samples A3 and F1, a Zn depletion. HR-FESEM-EDS of the line structures at nanoscale shows similarities between sample F14 (Figure 8) and sample F1 (Figure 3). Indeed, the strain lines observed in the *quadrans* F14 are discontinuous and heterogeneous in colour and are characterized by Cu nanodomains, compared to the undegraded alloy. The nanostructures observed in Figure 8c and Figure 8d show a deep de-alloying and the evidences of corrosion processes, as suggested by the darker grey colour composing the lines and the irregular border of the linear structures. These altered areas can have a thickness smaller than 1 µm.

The dezincification process, as showed by HR-FESEM images, follows the stress lines and the grain boundaries of the alloy.

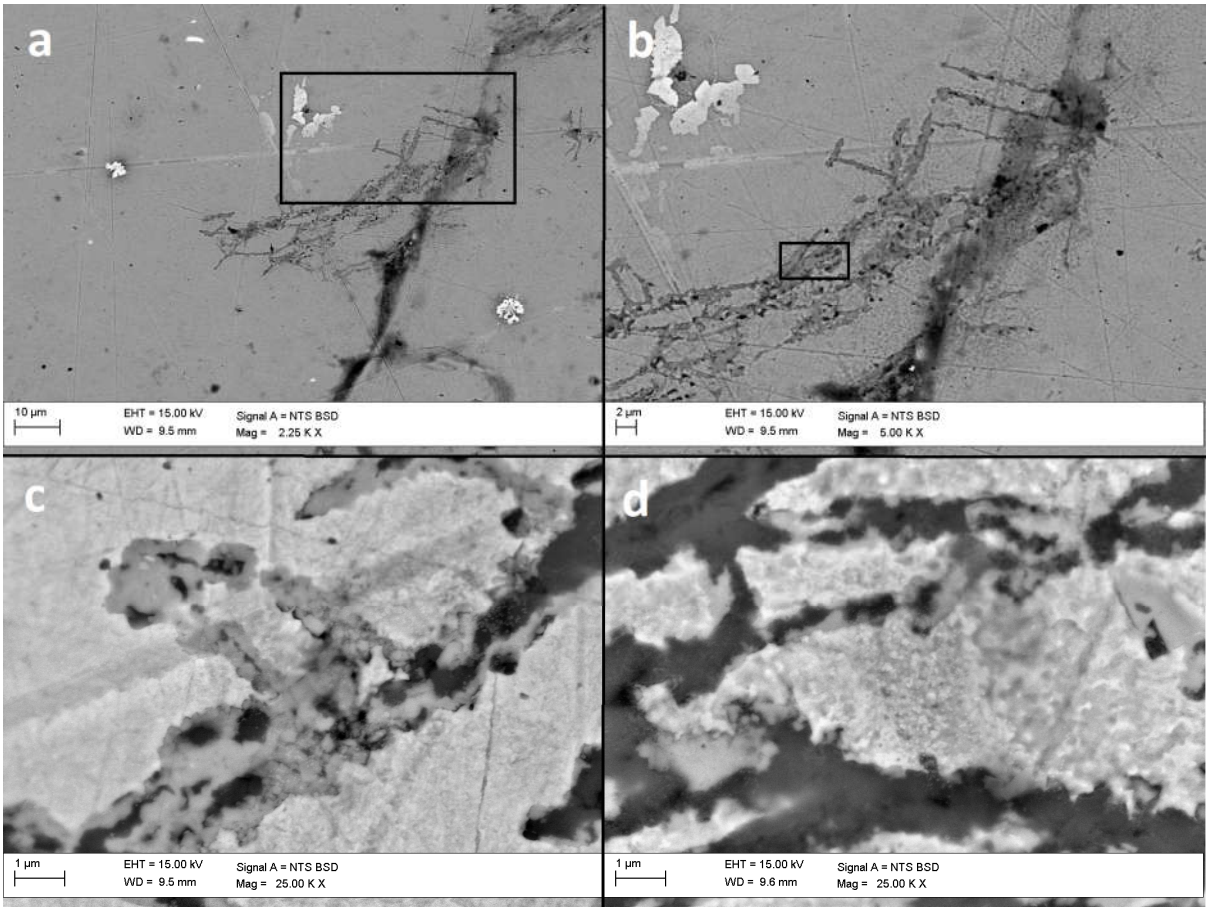

Figure 8 BSE image at nanoscale of cross section of sample F14. From (a) to (d) the magnification is increased: the highlighted area in (a) is expanded in (b), the highlighted area in (b) is expanded in (c) and (d).

4.5 Discussion

SEM-EDS analyses revealed that a coarse-type structure (Robbiola et al., 1998) occurs in the patina of the samples A3 and F1. This degraded surface layer is caused by the dezincification process and it usually occurs in artefacts having low amount of Sn in the alloy (Constantinides et al., 2002). In particular, in the studied samples the amount of Sn, where present, is below the detection limit of the EDS system. Indeed, as previously reported (Di Fazio et al., 2019b), quantitative analyses on orichalcum coins minted during the Roman Empire show a maximum Sn value of 2.27% and a minimum value of 0.01%. In

particular, EMP analyses on sample A3 indicate an average value of Sn of 0.84% in the alloy. Moreover, the altered patina of the samples is similar in thickness to that identified by Robbiola et al. (1998) as Type II structure patina ("coarse patina"), i.e. from ~200 µm to several mm.

The strain lines, highlighted by SEM and FESEM imaging investigation, are the evidence of a heavy cold-working during the minting process. The hammering, required for coining, causes the slip of crystal planes and, as consequence, a series of parallel movements, producing fine lines (Scott, 1991). However, the strain twin lines observed do not show additional deformation, as showed by SEM figures (Figure 2b, c, Figure 3, Figure 6a, b, Figure 8). This seems to suggest that further hammering actions were not performed on coins, after minting. Studying the stress lines at high magnification, a heterogeneity in composition at nanoscale is evidenced. This means that the slip lines have been preferentially dezincified respect to the not-stressed zones of alloy as highlighted by HR-FESEM images of sample F14 (Figure 8c, d). Micrographic investigations on other ancient alloys proved that the dendritic arms in casted objects were preferentially corroded than the inter-dendritic areas, that are preferentially preserved (Scott, 1991). Therefore, it can be affirmed that the typical strain lines due to hammering, represent a preferential point of corrosion in samples in orichalcum, like the dendritic structures for other copper-based alloys.

The trans-granular corrosion and the resulting dezincification, well observed in X-ray maps of elemental distribution of sample F1 (Figure 5), can be attribute to the Cu-Zn ratio; indeed, as observed by Sieradzki et al. (1987), corrosion process can be induced in trans-granular zones in alloys with Zn content between 20% and 30%. According to Sieradzki and al. (1987), the trans-granular stress corrosion can be correlated with the dislocation structures of the deformed alloys, if in contact with basic solutions.

The occurrence of Cl (Figure 4 and Figure 5), as exogenous element from the environment, provided an ideal medium for galvanic reactions between the Cu and Zn, involving corroded area and penetrating to the inner zones of the coins. Indeed, the first ionization of Zn determines superficial dezincification and, thus, Cu-enrichment surface layer. Moreover, also Cu can be lost, causing decuprification and, thus, porosity structures (Constantinides et al., 2002; Marshakov, 2005), well visible in Figure 2. In addition, the increase of Cl at the corroded-uncorroded interface has already been found in previous

studies on archaeological artefacts and artificial references materials for historical metals (Constantinides et al., 2002; Robbiola et al., 1998). According to these studies, the Cl increase is typical of an intense interaction between the samples and the environmental agents and confirms that the patina of samples A3 and F1 belong to the so-called Type II.

The occurrence of Si as exogenous element in the patinas of samples F13 and F14 protected the two *quadrantes* from degradation, as the good Si value of resistivity. Based on the low occurrence of Zn and soil elements, these patinas can be described as Type I structure patina ("even" patina), according to Robbiola et al. (1998). Indeed, SEM imaging revealed the good degree of conservation of the metal core of these two samples, considering the external layer as a passive and protective, so called, "noble patina". The natural coating effect of the Si-rich patina is confirmed by the absence of Cl at the patina-core interface.

4.6 Conclusion

The micro and nanostructures of Roman orichalcum coins were investigated applying SEM and HR-FESEM at different resolution and X-ray elements mapping, obtaining information about technological processes applied by the Roman and the processes of dezincification and decuprification, *i.e.* the corrosion processes of Zn and Cu, respectively. The investigation of the patinas revealed selective trans-granular corrosion, attributed to the Cu-Zn ratio and to the occurrence of exogenous Cl.

SEM-EDS and HR-FESEM-EDS investigation confirmed the use of cold-working by hammering to struck coins. The X-ray maps of elements and the nano-investigation showed the presence of corrosion also inside the strain parallel lines caused by the slip of crystal planes, due to hammering. These lines are heterogeneous in composition and Zn depleted. This consideration suggests that the structures produced by mechanical stress could be the trigger area of corrosion and degradation processes on this ancient alloy.

Acknowledgements

Financial support was provided by Sapienza University of Rome (Ateneo funding, 2018). PhD grants of the Department of Earth Sciences, Sapienza University of Rome, are gratefully. The authors are indebted to Private Collectors for generously providing the coins which were sacrificed for the study. The SNN-lab of the Center for Nanotechnology for Engineering (CNIS) , Sapienza University of Rome, are gratefully acknowledged.

References

Ager, F. J., Gómez-Tubío, B., Paúl, A., Gómez-Morón, A., Scrivano, S., Ortega-Feliu, I., et al. (2016). Combining XRF and GRT for the analysis of ancient silver coins. *Microchem. J.* 126, 149–154. doi:10.1016/j.microc.2015.12.017.

Amela Valverde, L. (2004). RRC 476 y 550, dos emisiones en oricalco de C. Julio César. *Nvmisma* 248, 7–22.

Ashkenazi, D., Inberg, A., Langgut, D., Hendler, N., and Cvikel, D. (2016). Brass–iron couple and brass–iron–wood ternary system of metal objects from the Akko 1 shipwreck (Israel). *Corros. Sci.* 110, 228–241. doi:10.1016/j.corsci.2016.04.003.

Ashkenazi, D., Nusbaum, I., Shacham-Diamand, Y., Cvikel, D., Kahanov, Y., and Inberg, A. (2017). A method of conserving ancient iron artefacts retrieved from shipwrecks using a combination of silane self-assembled monolayers and wax coating. *Corros. Sci.* 123, 88–102. doi:10.1016/j.corsci.2017.04.007.

Barrena, M. I., Gómez de Salazar, J. M., and Soria, A. (2008). Corrosion of brass archaeological blinker: Characterisation of natural degradation process. *Mater. Lett.* 62, 3944–3946. doi:10.1016/j.matlet.2008.05.015.

Caley, E. R. (1964). *Orichalcum and related ancient alloys*. New York: American Numismatic Society.

Caponetti, E., Armetta, F., Brusca, L., Chillura Martino, D., Saladino, M. L., Ridolfi, S., et al. (2017). A multivariate approach to the study of orichalcum ingots from the underwater Gela's archaeological site. *Microchem. J.* 135, 163–170. doi:10.1016/j.microc.2017.09.003.

Catalli, F. (2003). *Numismatica greca e romana*. Roma: Istituto Poligrafico e Zecca dello Stato.

Constantinides, I., Adriaens, A., and Adams, F. (2002). Surface characterization of artificial corrosion layers on copper alloy reference materials. *Appl. Surf. Sci.* 189, 90–101. doi:10.1016/S0169-4332(02)00005-3.

Corsi, J., Grazzi, F., Lo Giudice, A., Re, A., Scherillo, A., Angelici, D., et al. (2016). Compositional and microstructural characterization of Celtic silver coins from northern Italy using neutron diffraction analysis. *Microchem. J.* 126, 501–508. doi:10.1016/j.microc.2016.01.006.

Craddock, P. T. (1978). The composition of the copper alloys used by the Greek, Etruscan and Roman civilizations. *J. Archaeol. Sci.* 5, 1–16. doi:10.1016/0305-4403(78)90015-8.

Di Fazio, M., Di Turo, F., Medeghini, L., Fabrizi, L., Catalli, F., and De Vito, C. (2019a). New insights on medieval Provisini silver coins by a combination of non-destructive and micro-invasive techniques. *Microchem. J.* 144, 309–318. doi:10.1016/j.microc.2018.09.016.

Di Fazio, M., Felici, A. C., Catalli, F., and De Vito, C. (2019b). Microstructure and chemical composition of Roman orichalcum coins emitted after the monetary reform of Augustus (23 B.C.). *Sci. Rep.*, Submitted.

Di Turo, F., Montoya, N., Piquero-Cilla, J., De Vito, C., Coletti, F., Favero, G., et al. (2017). Archaeometric analysis of Roman bronze coins from the Magna Mater temple using solid-state voltammetry and electrochemical impedance spectroscopy. *Anal. Chim. Acta* 955, 36–47. doi:10.1016/j.aca.2016.12.007.

Di Turo, F., Montoya, N., Piquero-Cilla, J., De Vito, C., Coletti, F., Favero, G., et al. (2018). Dating Archaeological Strata in the Magna Mater Temple Using Solid-state Voltammetric Analysis of Leaded Bronze Coins. *Electroanalysis* 30, 361–370. doi:10.1002/elan.201700724.

Doménech-Carbó, M. T., Di Turo, F., Montoya, N., Catalli, F., Doménech-Carbó, A., and De Vito, C. (2018). FIB-FESEM and EMPA results on Antoninianus silver coins for manufacturing and corrosion processes. *Sci. Rep.* 8, 10676. doi:10.1038/s41598-018-28990-x.

Fabrizi, L., Di Turo, F., Medeghini, L., Di Fazio, M., Catalli, F., and De Vito, C. (2019). The application of non-destructive techniques for the study of corrosion

patinas of ten Roman silver coins: The case of the medieval Grosso Romanino. *Microchem. J.* 145, 419–427. doi:10.1016/j.microc.2018.10.056.

Finetti, A. (1987). *Numismatica e tecnologia: produzione e valutazione della moneta nelle società del passato*. Roma: La Nuova Italia scientifica.

Ingo, G. M., Riccucci, C., Faraldi, F., Pascucci, M., Messina, E., Fierro, G., et al. (2017). Roman sophisticated surface modification methods to manufacture silver counterfeited coins. *11th Int. Conf. Surf. Coat. Nanostructured Mater.* 421, 109–119. doi:10.1016/j.apsusc.2017.01.101.

Ingo, G. M., Riccucci, C., Pascucci, M., Messina, E., Giuliani, C., Biocca, P., et al. (2018). Combined use of FE-SEM+EDS, ToF-SIMS, XPS, XRD and OM for the study of ancient gilded artefacts. *12th Int. Conf. Surf. Coat. Nanostructured Mater. - NANOSMAT 2017* 446, 168–176. doi:10.1016/j.apsusc.2018.01.278.

Marshakov, I. K. (2005). Corrosion Resistance and Dezincing of Brasses. *Prot. Met.* 41, 205–210. doi:10.1007/s11124-005-0031-2.

Papadopoulou, O., Alessandri, O. C., Vassiliou, P., Grassini, S., Angelini, E., and Gouda, V. (2016). Soil-induced corrosion of ancient Roman brass - A case study. *Mater. Corros.* 67, 160–169. doi:10.1002/maco.201408115.

Pronti, L., Felici, A. C., Alesiani, M., Tarquini, O., Bracciale, M. P., Santarelli, M. L., et al. (2015). Characterisation of corrosion layers formed under burial environment of copper-based Greek and Roman coins from Pompeii. *Appl. Phys. A* 121, 59–68. doi:10.1007/s00339-015-9351-5.

Robbiola, L., Blengino, J.-M., and Fiaud, C. (1998). Morphology and mechanisms of formation of natural patinas on archaeological Cu–Sn alloys. *Corros. Sci.* 40, 2083–2111. doi:10.1016/S0010-938X(98)00096-1.

Scott, D. A. (1991). *Metallography and microstructure of ancient and historic metals*. [Marina del Rey, CA]: Getty Conservation Institute in association with Archetype Books.

Sieradzki, K., Kim, J. S., Cole, A. T., and Newman, R. C. (1987). The Relationship Between Dealloying and Transgranular Stress-Corrosion Cracking of Cu-Zn

and Cu-Al Alloys. *J. Electrochem. Soc.* 134, 1635–1639. doi:10.1149/1.2100726.

Sutherland, C. H. V. (1984). *The Roman Imperial Coinage: From 31 BC to AD 69: with introd. to the mints.* London: Spink.

Conclusion

This thesis aimed to improve and enrich the scientific knowledge on the production of the ancient and legendary alloy of orichalcum, as well as its degradation over two millennia. The use of oricalchum for the production of objects high in value and coins marked a turning point in terms of metal alloy production technology as well as from a political and economic point of view. In particular, the emissions in orichalcum, started as an experiment, represent the need of the Imperial authority to reform the entire monetary system, probably due to the absence of strict rules in the Republican Era.

With this purpose, ancient Roman orichalcum coins were investigated by a combined use of non-invasive (VIMP, XRF), micro-destructive (ATR-FTIR, FIB-FESEM-EDS) and destructive techniques (SEM-EDS, HR-FESEM-EDS, EMPA). The application of a multi-analytical approach allowed exploring the patterns of corrosion of the patinas and the chemical composition of the un-corroded nucleus. Based on the results reported in the previous chapters, the following conclusions can be drawn:

The external layers of the orichalcum samples are deeply corroded and have a porous microstructure, showing the signs of dezincification and decuprification processes, with Zn-depleted/Cu-enriched areas at different degrees of degradation. X-ray maps analyses highlighted variations in the distributions of the main elements of the alloy in patinas, picturing the enrichments and the depletions mentioned above. In addition, the corrosion layer can reach up more than 1mm in depth. In particular this information, from necessary destructive analyses, proves the impossibility of obtaining quantitative information from superficial investigation.

Studying the inner areas of the samples with X-ray maps, it has been noticed that the uncorroded cores of coin are homogeneous in composition, indicating a good technological level reached from Roman smiths. Scanning electron imaging analyses on cross sections, at different scales and resolution, show a typical orichalcum microstructure with α-grains, microdomains arranged in irregular shape and structure, with Cu-rich regions more corroded than Zn-Cu areas, and evidences of hard cold-working to struck coins. From a quantitative point of view, the inner un-corroded cores have a chemical composition which varies from 68 to 82 wt% for Cu and from 17 to 31 wt% for Zn. This is an evidence of the fluctuating of the average value of Zn in orichalcum during time (in particular, the studied samples were coined between 88 BC and 96 AD),

suggesting that these data cannot be used for dating the coin, as previously reported in literature.

Following historical sources, the monetary reform of Augustus in 23 BC was unchanged until the kingdom of Nero. However, this information is not confirmed by qualitative and quantitative analyses reported in this PhD thesis. Indeed, the research project shows that the respect of the Emperors' dictations has not been strictly followed. The results here presented could endorse the historic-numismatic hypotheses about an event, after the monetary reform of Augustus, that induced Nero to promulgate a new reform in 63-63 AD, necessary to put order in the uncontrolled monetary system, as the Augustus reform bring order in the Republican economic organisation (see Chapter 1 – Historical background). To confirm this, using the data obtained from the VIMP methodology it was possible grouping the coins by emission, evaluating the differences in composition between issues from different authorities.

In conclusion, this research could attempts to fill the scientific gap existing in the knowledge of Roman orichalcum coinage, contributing to characterize this ancient alloy, to better understand the dezincification process and to highlight possible differences among samples minted in different years.

I. Appendix A – Point-by-point EMP analyses

Here are presented additional selected data obtained using point-by-point EMP analyses on cross-section (rim-core-rim) of selected Roman orichalcum coins. EMPA data for quantitative chemical analyses were performed using a Cameca SX50 electron microprobe equipped with five wavelength-dispersive spectrometers (CNR–IGAG, Rome, c/o Department of Earth Sciences, Sapienza University of Rome). The operating conditions were: accelerating voltage 15 kV, beam current 15 nA. Element peaks and background were measured with counting times of 20 and 10 s respectively. Metallic Cu and metallic Zn were used respectively as a reference standard for Cu and Zn (LIF), galena for Pb (PET), cassiterite for Sn (PET), metallic Ni and metallic Co respectively for Ni and Co (LIF), synthetic GaAs for As (TAP), rhodonite and metallic Mn for Mn (PET), olivine and synthetic magnetite for Fe (LIF). Matrix corrections were calculated by the PAP method with software supplied by Microbeams Services. The detection limits under the specified working condition vary from 0.05 to 0.1 wt% with standard deviations from 0.02 to 0.04 wt%. The analytical error was ~1% rel. for the major elements.

Sample	Point analysis	Cu wt%	Zn wt%	Fe wt%	Sn wt%	Pb wt%	As wt%	Mn wt%	Ni wt%	Co wt%
A1	1	77.572	21.403	0.306	0.802	0.000	0.095	0.017	0.043	0.000
	2	74.465	21.205	0.318	0.947	5.640	0.046	0.000	0.043	0.012
	3	77.898	20.507	0.445	0.648	0.000	0.060	0.000	0.046	0.000
	4	77.111	20.472	0.410	0.545	0.000	0.037	0.000	0.000	0.045
	5	77.019	21.041	0.367	0.477	0.068	0.013	0.000	0.009	0.000
	6	77.391	21.515	0.274	0.552	0.062	0.000	0.000	0.011	0.018
	7	76.620	21.242	0.225	0.590	0.000	0.047	0.000	0.037	0.029
	8	76.941	21.261	0.347	0.605	0.068	0.010	0.004	0.022	0.000
	9	75.916	21.806	0.280	0.914	0.104	0.026	0.000	0.029	0.014
	10	76.625	21.397	0.288	0.964	0.000	0.000	0.000	0.044	0.019

Sample	Point analysis	Cu wt%	Zn wt%	Fe wt%	Sn wt%	Pb wt%	As wt%	Mn wt%	Ni wt%	Co wt%
A2	1	71.168	27.891	0.222	0.048	0.000	0.089	0.000	0.027	0.000
	2	70.633	27.994	0.240	0.057	0.136	0.031	0.000	0.011	0.000
	3	70.761	27.916	0.236	0.078	0.000	0.084	0.026	0.069	0.006
	4	70.357	27.606	0.280	0.085	0.148	0.024	0.000	0.017	0.013
	5	70.956	27.553	0.276	0.093	0.074	0.031	0.017	0.000	0.000
	6	70.889	27.561	0.216	0.068	0.062	0.042	0.000	0.024	0.000
	7	70.876	27.852	0.228	0.077	0.000	0.000	0.000	0.027	0.011
	8	70.752	27.675	0.268	0.089	0.025	0.086	0.000	0.019	0.034
	9	71.322	27.905	0.188	0.050	0.000	0.068	0.003	0.011	0.000
	10	71.427	27.722	0.240	0.029	0.062	0.000	0.000	0.010	0.003
A3	1	80.521	17.227	0.338	0.832	0.086	0.039	0.000	0.054	0.006
	2	79.984	17.081	0.337	0.767	0.000	0.000	0.003	0.029	0.001
	3	80.282	17.291	0.391	0.766	0.055	0.022	0.012	0.055	0.000
	4	80.408	16.931	0.356	0.688	0.037	0.027	0.005	0.000	0.009
	5	81.127	17.210	0.319	0.647	0.000	0.019	0.026	0.000	0.010
	6	81.381	17.869	0.254	0.722	0.000	0.034	0.014	0.019	0.000
	7	82.058	16.723	0.368	0.610	0.043	0.000	0.010	0.107	0.010
	8	80.628	17.399	0.318	0.737	0.049	0.000	0.000	0.046	0.009
	9	81.093	17.036	0.331	0.632	0.018	0.000	0.001	0.019	0.021
	10	80.672	16.971	0.365	0.689	0.006	0.000	0.000	0.067	0.029
A9	1	70.009	29.399	0.009	0.828	0.000	0.034	0.000	0.050	0.036
	2	68.349	30.961	0.021	1.144	0.019	0.000	0.000	0.000	0.000
	3	68.264	30.824	0.000	1.175	0.000	0.000	0.007	0.000	0.000
	4	67.898	30.386	0.025	1.360	0.012	0.023	0.000	0.000	0.036
	5	67.768	30.452	0.000	1.254	0.000	0.000	0.004	0.072	0.000
	6	67.846	30.740	0.000	1.185	0.099	0.000	0.000	0.000	0.012
	7	68.279	30.569	0.000	0.679	0.012	0.000	0.000	0.101	0.000
	8	68.355	30.443	0.048	1.025	0.000	0.013	0.006	0.038	0.025
	9	69.379	30.644	0.045	1.049	0.006	0.000	0.000	0.056	0.000
	10	68.701	29.594	0.020	1.168	0.043	0.000	0.000	0.002	0.000
A	1	81.980	18.597	0.366	0.090	0.098	0.000	0.004	0.061	0.000
	2	79.752	19.093	0.321	0.019	0.000	0.000	0.000	0.085	0.000
	3	78.040	20.621	0.352	0.121	0.000	0.000	0.020	0.000	0.000
	4	77.507	20.217	0.336	0.013	0.148	0.039	0.010	0.062	0.000
	5	77.455	20.019	0.303	0.056	0.043	0.000	0.000	0.000	0.002
	6	77.010	20.381	0.366	0.037	0.000	0.000	0.017	0.005	0.000
	7	77.936	20.385	0.319	0.123	0.025	0.000	0.019	0.000	0.000
	8	77.233	21.347	0.347	0.110	0.055	0.000	0.000	0.051	0.000
	9	79.272	21.522	0.297	0.072	0.000	0.000	0.000	0.075	0.000
	10	78.195	20.503	0.268	0.069	0.160	0.034	0.000	0.039	0.024

Sample	Point analysis	Cu wt%	Zn wt%	Fe wt%	Sn wt%	Pb wt%	As wt%	Mn wt%	Ni wt%	Co wt%
B4	1	81.192	17.260	0.108	0.104	0.000	0.013	0.000	0.000	0.000
	2	80.166	16.560	0.044	0.093	0.104	0.095	0.000	0.001	0.008
	3	80.374	17.287	0.045	0.174	0.000	0.061	0.009	0.007	0.000
	4	82.515	17.621	0.088	0.131	0.098	0.000	0.009	0.010	0.000
	5	82.871	17.371	0.103	0.086	0.063	0.034	0.021	0.000	0.000
	6	83.212	17.440	0.057	0.154	0.040	0.051	0.000	0.021	0.006
	7	82.741	16.867	0.025	0.111	0.006	0.045	0.000	0.055	0.000
	8	81.237	17.152	0.061	0.141	0.000	0.072	0.055	0.058	0.000
B5	1	75.552	22.748	0.260	0.254	0.052	0.032	0.012	0.023	0.072
	2	75.828	23.089	0.337	0.070	0.254	0.065	0.000	0.050	0.023
	3	75.576	23.734	0.198	0.401	0.006	0.069	0.009	0.000	0.037
	4	77.855	22.720	0.308	0.190	0.162	0.135	0.000	0.059	0.009
	5	78.008	23.043	0.304	0.156	0.144	0.029	0.001	0.016	0.018
	6	77.128	23.027	0.239	0.146	0.000	0.006	0.024	0.004	0.000
	7	76.387	23.464	0.211	0.264	0.064	0.098	0.026	0.000	0.000
	8	76.596	22.874	0.218	0.143	0.185	0.042	0.000	0.007	0.000
	9	77.572	22.710	0.226	0.121	0.064	0.076	0.000	0.000	0.000
	10	83.889	0.357	0.029	0.098	0.046	0.025	0.000	0.034	0.004
B14	1	84.866	0.000	0.120	0.020	0.023	0.070	0.000	0.000	0.043
	2	78.807	20.943	0.240	0.074	0.017	0.060	0.025	0.000	0.000
	3	79.709	21.009	0.247	0.053	0.052	0.147	0.010	0.013	0.000
	4	79.170	21.027	0.206	0.031	0.017	0.111	0.051	0.012	0.027
	5	79.662	21.446	0.254	0.060	0.000	0.066	0.000	0.000	0.001
	6	79.748	21.092	0.207	0.044	0.000	0.000	0.000	0.023	0.002
	7	79.460	20.769	0.240	0.000	0.000	0.105	0.000	0.011	0.000
	8	79.561	21.347	0.310	0.011	0.092	0.071	0.000	0.026	0.015
	9	79.944	21.529	0.220	0.037	0.098	0.015	0.000	0.000	0.000
	10	81.253	1.164	0.111	0.017	0.092	0.068	0.018	0.046	0.023
20#	1	83.642	15.202	0.259	1.003	0.000	0.002	0.035	0.038	0.029
	2	82.381	15.367	0.322	2.255	0.046	0.051	0.000	0.061	0.000
	3	83.494	15.591	0.267	2.090	0.046	0.003	0.000	0.016	0.036
	4	83.031	15.328	0.260	2.145	0.023	0.011	0.000	0.067	0.000
	5	83.134	15.388	0.286	2.214	0.109	0.032	0.000	0.002	0.011
	6	83.549	15.337	0.273	2.145	0.000	0.000	0.000	0.063	0.000
	7	83.619	15.532	0.317	2.313	0.000	0.000	0.000	0.046	0.016
	8	82.945	15.483	0.315	2.155	0.000	0.041	0.009	0.005	0.000
	9	81.726	15.342	0.304	2.056	0.057	0.000	0.000	0.059	0.000
	10	83.469	15.670	0.239	2.243	0.000	0.000	0.044	0.017	0.000

Sample	Point analysis	Cu wt%	Zn wt%	Fe wt%	Sn wt%	Pb wt%	As wt%	Mn wt%	Ni wt%	Co wt%
10#	1	81.369	19.084	0.206	0.041	0.035	0.079	0.000	0.000	0.000
	2	81.558	19.090	0.187	0.060	0.035	0.053	0.008	0.000	0.021
	3	81.839	18.753	0.206	0.069	0.040	0.050	0.000	0.000	0.000
	4	81.059	18.738	0.187	0.036	0.046	0.101	0.035	0.025	0.018
	5	81.739	19.139	0.228	0.114	0.092	0.018	0.033	0.022	0.000
	6	81.482	19.069	0.172	0.040	0.075	0.053	0.039	0.008	0.001
	7	82.132	18.665	0.241	0.040	0.000	0.052	0.019	0.000	0.009
	8	81.082	18.793	0.226	0.029	0.023	0.089	0.000	0.004	0.000
	9	81.503	18.798	0.214	0.073	0.184	0.061	0.000	0.035	0.020
	10	81.618	19.203	0.194	0.097	0.282	0.079	0.017	0.000	0.010
5#	1	89.335	10.060	0.131	0.011	0.000	0.000	0.014	0.011	0.024
	2	86.410	12.420	0.051	0.061	0.132	0.000	0.000	0.031	0.000
	3	85.397	14.477	0.090	0.068	0.000	0.006	0.036	0.000	0.043
	4	76.113	23.323	0.139	0.127	0.087	0.037	0.032	0.021	0.000
	5	77.179	23.493	0.100	0.123	0.058	0.000	0.026	0.000	0.003
	6	76.524	23.400	0.156	0.093	0.000	0.000	0.000	0.038	0.000
	7	77.203	23.640	0.124	0.130	0.029	0.023	0.000	0.037	0.000
	8	77.730	23.727	0.120	0.104	0.000	0.013	0.008	0.000	0.016
	9	90.731	9.335	0.044	0.044	0.115	0.000	0.000	0.047	0.020
	10	95.001	5.413	0.055	0.000	0.000	0.033	0.019	0.012	0.000
C9	1	98.343	0.000	0.002	0.000	0.000	0.030	0.000	0.050	0.003
	2	98.029	0.000	0.004	0.000	0.040	0.026	0.000	0.000	0.009
	3	97.328	0.092	0.080	0.055	0.064	0.000	0.000	0.011	0.000
	4	99.552	0.541	0.062	0.012	0.000	0.002	0.029	0.043	0.014
	5	78.657	21.586	0.171	0.000	0.000	0.015	0.022	0.000	0.000
	6	77.359	22.339	0.149	0.111	0.000	0.028	0.000	0.036	0.004
	7	77.733	22.322	0.175	0.037	0.047	0.010	0.000	0.032	0.004
	8	77.924	22.326	0.148	0.015	0.000	0.000	0.000	0.054	0.001
	9	77.249	22.285	0.163	0.032	0.052	0.064	0.041	0.000	0.039
	10	98.447	0.039	0.000	0.000	0.064	0.000	0.025	0.002	0.008

II. Appendix B – XRF spectra

Additional representative X-ray fluorescence spectra of the patinas of the orichalcum sample are showed below. They were carried out by energy-dispersive X-ray fluorescence spectroscopy (EDXRF - Department of Basic and Applied Sciences for Engineering, Sapienza University of Rome, Italy) The spectrometer consists of an X-ray generator (Amptek MiniX) with an anode target of rhodium and a beryllium window of 127µm of thickness. The detector is a Peltier cooled silicon drift with integrated amplifier and multi-channel analyser (Amptek 123-SDD). The detector has a surface of 25 mm^2, a thickness of 450µm, a beryllium window of 12.5 µm of thickness and its energy resolution is 140 eV, full width half maximum at 5.9 keV. The incident and the revealed beams form an angle of 45° with respect to the surface of the sample. The analysed surface is distant 3 cm from the X-ray generator anode and 3.5 cm from the detector surface. The X-ray generator was equipped with a 2 mm diameter collimator and was powered with an accelerating potential difference of 35 kV and an electronic current of 15 µA. For each sample, three measures were obtained, with an acquisition time of 200s each.

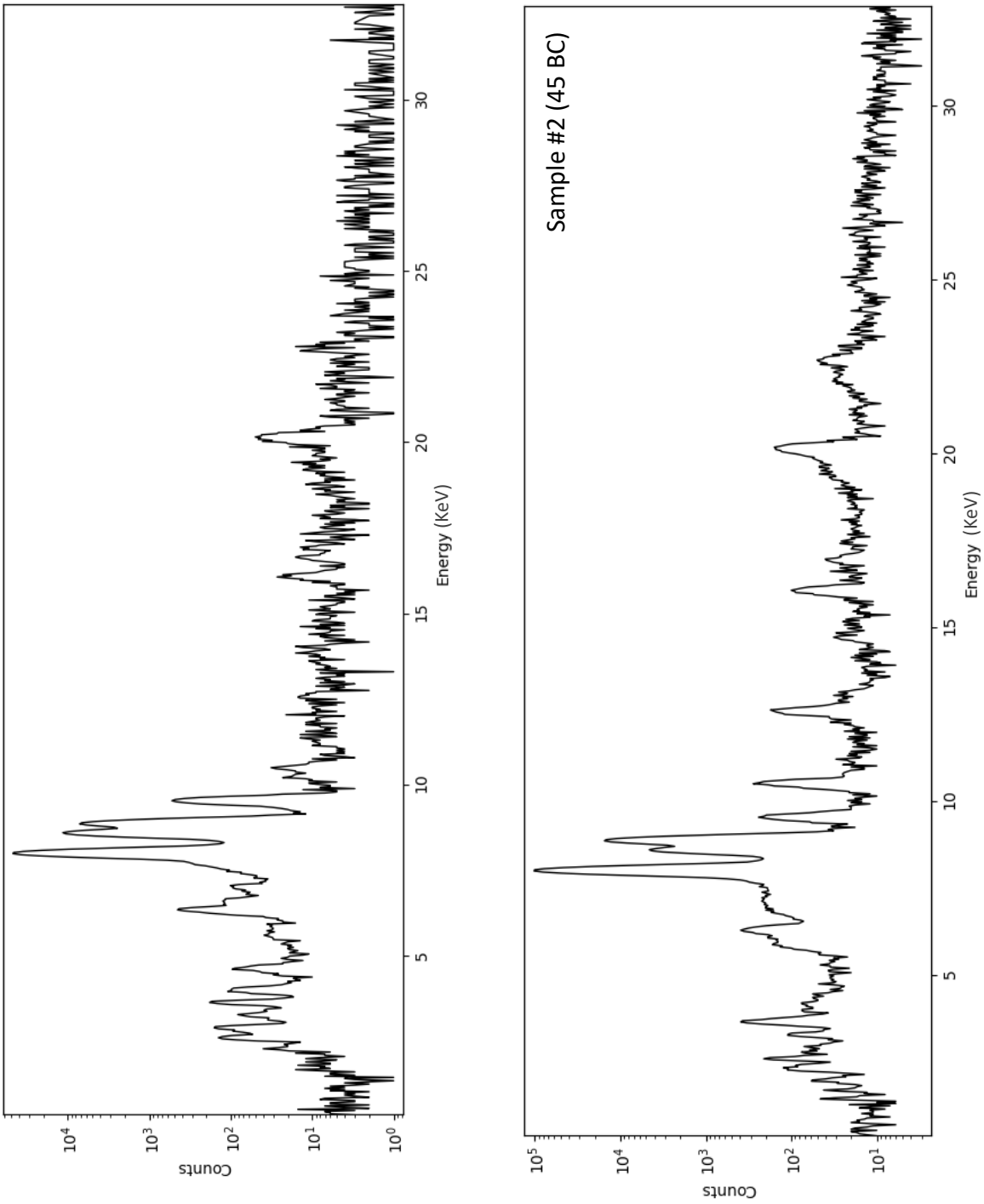
Sample #2 (45 BC)
Counts
Energy (KeV)
Counts
Energy (KeV)

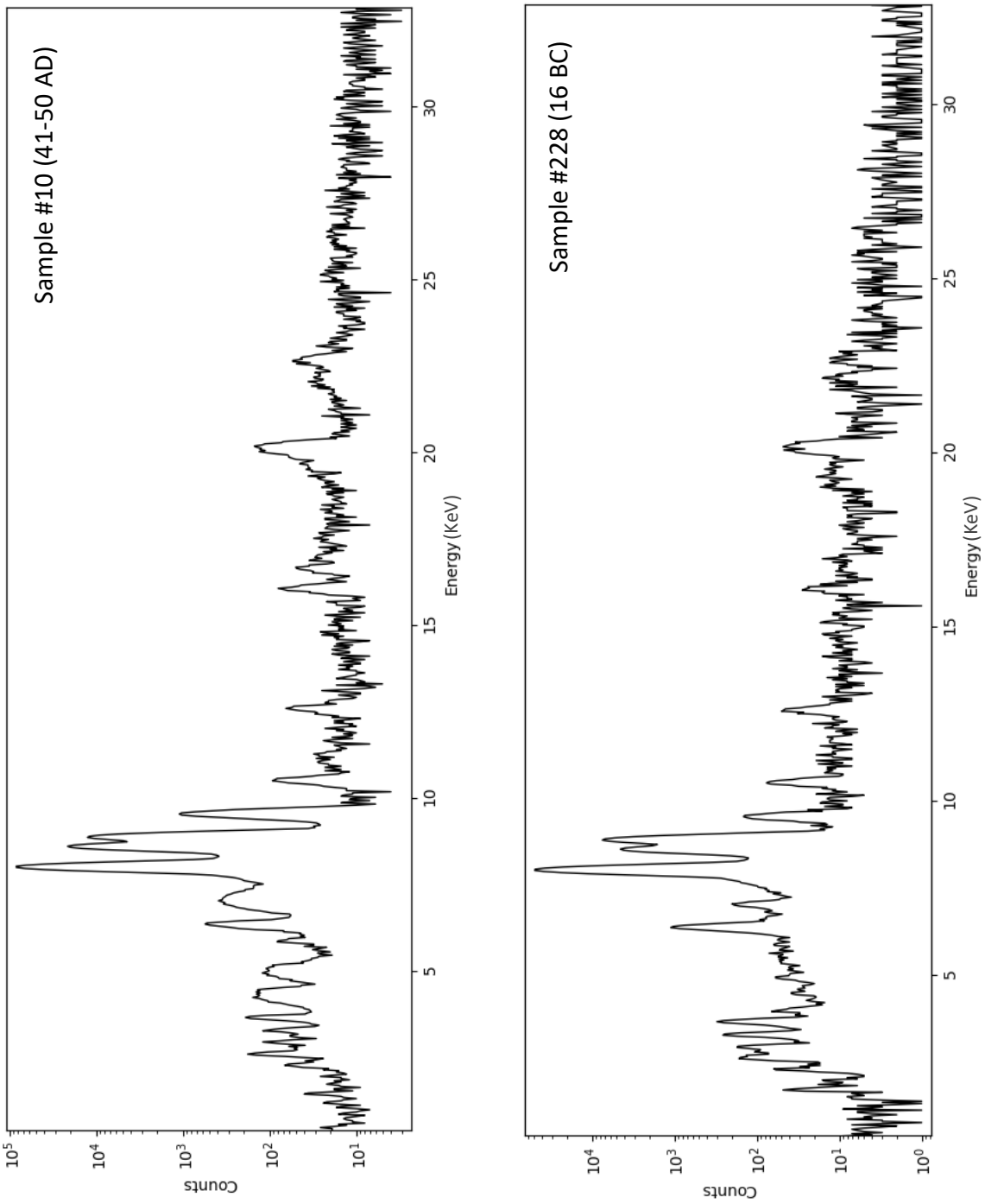
Sample #10 (41-50 AD)
Counts
Energy (KeV)
Sample #228 (16 BC)
Counts
Energy (KeV)

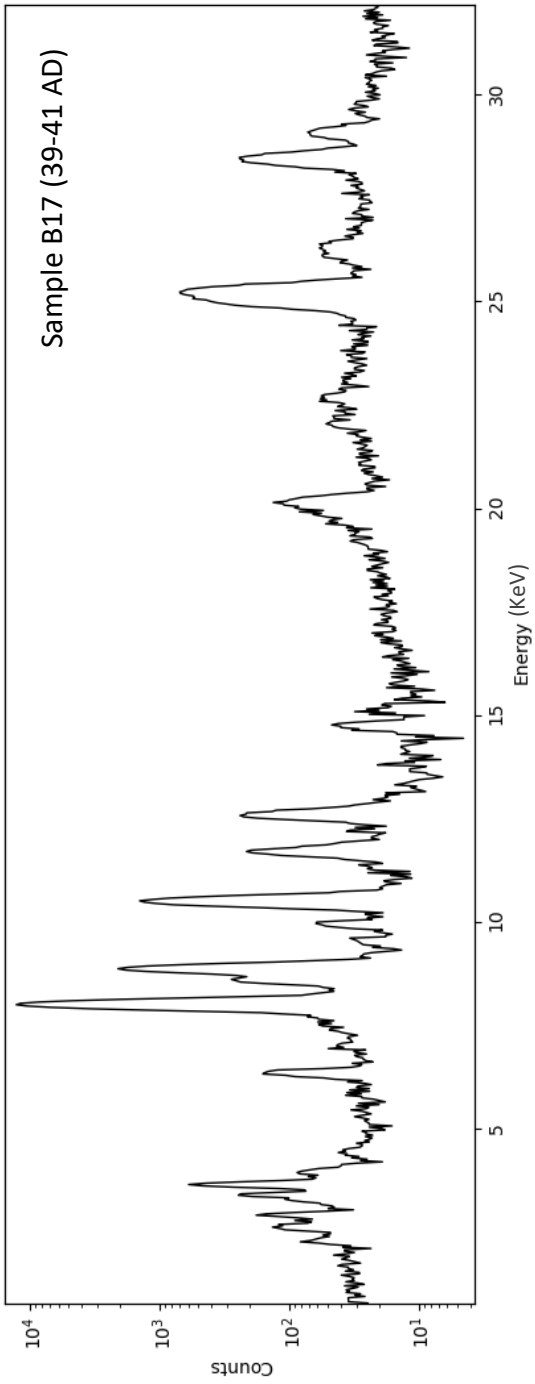
Sample B17 (39-41 AD)
Counts
Energy (KeV)

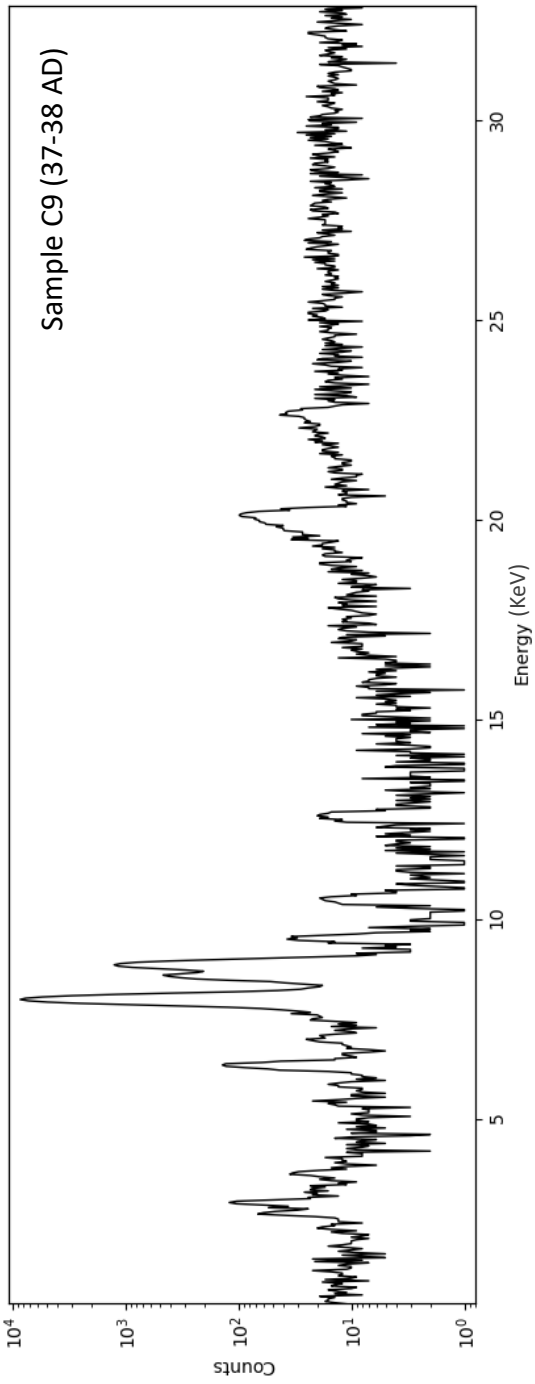
Sample C9 (37-38 AD)
Counts
Energy (KeV)

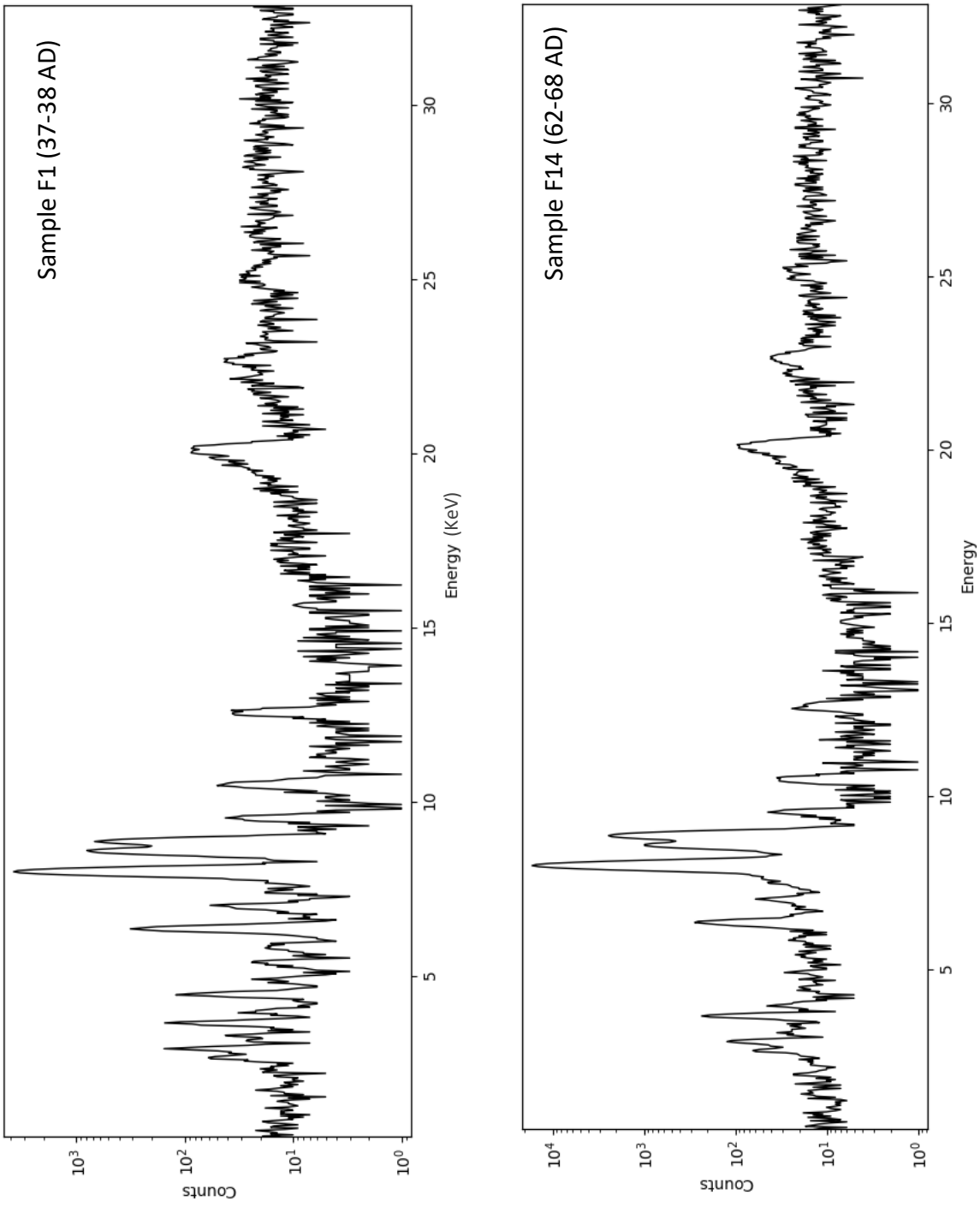
Sample F1 (37-38 AD)
Counts
Energy (KeV)
Sample F14 (62-68 AD)
Counts
Energy

Appendix C – Voltammograms

Here are presented selected voltammograms obtained using Voltammetry of Microparticles (VIMP).Analyses were performed at 298 K in a three-electrode cell using a CH I660C device (Departament de Química Analítica, Universitat de València, Valencia, Spain), using air-saturated aqueous 0.25 M HAc/NaAc aqueous buffer solution at pH 4.75. A sample-modified graphite bar (Alpino, HB type, 3 mm diameter) was used as a working electrode, the three-electrode arrangement being completed by a platinum wire auxiliary electrode and an Ag/AgCl (3 M NaCl) reference electrode.

Square wave voltammetry (SWV) was used as a detection mode determining successively the negative- and the positive-going potential scans using as parameters: potential step increment 4 mV; square wave amplitude 25 mV; frequency 5 Hz.

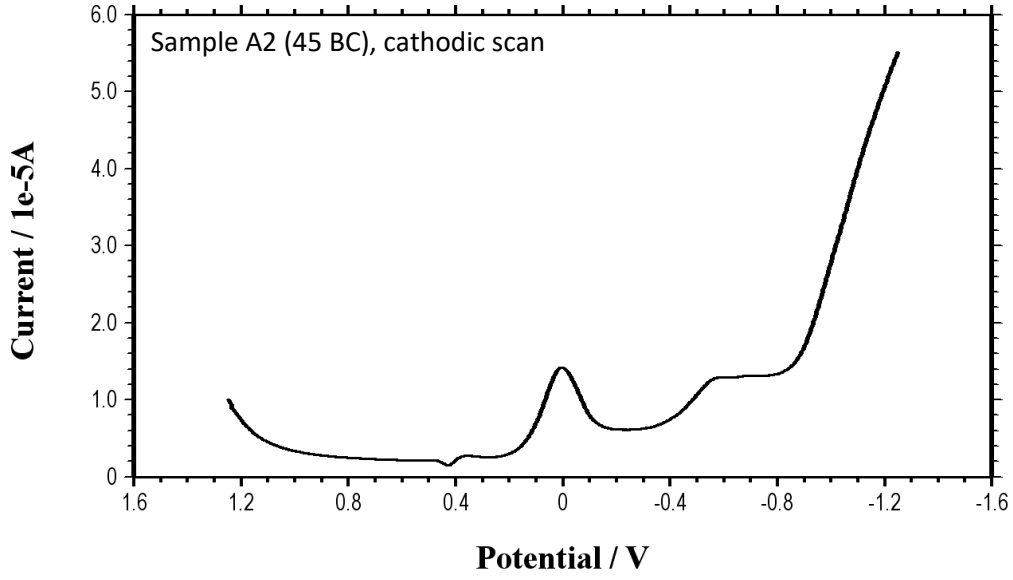
Sample A2 (45 BC), cathodic scan
Current / 1e-5A
Potential / V
6.0
5.0
4.0
3.0
2.0
1.0
0
1.6
1.2
0.8
0.4
0
-0.4
-0.8
-1.2
-1.6

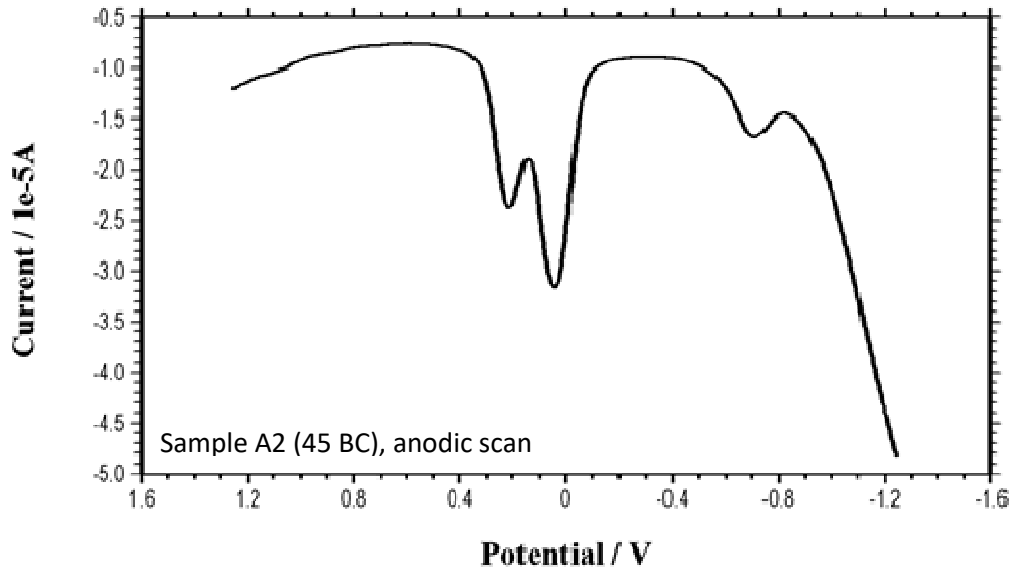
Sample A2 (45 BC), anodic scan
Current / 1e-5A
Potential / V
-0.5
-1.0
-1.5
-2.0
-2.5
-3.0
-3.5
-4.0
-4.5
-5.0
1.6
1.2
0.8
0.4
0
-0.4
-0.8
-1.2
-1.6

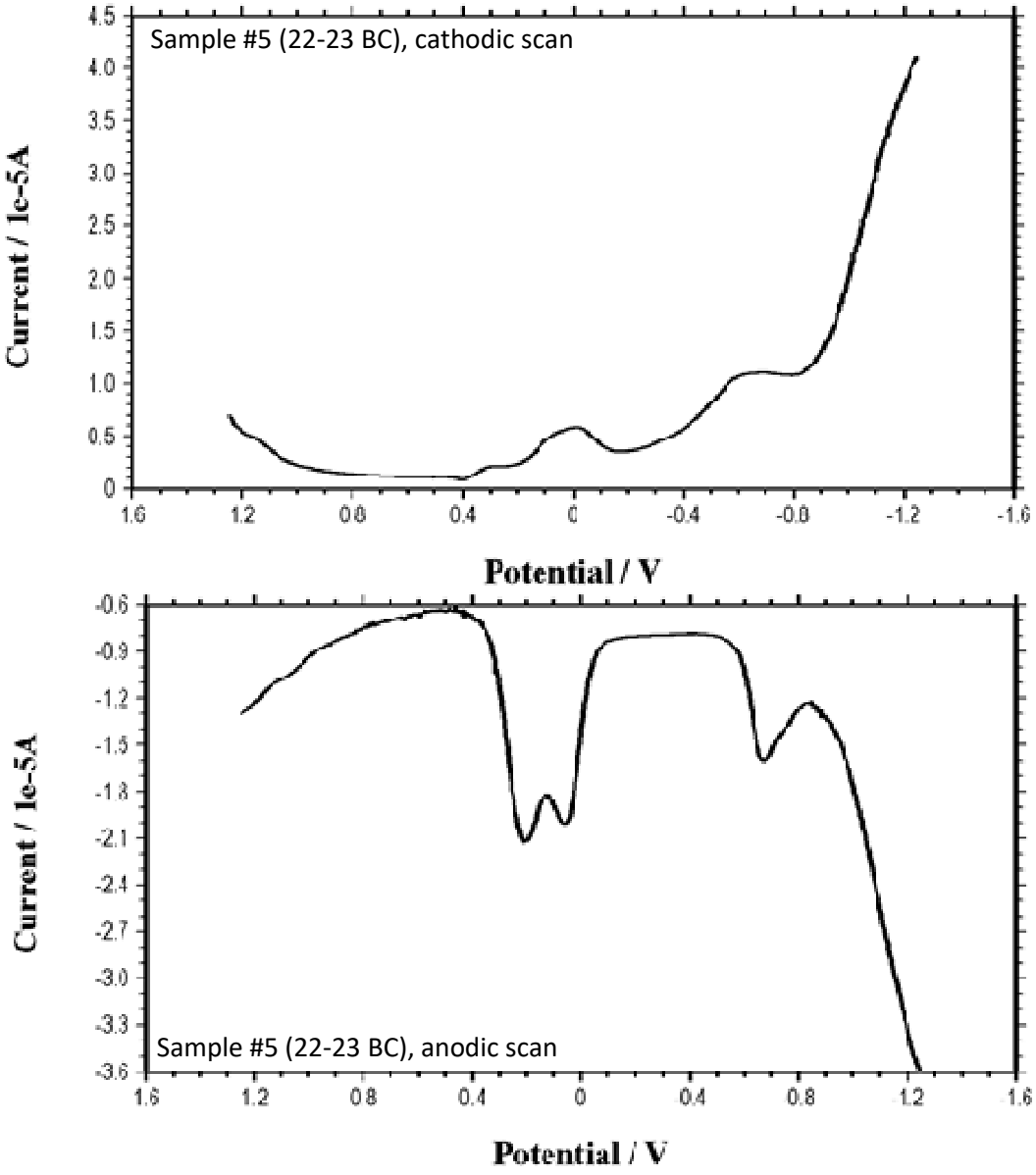
Sample #5 (22-23 BC), cathodic scan
Current / 1e-5A
Potential / V
Sample #5 (22-23 BC), anodic scan
Current / 1e-5A
Potential / V

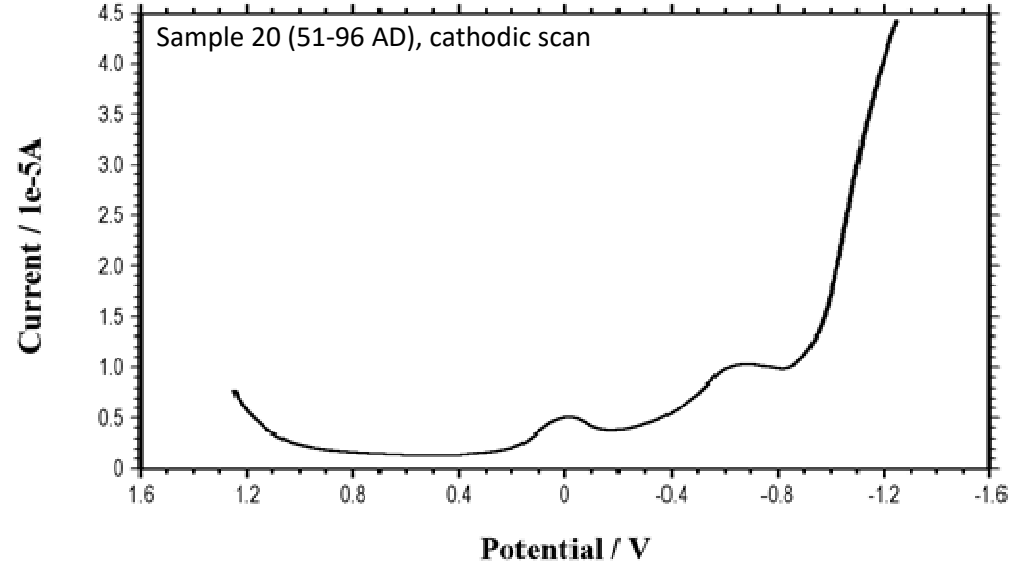
Sample 20 (51-96 AD), cathodic scan
Current / 1e-5A
Potential / V
4.5
4.0
3.5
3.0
2.5
2.0
1.5
1.0
0.5
0
1.6
1.2
0.8
0.4
0
-0.4
-0.8
-1.2
-1.6

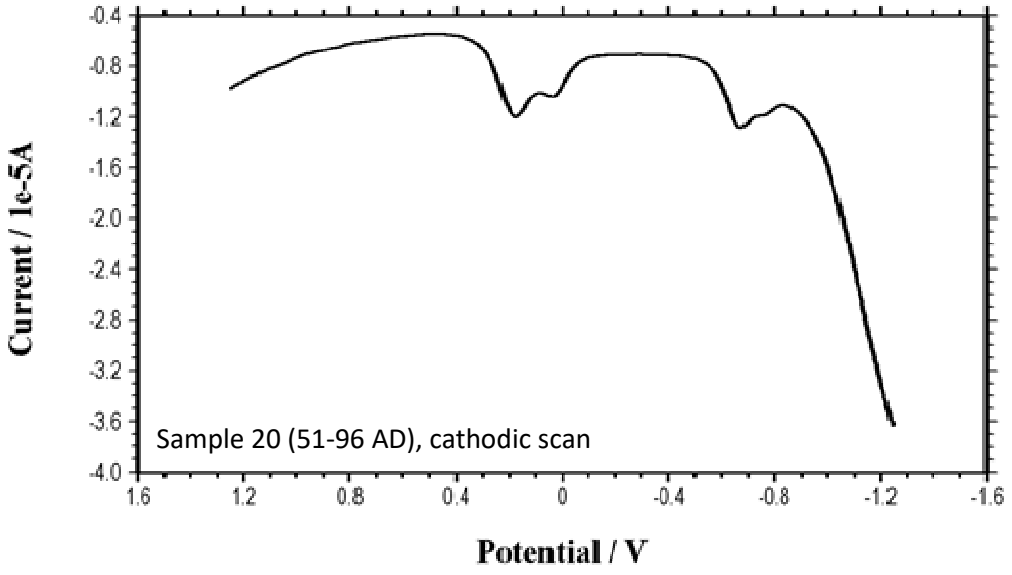
Sample 20 (51-96 AD), cathodic scan
Current / 1e-5A
Potential / V
-0.4
-0.8
-1.2
-1.6
-2.0
-2.4
-2.8
-3.2
-3.6
-4.0
1.6
1.2
0.8
0.4
0
-0.4
-0.8
-1.2
-1.6

List of acronyms

XRF	X-ray fluorescence
ATR-FTIR	Attenuated total reflectance – Fourier transform infrared spectroscopy
FIB-FESEM-EDS	Focused ion beams – field emission scanning electron microscope – energy dispersive X-rays spectroscopy
VIMP	Voltammetry of immobilized particles
HR-FESEM	High resolution field emission scanning electron microscopy
EMPA	Electron microprobe analysis
SEM-EDS	Scanning electron microscope – energy dispersive X-ray spectroscopy
LIF	Lithium fluoride crystal
PET	Pentaerythritol crystal
TAP	Thallium acid phthalate crystal
SWV	Square wave voltammetry
ORR	Oxygen reduction reaction
HER	Hydrogen evolution reaction
CE	Current era
BCE	Before current era
AD	Anno Domini
BC	Before Christ
RIC	Roman Imperial Coinage (Catalogue)
SE	Secondary electron
BSE	Backscattered electron